NAVAL POSTGRADUATE SCHOOL

MONTEREY, CALIFORNIA

THESIS

A FOLLOW-UP STUDY ON WIRELESS POWER TRANSMISSION FOR UNMANNED AIR VECHICLES

by

Leng Huei Toh

December 2007

Thesis Advisor:	David C. Jenn
Second Reader:	Michael A. Morgan

Approved for public release; distribution is unlimited

THIS PAGE INTENTIONALLY LEFT BLANK

REPORT DOCUMENTATION PAGE			Form Approved OMB No. 0704-0188
Public reporting burden for this collection of information is estimated to average 1 hour per response, including the time for reviewing instruction, searching existing data sources, gathering and maintaining the data needed, and completing and reviewing the collection of information. Send comments regarding this burden estimate or any other aspect of this collection of information, including suggestions for reducing this burden, to Washington headquarters Services, Directorate for Information Operations and Reports, 1215 Jefferson Davis Highway, Suite 1204, Arlington, VA 22202-4302, and to the Office of Management and Budget, Paperwork Reduction Project (0704-0188) Washington DC 20503.			
1. AGENCY USE ONLY *(Leave blank)*	**2. REPORT DATE** December 2007	**3. REPORT TYPE AND DATES COVERED** Master's Thesis	
4. TITLE AND SUBTITLE: A Follow-up Study on Wireless Power Transmission for Unmanned Air Vehicles		**5. FUNDING NUMBERS**	
6. AUTHOR(S) Leng Huei Toh			
7. PERFORMING ORGANIZATION NAME(S) AND ADDRESS(ES) Naval Postgraduate School Monterey, CA 93943-5000		**8. PERFORMING ORGANIZATION REPORT NUMBER**	
9. SPONSORING /MONITORING AGENCY NAME(S) AND ADDRESS(ES) N/A		**10. SPONSORING/MONITORING AGENCY REPORT NUMBER**	
11. SUPPLEMENTARY NOTES The views expressed in this thesis are those of the author and do not reflect the official policy or position of the Department of Defense or the U.S. Government.			
12a. DISTRIBUTION / AVAILABILITY STATEMENT Approved for public release; distribution is unlimited		**12b. DISTRIBUTION CODE**	

13. ABSTRACT (maximum 200 words)

This thesis was a continuation in part of a NPS project relating to microwave wireless power transmission for micro air vehicles (MAVs). The concept of using microwaves for transferring power in free space has existed since the beginning of the 20th century. The emphasis of this thesis is the experimental study of powering micro air vehicles via the use of using a microstrip rectenna (rectifying antenna) at 10 GHz. A microstrip rectenna was built and experiments were conducted to measure the efficiency of the rectenna elements.

The conversion of radio frequency (RF) power into usable DC power was performed by a rectenna. Its function could be broken down into the following four stages: reception of radio frequency (RF) power, pre-rectification filtering, rectification, and post-rectification filtering. A rectenna model based on past research by NPS students was simulated, built, and tested. The analysis and findings of the rectenna model were presented, with suggested improvements highlighted.

14. SUBJECT TERMS: Rectenna, Schottky Diode, MAV, WPT, Low-pass Filter, 10 GHz Antenna.			**15. NUMBER OF PAGES** 109
			16. PRICE CODE
17. SECURITY CLASSIFICATION OF REPORT Unclassified	**18. SECURITY CLASSIFICATION OF THIS PAGE** Unclassified	**19. SECURITY CLASSIFICATION OF ABSTRACT** Unclassified	**20. LIMITATION OF ABSTRACT** UU

NSN 7540-01-280-5500

Standard Form 298 (Rev. 2-89)
Prescribed by ANSI Std. 239-18

THIS PAGE INTENTIONALLY LEFT BLANK

Approved for public release; distribution is unlimited

A FOLLOW-UP STUDY ON WIRELESS POWER TRANSMISSION FOR UNMANNED AIR VECHICLES

Toh Leng Huei
Defence Science & Technology Agency (DSTA)
B.E (Electrical & Electronic Engineering), University of Birmingham, 1998

Submitted in partial fulfillment of the
requirements for the degree of

MASTER OF SCIENCE IN ELECTRICAL ENGINEERING

from the

NAVAL POSTGRADUATE SCHOOL
December 2007

Author: Leng Huei Toh

Approved by: Professor David C. Jenn
Thesis Advisor

Professor Michael A. Morgan
Second Reader

Professor Jeffrey B. Knorr
Chairman, Department of Electrical and Computer Engineering

THIS PAGE INTENTIONALLY LEFT BLANK

ABSTRACT

This thesis was a continuation in part of a NPS project relating to microwave wireless power transmission for micro air vehicles (MAVs). The concept of using microwaves for transferring power in free space has existed since the beginning of the 20th century. The emphasis of this thesis was the experimental study of powering micro air vehicles via the use of a microstrip rectenna (rectifying antenna) at 10 GHz. A microstrip rectenna was built and experiments were conducted to measure the efficiency of the rectenna elements.

The conversion of radio frequency (RF) power into usable DC power was performed by a rectenna. Its function could be broken down into the following four stages: reception of radio frequency (RF) power, pre-rectification filtering, rectification and post-rectification filtering. A rectenna model based on past research by NPS students was simulated, built and tested. The analysis and findings of the rectenna model were presented, with suggested improvements highlighted.

THIS PAGE INTENTIONALLY LEFT BLANK

TABLE OF CONTENTS

LIST OF FIGURES

THIS PAGE INTENTIONALLY LEFT BLANK

LIST OF TABLES

THIS PAGE INTENTIONALLY LEFT BLANK

ACKNOWLEDGMENTS

I would like to thank Professor David C Jenn for his guidance on this thesis topic and his encouragement throughout the months that I was working with him on this thesis topic. This thesis proved to be extremely challenging, with the requirement to understand the work done by previous students and the requirements to learn Microwave Studio, Agilent ADS and test the rectenna system within months. Without the assistance of Professor Jenn, the project would not have been able to be completed.

I would like to thank Mr Robert D. Broadston for his advice and assistance rendered for the use of Microwave Laboratory and Professor Michael A. Morgan for his comments on the thesis.

Lastly, I would like to thank my wife, Susy, for her support and understanding.

THIS PAGE INTENTIONALLY LEFT BLANK

EXECUTIVE SUMMARY

The concept and background history of using radio frequency for power transfer in free space for micro air vehicle (MAV) propulsion is presented in this thesis. The theory of power transmission using radio frequencies can traced back to a century ago. However, micro air vehicles (MAVs) belong to a new category of unmanned aerial vehicles (UAVs) that are currently being developed at many institutes. According to the Defense Advanced Research Project Agency (DARPA), the definition of a MAV is a fully functional UAV no larger than 15 cm in length, width and height. With the improvement of integrated circuit performance and advances in micro electronics over the past few decades, the possibility of building a micro air vehicle powered by microwaves is a possibility.

In this thesis, the proposed rectenna design by past NPS students was re-evaluated. The design of a 10 GHz rectifier antenna (rectenna) for MAV application using a low-pass filter, Schottky diode and quarter-wave impedance matching unit was analyzed and simulated in CST Microwave Design Studio and Agilent ADS software. The single Schottky diode acts as a half-wave rectifier to rectify the incoming alternating current (AC) signal to a direct current (DC) signal. The rotor motor proposed by past NPS student was re-tested to verify its operating characteristics.

The proposed circuit was fabricated using dielectric material with a dielectric constant of three. Several individual rectenna elements were tested and had an efficiency of 26% to 36% which was an an improvement over the previous design by more than 400%.

The rectenna elements were arranged in series and parallel configurations to increase the current and voltage to power the MAV. The 4 x 4 rectenna array did not produce sufficient current and voltage to drive the MAV motor to hover as there were too few rectenna elements. The propellers of the MAV rotated at a regular speed when illuminated with approximately 23 dBm into

the horn antenna at the aperture. In order for the MAV to hover, the efficiency of the rectenna element needs to be improved.

An improved rectenna design was proposed using a full-wave rectifier. The new design needs to reconsider the impedance matching unit values as the impedance of an HSMS 8202 series Schottky diode would be different from the HSMS 8101 single Schottky diode package.

I. INTRODUCTION

A. MICROWAVE WIRELESS POWER TRANSMISSION

The concept of power transmission dates back to Heinrich Hertz [1] and Nikola Tesla [2]. Tesla aimed to develop a high power transmitter to ascertain the law of propagation of current through the earth and the atmosphere. Although he failed to build any practical system, his concept proved to be important when the study of electromagnetic wave propagation began a few decades later.

Micro air vehicles (MAVs) belong to a new category of unmanned air vehicles (UAVs) that are currently being developed by many institutes around the world. According to the Defense Advanced Research Project Agency (DARPA), the definition of a MAV is a fully functional UAV no larger than 15 cm in length, width and height. With the improvement of integrated circuit performance and advances in micro electronics over the past few decades, the possibility of building a micro air vehicle is no longer a dream.

The sustenance of flight for a long period without the need for the aircraft to carry large amounts of fuel, primarily for ground surveillance and communication relay applications, was the main reason behind the thrust for microwave wireless power transmission (WPT) for the military. If an air platform could be powered by an antenna and rectifier, herein known as a rectenna system, there would be no need for an air platform to carry fuel. The air platform could increase its payload and its flight duration could be lengthened. Furthermore, the air platform could be remotely controlled by the ground station if a control unit was included.

The concept of WPT is simply to transmit electrical power from one point to another through the atmosphere without the physical need of transmission lines. WPT could be realized by microwave or laser. This process usually entails direct current (DC) to alternating current (AC) power conversion, followed by the transmission of this electromagnetic wave through radiation from the antenna. At

the receiving side, the electromagnetic wave is collected and converted into DC to power the load. The load is either a battery or the propulsion power plant itself.

The difference between WPT and microwave transmission for communication is the concentration of electromagnetic energy. WPT tends to be focused with a higher concentration of beam energy towards the receiver as illustrated in Figure 1. Usually microwave WPT involves conversion of DC power to radio frequency (RF) for transmission. At the receiving station, the radio frequency is collected and converted back into DC power. In practice a 100% conversion efficiency is not likely. Since the transmission is through the air, power attenuation due to atmospheric absorption and scattering is present. The conversion factor of a rectenna system became one of the most important factors in determining the performance of the system, which consists of antennas, filters and diodes for rectification.

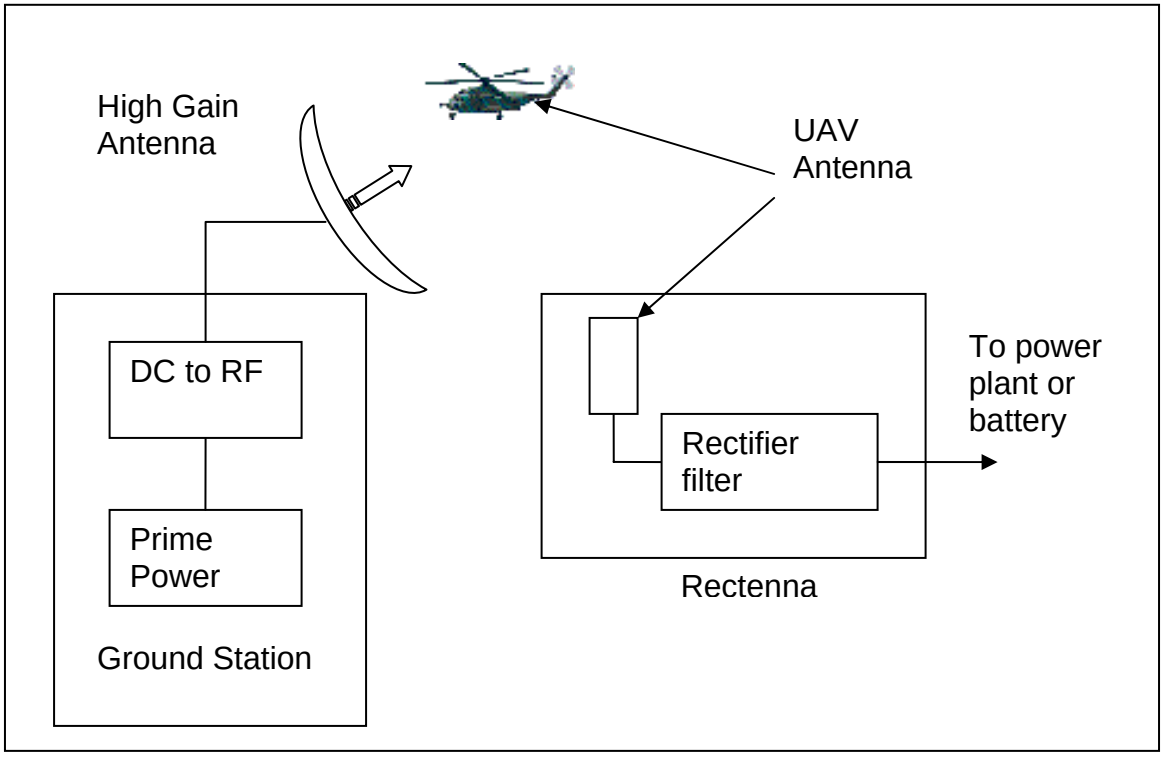

Figure 1. WPT for UAV Applications.

In this thesis, a rectenna model based on the studies performed by Tsolis [3] and Tan [4] was redesigned, built, and simulated. Various experiments were done to verify and validate the theoretical calculation of the rectenna system. The robustness of the rectenna design was investigated and improvement on the initial designed was performed.

The measured level of efficiency of the original NPS rectenna was only 7% [3]. This thesis follows up on determining the probable causes of low efficiency in order to establish a better overall design. The recommended design changes should yield higher manufacturing tolerances and lighter weight.

B. OBJECTIVE

The theoretical efficiency of the rectenna designed by Tan claimed to be approximately 60%, which was sufficient to power the micro air vehicle prototype designed by Tsolis. The purpose of this thesis is to verify and analyze the design of the rectenna systems, make improvement in the design of the rectenna system, and integrate the MAV with the rectenna system.

C. THESIS OUTLINE

This thesis is divided into six chapters organized as follows. Chapter II covers the background of WPT and the development of WPT from early work through today. Applications of WPT and advances in WPT development are also covered in this chapter. An overview of the two related thesis projects that were conducted at the Naval Postgraduate School is presented.

Chapter III discusses the rectenna design and architecture of a rectenna element, as well as how a rectenna is able to convert RF energy into usable DC power. Details of each rectenna subsystem are presented. The design of the MAV by Tsolis, analysis of the rectenna system, and verification of its performance is also presented. Analysis of the Schottky diode, dielectric material, and antenna dimensions are covered in this chapter. Chapter III also discusses the pre- and post-rectification filtering process. The analysis for designing a filter

system on a microstrip circuit board is documented and a comparative study of the performance of the pre- and post-designs is analyzed.

Chapter IV focuses on the implementation of the rectenna system and the need for the impedance matching units. Mutual coupling of the rectenna array is discussed and results of the simulations are also presented.

Chapter V documents the test and evaluation of the rectenna system. The performance of the rectenna system is presented.

Chapter VI summarizes the findings of the research and experiments. Conclusions and recommendations for an overall better rectenna design are also presented.

II. BACKGROUND

A. HISTORY OF WIRELESS POWER TRANSMISSION

Free space microwave power transmission began in the 1950s but the concept of wireless transmission has existed since the beginning of the 20th century. German physicist Henrich Hertz successfully demonstrated the existence of electromagnetic waves in 1888. According to an article by Brown [3], Nokola Tesla carried out numerous experiments on high power transmission in the early 1900s in Colorado Springs with a grant of $30,000 from Colonel John Jacob Astor. Subsequent RF experiments by Tesla, with a grant from J. Piermont Morgan to build a large wooden transmitter tower with a giant copper electrode at the top, were not completed due to the exhaustion of funds. Although no practical system was constructed and no fruitful results were obtained for his numerous experiments, his concept proved to be important for the development of wireless transmission in the later half of the century.

The invention of the klystron tube in the early 1930s was a large step in the development of wireless power transmission and, eventually, it lead to the development of high power amplifier tubes for radar, such as the cavity magnetron, during World War II. Microwave power tubes, and DC converter diodes, which were capable of converting microwave power to DC power, made WPT realizable. The magnetron was more suitable for WPT application as it had higher efficiency.

B. EARLY EXPERIMENTATION

The ability to focus electromagnetic waves into a beam for high efficiencies and advances in amplifier tubes to create the required transmitting power [5, 6] allowed the efficient transmission of microwave power and contributed to the development of WPT in the 1950s. The advances in different technology fields coupled with the investigation of semiconductor diodes for DC power rectification by Sabbuagh and George at Purdue were a few of the important milestones achieved in the development of the rectenna [1].

The convergence of these technologies motivated the Raytheon Company to build a microwave-powered air platform prototype for the U.S. Air Force. According to Ref. [1], the first microwave-powered helicopter flight was made on July 1, 1964 in Raytheon's Spencer laboratory. This was the first air platform solely powered by microwaves with the use of a rectenna. The first rectenna conceived by the Raytheon Company is shown in Figure 2. The rectenna system consisted of 4,480 diodes and had a maximum power output of 270 W.

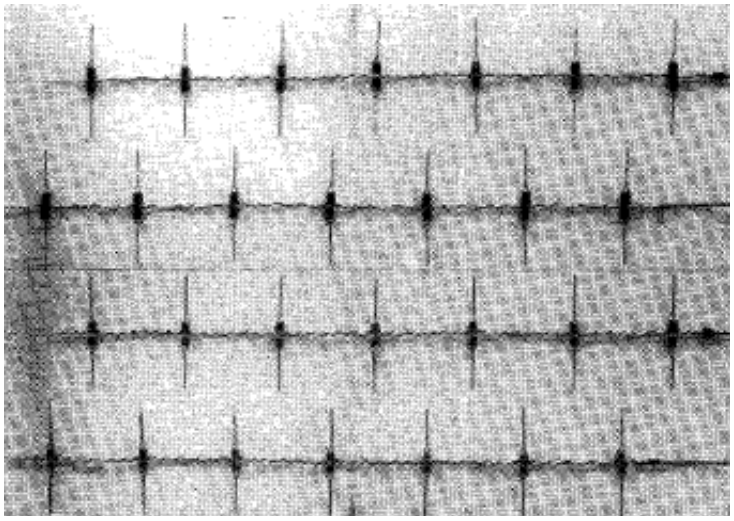

Figure 2. The First Rectenna had a Power Output of 7 W and 40 Percent Efficiency (From [1]).

In November 1964, a non-stop 10 hour microwave-powered hovering of a helicopter was demonstrated to the mass media (Figure 3). The presentation received wide media coverage. Hewlett-Packard Associates subsequently developed the Schottky barrier diodes which had a better performance than the point contact diode used by George.

More research and experiments were conducted following the successful endurance flight at the Raytheon Company of the microwave-powered helicopter with the intent of improving the design for the use of a free-flying remotely controlled helicopter. As a result, a beam-riding microwave WPT helicopter was demonstrated. However, the Air Force and the industry showed little interest in subsequent years until 1970 when NASA got involved in the development of a rectenna for its space program.

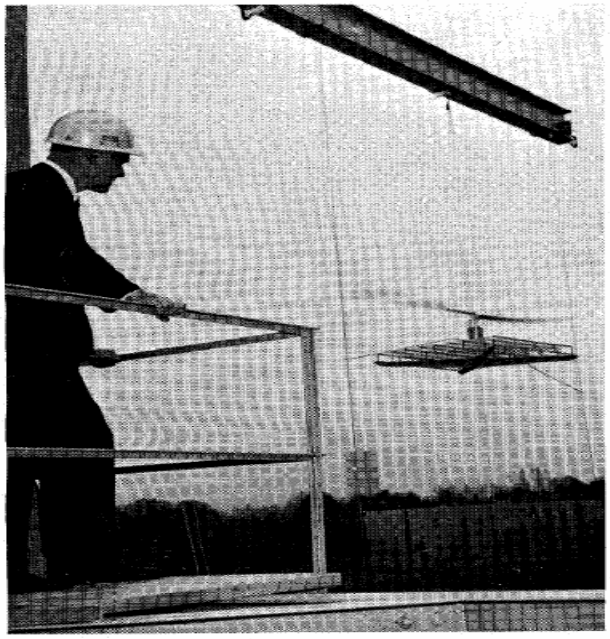

Figure 3. A Powered Helicopter Demonstration to the Mass Media in November 1964 (From [1]).

The NASA solar-power satellite (SPS) program concept was conceived in the 1960s and 1970s. It involved the research and development of many microwave WPT activities. Under the SPS concept, a large rectenna consisting of dipole antennas was to be built on earth to collect the solar energy relayed by satellites in space. Ultimately, when the SPS concept study program ended in 1980, the impact of the SPS program upon the WPT was to redirect the design of the transmitter away from high power tubes to active phase arrays made from a large number of low power magnetrons [1]. The SPS program was discontinued due to the cost factor.

After the 1980s, semiconductor devices were widely used to replace the microwave tubes for WPT applications. Component improvements resulting from the wireless revolution had contributed to the progress of WPT supporting elements. Solid state silicon-based PN (PN refers to the P-type and N-type semiconductor) junction diodes, which have a high turn on voltage, were less preferred than fast switching Schottky diodes that exhibit very fast switching capabilities suitable for high frequency rectification processes. Semiconductor phased array amplifiers were researched and developed for WPT applications [7,

8]. The world's first microwave-powered flight was conducted on September 17, 1987 [9]. The plane powered by microwaves flew in a circular path for 20 minutes above the antennas.

In the 1990s, Europe, Japan, Canada, and Korea were active in the area of solar power generation research and development. The SPS2000 concept study by Japan in 1994 concluded that the enabling technology for SPS realization was not available and critical components were lacking. Key electric technologies such as highly efficient solar cell and phased array antennas were not ready for SPS. There was a lack of technical knowledge and experience in many of the key areas for the design of SPS [10, 11]. Furthermore, the cost of SPS development was too high. Nevertheless, Japan continued to explore the possibility of a launching a SPS in the future.

Due to the advancement of technology, large scale space solar power (SSP) systems were once again considered by NASA in 1995. Feasibility studies and analysis of SSP systems for commercial and government usage were explored [12]. System studies and small scale SSP conceptual demonstrations were performed by the NASA SSP Exploratory Research and Technology (SERT) program. Enabling technologies needed for SSP systems were investigated and explored by NASA. In 1999, the Korea Electrotechnology Research Institute conducted a study on a WPT system [13] having a single rectenna conversion efficiency of 75.6% and an overall system efficiency of 33%.

C. RECENT DEVELOPMENT OF WPT

The development of microwave WPT continues under sponsorship by NASA for microwave-powered high altitude communication and surveillance air platforms. In recent years, there has been a renewed interest in SSP systems. Other agencies such as the U.S. National Science Foundation (NSF) and Electric Power Research Institute (EPRI) were involved in the SSP programs. McSpadden and Makins gave an insight of NASA research on SSP and WPT in an article published by *IEEE Microwave Magazine* in December 2002 [14]. Four key areas were identified and emphasized for future research in year 2002 with

solid state transmission by microwave WPT being one of them. Critical components such as the transmitter, power management system, and rectenna for SSP were identified for further research and development. Both mentioned that technology had not achieved the state of maturity for successful implementation of SSP, but strategic roadmaps were highlighted for further investigation.

The December 2002 *IEEE Microwave Magazine* issue contained an article on SPS and microwave WPT research in Japan [15]. In the conclusion section, Matsumoto believed that the target goal of overall efficiency of 80% solar-to-DC conversion factor would be achieved by the solar panels in the near future at both the transmitting and receiving stations. The Japan Aerospace Exploration Agency (JAXA) continued the feasibility studies of a space solar power system (SSPS). According to Nagayama's article in October 2003 [16], more than 180 persons from industrial and academic sectors were involved in the SSPS research program. Two kinds of WPT (microwave and laser) were explored. The ultimate goal was to transmit energy to earth for commercial usage. In addition to technical studies, JAXA had proposed a roadmap that included a stepwise approach to realize commercial SSPS in 20-30 years.

With the increase in oil prices and the demand for oil consumption increasing over the past decades, WPT has became more attractive as solar power, being available 24 hours in space with the use of satellites as relay and collection stations. The collected solar power in the satellites would be transmitted to an earth rectenna station using microwave WPT. The advantages of using solar energy as a non-fossil fuel include environmentally clean, non-depletable, and low cost. Figure 4 depicts a typical ground rectenna station for collecting power from the transmitted microwaves. An IEEE article published in 2005 claimed that a geo-synchronous SPS system could be illuminated 99% of time since the satellite would be in the earth's shadow for only a few days at the spring and fall equinoxes [17].

Figure 4. A Typical Ground Rectenna Illuminated by Space Solar Power Satellite (From [15]).

In 2004, the Chinese Academy of Science demonstrated the feasibility of a rectenna working at 35 GHz via the use of commercial diodes with an efficiency of 52% and an output of 25.6 mW [18].

In 2004, the Space Power Infrastructure (SPI) project by the European Aeronautic Defense and Space Company (EADS) demonstrated WPT using a Diode/Nd YAG laser for a remote rover vehicle involving an airship as a relay station to supply power to the ground vehicle. A laser was chosen to avoid the drawback of microwave side lobes, their difficult control in failure cases, and the much higher mass of using microwave transmitting elements as compared to a laser system [19]. Although microwave systems were relatively more efficient and have less attenuation by atmospheric effects, lasers were explored by EADS because electronic steering for laser beams would require less complex mechanical parts than a microwave system. Furthermore, in term of launching the SPS system, a laser system was viewed to be easier for transportation without the need for big antennas and assembly efforts, as would be the case for a microwave system which would be more complex.

Another article was published in April 2006 that demonstrated a 5.8 GHz dual-diode rectenna and its array with a band-pass filter to block the harmonic signals generated from the diodes. The rectenna could provide a maximum efficiency of 76% with twice as much output voltage as compared to a single-shunt diode rectenna. The parallel-connected rectenna array could be extended to form a traveling wave antenna for long distance power transmission [20].

Recently, in July 2007, *IEEE Transactions on Antennas and Propagation* reported a compact dual-frequency rectifying antenna with an overall efficiency of 65% [21].

D. EVOLUTION OF MICROWAVE RECTENNAS

The development of microwave WPT has progressed significantly over the past century due to a number of activities and research being done by numerous institutes and scientists. Tesla's experiments showed that large antennas had to be constructed for the experiments. With the invention of microwave tubes such as klystrons and traveling wave tubes and advances in radio frequency technology and diodes, a small scale antenna, transmitter and rectifier could be built to handle high frequency and high power.

The use of a cyclotron wave converter (CWC) for DC conversion showed that 90% rectenna efficiency could be achieved [22, 23]. The input microwave power is converted into the kinetic energy of an electron beam through cyclotron resonance and then to DC power by decelerating the electron beam.

A 35 GHz rectenna with 52% efficiency was demonstrated during 2004 as mentioned in the previous section. The major improvements made for microwave WPT over the last few decades were mostly related to large scale space solar power research programs. The technological spin-offs out of the solar power platform development are an important aspect of the activities.

An IEEE paper published in January 2006 [24] showed that a hybrid sensitive rectenna system using a commercial zero bias Schottky diode and a dielectric constant of 4.4 for the substrate could achieve 56% efficiency at 2.54

GHz. An improved monolithic rectifier design demonstrated that RF to DC conversion efficiency of 65% and 25 dBm input power was achievable with a second diode acting as a variable resistor. The circuit diagram of the improved rectenna system is depicted on Figure 5. The dimensions of the circuit were 1340 µm x 476 µm.

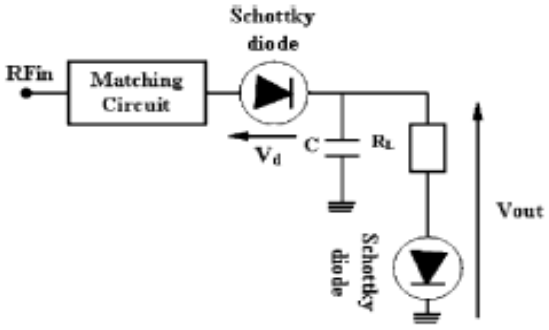

Figure 5. The Improved Hybrid Rectenna Circuit Diagram (From [21])

E. NPS RESEARCH

At NPS, a few students have looked into the aspects of WPT for MAV propulsion.

Vitale [25] used a metal semi-conductor diode for power rectification and was able to experimentally determine the S parameters of the diode. He recommended that future research be in the areas of employing GaAs Schottky diodes for better rectification efficiency and the use of high power sources for future improvement on the MAV antenna design.

Tsolis [3] continued Vitale's work by utilizing Schottky diodes with a patch antenna. Two prototypes of a counter-rotating helicopter-type MAV were fabricated and tested. The overall gain efficiency was verified by Tan [4] to be only 7% due to the mismatch of impedance. Tan investigated various designs of antennas suitable for the rectenna and concluded that a round patch antenna and sixth order filters were the better option, and simulated his design using software.

F. SUMMARY

The history of WPT was briefly covered and the major milestones in the development of WPT were highlighted. Much interest and research has been conducted to determine the feasibility of implementing WPT and its applications range from futuristic large scale systems to miniaturize versions of remotely powered vehicles.

THIS PAGE INTENTIONALLY LEFT BLANK

III. RECTENNA DESIGN

A. BASIC RECTENNA DESIGN

The rectenna is composed of several subsystems. These subsystems are namely the receiving antenna, pre-rectification filter, rectifier, and post-rectification filter. The basic configuration of the NPS rectenna system is shown in Figure 6.

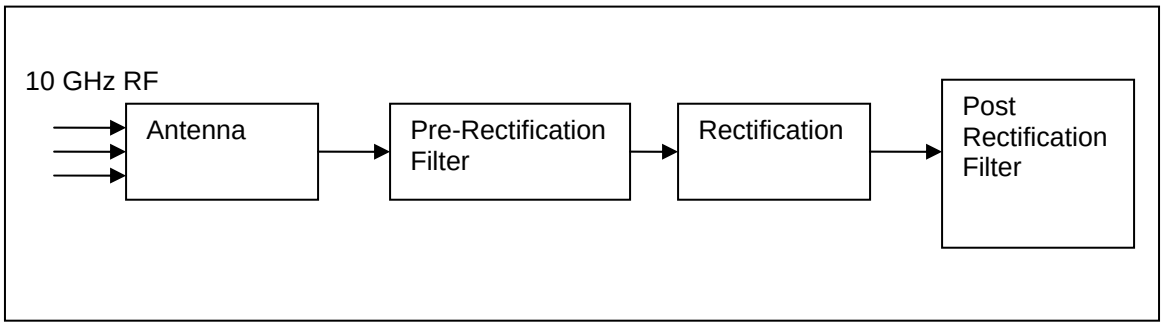

Figure 6. Basic Configuration of a Rectenna System.

1. Antenna

Antennas come in various shapes and designs. The most commonly used antennas include the half-wave dipole, parabolic dish, horn, helix antenna, and microstrip antenna. The choice of antenna design is influenced by the specific needs of the application. The main factors to be considered in antenna design for a UAV rectenna system are power handling capability, radiation efficiency of the antenna, weight and size of the antenna, and reflection coefficient of the antenna at the desired frequency.

For high power handling capability and weight consideration, a microstrip antenna is the good choice compared to other designs, especially when the principal consideration is to keep the rectenna system as light as possible for MAV applications. Reference [4] explored the various antenna designs for the rectenna system and concluded that a round patch antenna with a center feed is the best option. A circular patch antenna would reduce and suppress the re-radiation of high order harmonics as the resonance frequencies of a circular patch antenna are a function of the Bessel function zeros, which are not multiple

integers of the operating frequencies. For square or rectangle patches, the resonance frequencies are usually integer multiples of the lowest resonating mode frequency, which will likely re-radiate higher order harmonics if they were present. Bandwidth enhancement techniques for microstrip antennas can be found in [26]. These include slots, multi-stacking, and arraying, which are not suitable for the current application as it will add weight.

The purpose of the antenna in the rectenna system is to collect radio waves impinging on its surface and transfer this energy into the pre-rectification filter stage for direct current conversion. Therefore, a wider bandwidth is desirable at the receiving antenna to allow for transmitter frequency drift and Doppler shift due to the motion of the UAV. A wider bandwidth would allow for better design tolerance since impedance matching would affect the efficiency of the rectenna system in the subsequent stages.

2. Pre-rectification and Post-rectification Filter

The pre-rectification filter limits the frequency of the incoming RF signal to ensure that the incoming RF signal is operating at the desired frequency for the rectifier and prevents the re-radiation of higher order harmonics produced by the non-linear I-V characteristics of the diode. It will also reject out-of-band interference signals

The post-rectification filter function is to extract the DC component and reflect the rest of the frequencies back to the rectifier. As it is not possible to achieve an ideal cut-off low-pass filter response, some low frequency components may still be present at the output end of the rectenna, which will show up as ripples in the DC voltage.

Pre- and post-rectification filters for a rectenna system are usually implemented either as a microstrip low-pass filter or band-pass filter with a capacitor and resistive load to minimize interference of high order harmonic radiation to other parts of the system.

3. Rectification

The purpose of the rectifier is to convert the incoming RF signal into DC to drive the DC load. This function is usually undertaken by a fast switching and high power handling diode with other lumped elements. The selection of the diode is based on its power handling capabilities, switching speed, I-V characteristics, operating frequency, forward and reversed bias voltage, saturation current, efficiency, weight and cost.

For rectenna applications, small turn-on voltage or zero-bias current with large reverse breakdown voltage and low capacitance is preferable. This is usually performed by a Schottky diode since it has the previously discussed desirable characteristics.

B. DISCUSSION OF ANTENNA DESIGN

Reference [3] tested a rectenna system shown in Figure 7 at 10 GHz. The overall efficiency of the rectenna system was dependent on the individual sub-components which were the antenna, rectifier, pre- and post-rectification filter, and its matching units.

According to [4], the efficiency of the circular patch antenna design in [3] has achieved a gain efficiency of only about 7% due to the mismatch of impedance. The resonant frequency of the circular antenna has a return loss of -7dB at 10 GHz and 20% of the energy is reflected back. The circular patch was not optimized to perform at 10 GHz. Furthermore, thin substrate thickness of 0.127 mm was used, which resulted in a very narrow bandwidth of 0.4% for a voltage standing wave ratio (VSWR) of 2. This allows for very little manufacturing deviation and design margin for the rectenna performance at subsequent sub-systems for impedance matching.

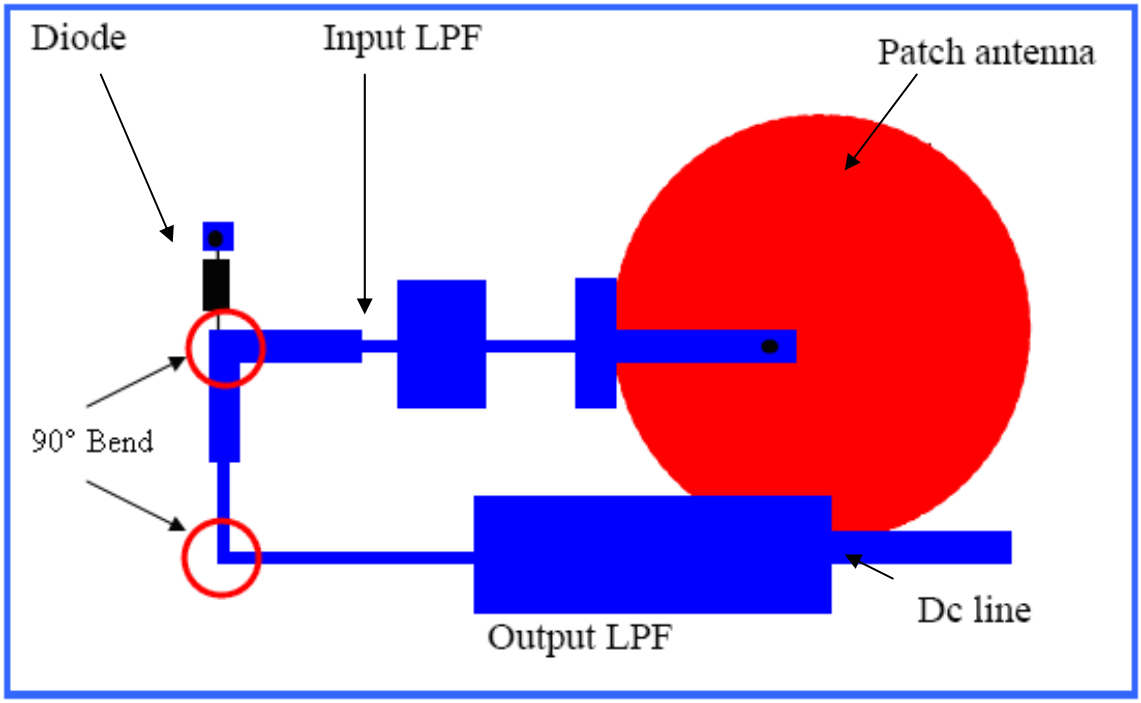

Figure 7. Rectenna Design at 10 GHz (From [3]).

Therefore, it is important to analyze each of these subsystems carefully to understand its function and to minimize possible causes of inefficiency in each component. The next chapter will ascertain the design and simulation results obtained for the rectenna system proposed by [3] and [4] for the MAV application. The proposed design and results of each rectenna sub-component were simulated using CST Microwave Studio and Agilent ADS2006 software. The rectenna system design parameters such as the frequency selection, patch antenna design, filter design, microstrip impedance matching units, and motor selection proposed by [3] and [4] will be discussed in the next chapter.

1. Use of 10 GHz Operating Frequency

The primary reason for choosing a 10 GHz operating frequency for the rectenna system was to reduce the size of the antenna patch, which in turn reduces the weight of the rectenna sub-components. Antenna dimensions are a function of the wavelength of transmission.

For the application of a DC-powered MAV, the requirement for a lightweight and small antenna superseded other considerations as any increase in weight would require more power for the MAV. Another factor for choosing 10 GHz is due to the availability of a high power 10 GHz transmitter in the NPS laboratory.

2. Circular Patch Antenna

Based on [4], a circular patch was chosen because of its inherent advantage of being smaller than the square or rectangular patches for a given resonance frequency. It does not need a preferred axis and the feeder can be placed along the radius on the patch without worrying about aligning on the x and y axes. Table 1 from [27] shows the bandwidths of circular patches when compared with annular rings and quarter-wave patches at 2 GHz. A circular patch usually has a smaller area for the same dimension of a rectangular patch. Rectangular patch bandwidth increases as the dimension increases. A typical microstrip antenna design tends to have a narrow bandwidth. Therefore, multi-modes and slots are sometimes used to increase the bandwidth. These enhancements usually lead to increases in size and complexity of the circuit.

Comparison of VSWR = 2 Bandwidth, $\varepsilon_r = 2.32, h = 1.59\,\text{mm}, f = 2\,\text{GHz}$.		
Element Shape	**Element Size**	**Bandwidth (%)**
Narrow rectangular patch	L = 4.924 cm, W = 2.0 cm	0.7
Wide rectangular patch	L = 4.97 cm, W = 7.2 cm	1.6
Square patch	L = W = 4.82 cm	1.3
Circular disk	a = 2.78 cm	1.3
Annular Ring	b = 8.7 cm, a = 4.45 cm	3.8
Quarter-wave patch	L = 2.462 cm, W = 2.0 cm	1.05

Table 1. Bandwidth of Various Antenna Shapes at VSWR =2 (After [27]).

For the current application, a circular patch was chosen due to its simplicity of design and construction, although its bandwidth is narrower than a slot antenna and annular ring. Furthermore, a circular patch resonates in

harmonics governed by the Bessel function of order *n.* The equation of resonance [28] for a circular patch of radius r_{patch} is approximated by

$$J_n'\left(\sqrt{\varepsilon_r}k_0 r_{patch}\right)=0 \tag{3.1}$$

where $k_0=\frac{2\pi}{\lambda_0}$, λ_0 is the free space wavelength, and ε_r is the relative dielectric constant of the substrate. The primed notation denotes the derivative with respect to the argument.

This implies that the circular patch's resonance frequencies are not synchronized with the harmonics generated by the rectification diode, which suited the present application as minimum interference would be expected.

The resonant frequency of an antenna is determined by the physical dimensions. For a circular patch antenna, the radius of the antenna will affect the operating frequency. According to [28], the resonant frequency is determined by the root of a Bessel function. For TM_{110} mode operation, the solution to Equation (3.1) is

$$(f_r)_{110}=\frac{1.8412c}{2\pi r_{patch}\sqrt{\varepsilon_r}} \tag{3.2}$$

Based on [28], for an accurate computation of patch radius, fringing electric fields experienced at the copper edge must be taken into consideration as fringing makes the patch look electrically larger. Therefore, to compute the effective patch radius:

$$r_{patch\_eff}=r_{patch}\left\{1+\frac{2h}{\pi r_{patch}\varepsilon_r}\left[\ln\left(\frac{\pi r_{patch}}{2h}\right)+1.7726\right]\right\}^{1/2} \tag{3.3}$$

where h is the dielectric substrate thickness. Substitute Equation (3.3) into (3.2) to obtain the radius of the circular patch antenna at the desired frequency. In this case $f_r=10$ GHz.

$$(f_r)_{110} = \frac{1.8412c}{2\pi r_{patch\_eff}\sqrt{\varepsilon_r}} \tag{3.4}$$

According to [28], Equation (3.4) is valid for a relative dielectric substrate height of $h < 0.05\lambda$. The radius of the antenna was theoretically calculated at 5.1 mm at 9.952 GHz. The dimension of the circular patch antenna was fine tuned to 10 GHz using CST Microwave Studio software. The optimum radius was found to be 4.57 mm.

3. Dielectric Materials

A microstrip patch with an inherently lower quality factor (Q) tends to have higher bandwidth as impedance bandwidth of a patch antenna varies inversely with Q of the patch antenna [27]. The Q factor is defined as

$$Q = \frac{\text{Energy Stored}}{\text{Power Lost}} \tag{3.5}$$

The dielectric substrate thickness (*h)*, width of the copper cladding of microstrip (*w*), and dielectric constant (ε_r) of the material used for fabrication could affect the impedance. A higher value h will translate to higher impedance bandwidth. A wider microstrip would result in lower impedance. Figure 6 from reference [28] shows the relationship of substrate thickness, efficiency, and percentage bandwidth. A lower value of dielectric constant would have a higher impedance bandwidth. Therefore, a dielectric constant (ε_r) of 3 is selected for the rectenna system.

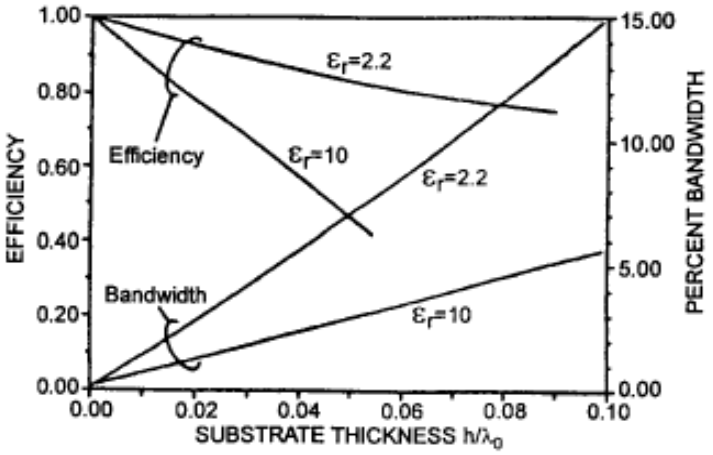

Figure 8. Effect of Substrate Thickness and Dielectric Constant on the Impedance Bandwidth (VSWR <2) and Radiation Efficiency (From [28]).

The details of the dielectric materials used for the rectenna system is given in Table 2. The dielectric material's specification is obtained from Rogers Corporation.

Dielectric Material Used	RO 3003 from Rogers Corporation
Dielectric Constant ε_r	3 ∓ 0.04
Dissipation Factor	0.0013
Loss Tangent, $\tan \delta$	0.0012 @ 10 GHz
Substrate Height, h	0.75 mm for circular Patch antenna; 0.13 mm for pre- and post-rectification filter
Copper Thickness	½ oz or 17 μm

Table 2. Dielectric Materials for Rogers Material RO 3003.

4. Feeder Position for Circular Patch Antenna

A probe feed was chosen over an edge feed as it allows two different thicknesses of substrate with different properties to be used for the rectenna system. Both substrates' ground plane can be soldered back-to-back to provide isolation from the fringing electric field caused by the antenna radiation. The pre- and post-rectification sub-components, which consisted of a low-pass filter,

requires the use of a thin substrate to reduce the overlapping of fringing E-fields from a microstrip's other sub-components. The use of a thin substrate will also reduce the weight of the rectenna system.

As the impedance of the circular patch antenna is affected by the position and dimension of the feeder, there is a need to determine the position of the probe feed. Theoretically, the closer the feeder to the center of the circular patch antenna, the lower the impedance of the antenna. Reference [3] used the PatchD program from [29] to determine the initial position of the feeder location before using a CST Microwave Studio full-wave simulation to fine tune the position of the probe feeder.

In order for a traveling wave to view the probe feed and relief hole of the circular patch antenna as a coaxial cable with impedance Z_o, the dimension of the probe feed and relief hole for the circular antenna needs to be determined. The dimension of the feeder radius and relief hole's radius can be determined using the following equation:

$$Z_o = \frac{60}{\sqrt{\varepsilon_r}} \ln(\frac{r_h}{r_p}) \tag{3.6}$$

where r_h and r_p are the radii of the relief hole and probe respectively [26]. Based on Equation (3.6), $Z_o = 51.3\Omega$ when $r_p = 0.125$ mm and $r_h = 0.55$ mm.

In order to increase the impedance bandwidth of the circular patch antenna, [3] proposed the use of a thick dielectric substrate with height *h*=0.75 mm instead of 0.127 mm for the antenna. As a thick substrate will lead to an inductive effect for the probe feed at resonant frequency, a small etched-out ring was introduced, as shown in Figure 9. The small etched out ring provided some capacitance to cancel out the inductance. The inductance caused by the probe feed for a thick substrate can be estimated using [29]

$$X_f \approx -\frac{\eta kh}{2\pi}\left[\ln\left(\frac{kd}{4}\right) + 0.577\right] \tag{3.7}$$

In the above equation, η is the intrinsic impedance of the dielectric substrate, h is the substrate height, and d is the diameter of the probe feed. The inductance can be cancelled out by varying the dimension of the small etched out ring. Figure 10 shows the internal construction of the probe feed and relief hole using CST Microwave Studio.

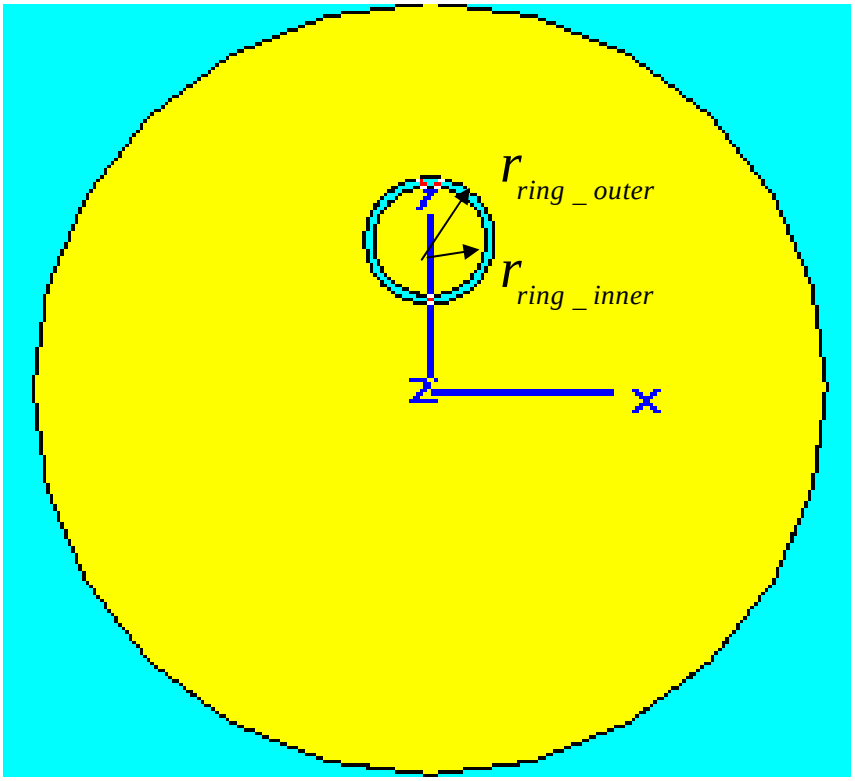

Figure 9. Circular Patch Antenna Showing the Small Ring Etched Out.

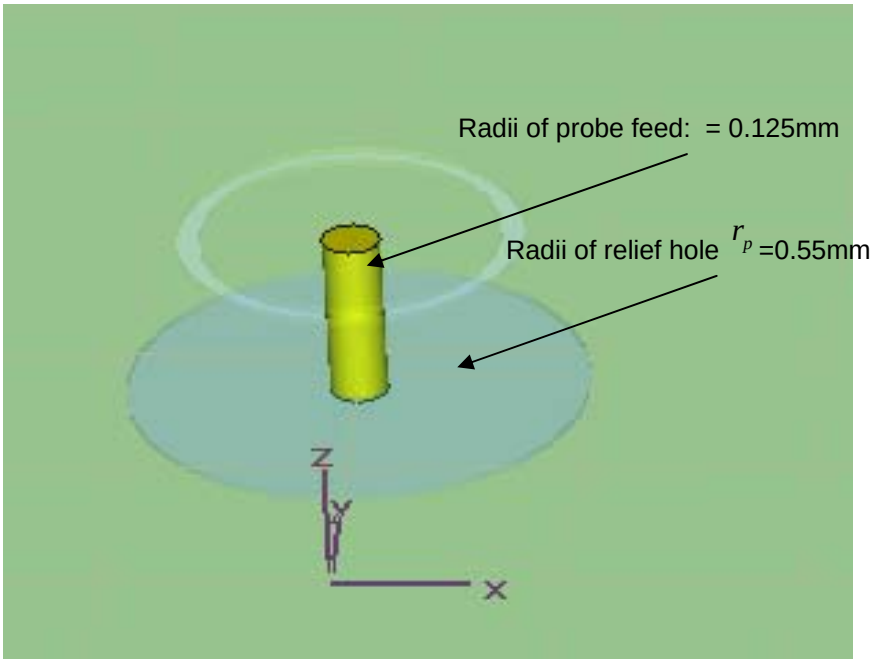

Figure 10. Internal Layout of the probe Feed and Relief Hole.

5. Performance of Proposed Antenna Design

Table 3 shows the design parameters of the proposed 10 GHz circular patch antenna by [3] and fine tuned by [4]. Various dimensions of the patch were simulated. The patch radius was finally adjusted to 4.57 mm with probe feed position at 1.75 mm away from the center of the circular patch.

Parameter	Symbol	Unit	Value
Patch Radius	r	mm	4.57
Inner Ring Radius	r_{ring_inner}	mm	0.65
Outer Ring Radius	r_{ring_outer}	mm	0.75
Probe Offset from Center Patch Antenna	x	mm	1.75
Probe Radius	r_{probe}	mm	0.125
Relief Hole Radius	$r_{relief\_}$	mm	0.55
Copper Cladding for Antenna Patch	h	µm *(Oz)*	17 (0.5)

Table 3. Design Parameters of Capacitive Probe Circular Patch Antenna.

Figure 11 from reference [4] shows the S11 response of the proposed 10 GHz circular patch antenna. S11 represents the input reflection coefficient of 50Ω terminated output*. From the S11 magnitude plot, the return loss is about 36 dB at 10 GHz. The impedance bandwidth is about 25 MHz at -10 dB, which is considered narrow for a microstrip antenna. A circular patch antenna based on the dimension provided by [4] was re-simulated using CST Microwave Studio with both sides of copper cladding set at $17\mu m$ (0.5 oz). The standard printed circuit board (PCB) comes with $17\mu m$ (0.5 oz) or $35\mu m$ (1 oz) copper cladding.

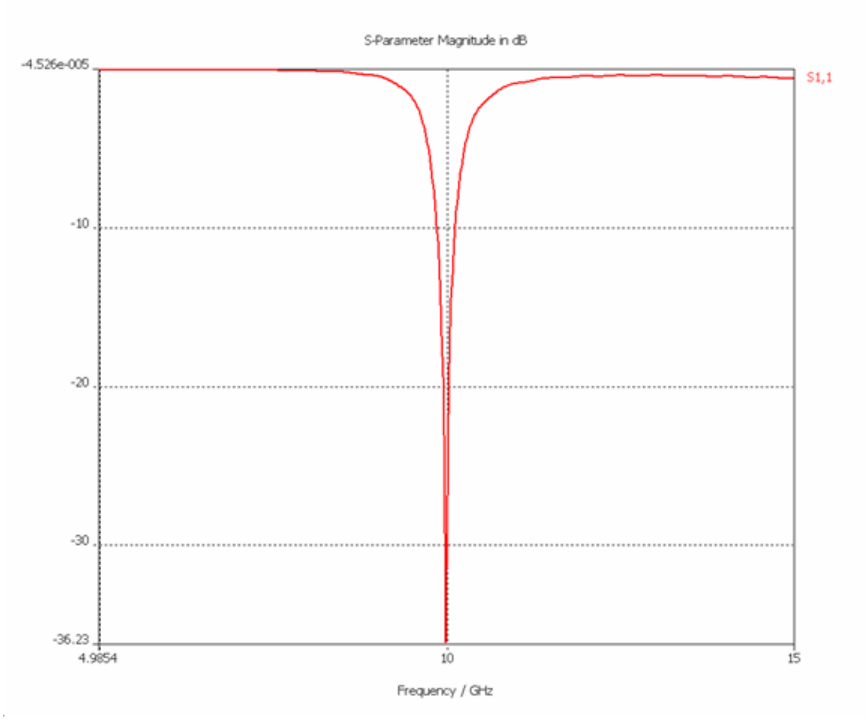

Figure 11. S11 Frequency Response of Circular Disc Design (From [4]).

The re-simulated S11 magnitude plot for the 10 GHz circular patch antenna based on [4] is shown in Figure 12. The return loss for the antenna is about 18 dB instead of 36 dB. There are several reasons for the different in results. The primary difference was basically due to impedance mismatch as [4] must have used a thicker copper cladding for the simulation instead of $17\mu m$ as stipulated in Table 9 [4]. Figure 12 was obtained using both copper cladding

* Return loss is the negative of S11 in dB.

with $17\,\mu m$. As observed from Figures 11 and 12, both antennas are still resonant at 10 GHz as the radius of the antennas remains the same. Ideally, S11 should be as low as possible in order to transfer more RF energy impinging onto the surface of the antenna for subsequent rectenna systems. However, from a practical aspect, a return loss of 15-20 dB is probably the best that can be achieved.

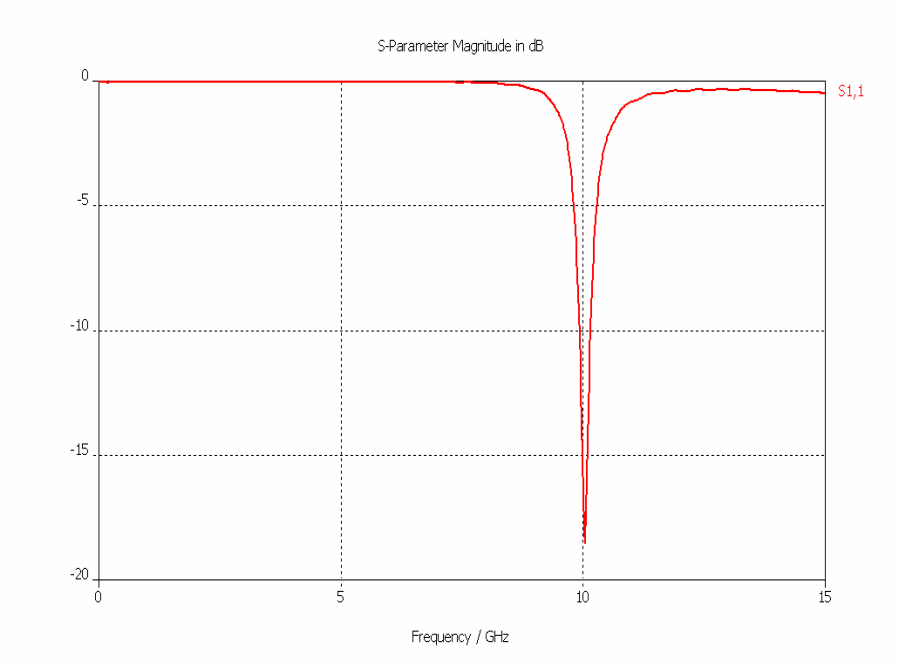

Figure 12. S11 Frequency Response of Circular Disc Design with Copper Cladding on Both Sides at $17\,\mu m$ (0.5 Oz).

Figure 13 shows the S11 response of the circular patch antenna with copper cladding thickness set at $35\,\mu m$ (1 Oz). The return loss is about 32 dB instead of 18 dB. This is almost twice that of the circular patch antenna with copper cladding set at $17\,\mu m$. The Smith chart for the antenna is shown in Figure 14. The impedance is $50.58 - j2.27\,\Omega$, which is close to $50\,\Omega$.

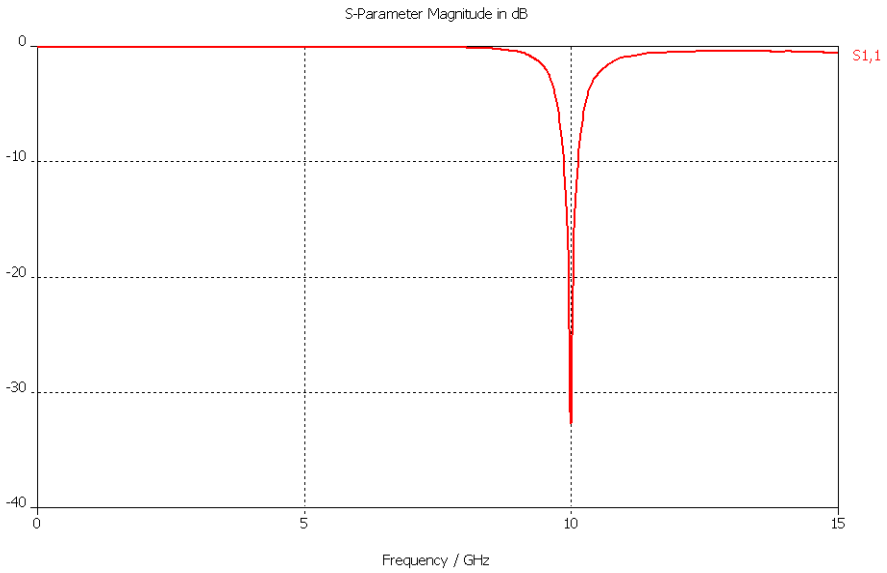

Figure 13. S11 Frequency Response of Circular Disc Design with Copper Cladding on Both Sides at $35\,\mu m$ (1 Oz).

Table 4 summarizes the results due to changes of the copper cladding height for the antenna. The other factor that causes the result to be different was due to the CST Microwave Studio transient simulation environment setup under the full wave global mesh cells setting, where users define the cell and accuracy for the simulation. Depending on the cell's size and setting, the result obtained from the simulation varies slightly.

	S11 (dB)	Impedance at 10 GHz (Ω)	Radiation Efficiency	Bandwidth (MHz) at -10dB	Antenna Gain (dBi)
Antenna patch with both side copper cladding $17\,\mu m$ with 1.75 mm offset	-15.34	$37.84 - j7.47$	0.9547	23.02	7.64
Antenna patch with both side copper cladding at $35\,\mu m$ with 1.75 mm offset	-32.34	$50.58 - j2.27$	0.9560	26.63	7.69
Antenna patch with both side copper cladding $17\,\mu m$ with 2 mm offset	-50.8	$49.74 - j0.12$	0.9554	26.90	7.65

Table 4. Summarized Results Caused by Different Copper Cladding Height and Probe Feed Offset Position.

By shifting the probe feed $2\,\mathrm{mm}$ offset from the center of the circular patch, the return loss of the antenna is about 50 dB as shown in Figure 14. The impedance of the antenna is $49.74 - j0.12\,\Omega$ at 10 GHz as shown on the Smith chart in Figure 15. This value is close to $50\,\Omega$. The gain and radiation efficiency of the antenna is shown in Figure 16. The directivity of the antenna with 2 mm offset is 7.65 dBi as compared to 6.50 dBi with 1.75 mm offset. For subsequent calculations for the pre-rectification filter, the impedance of the antenna is assumed to be $50\,\Omega$.

From the simulation, it was observed that minor changes in the probe feed position and copper cladding thickness would result in major changes in the impedance and return loss response. The simulation result using CST Microwave Studio demonstrated that a tight fabricating tolerance is needed.

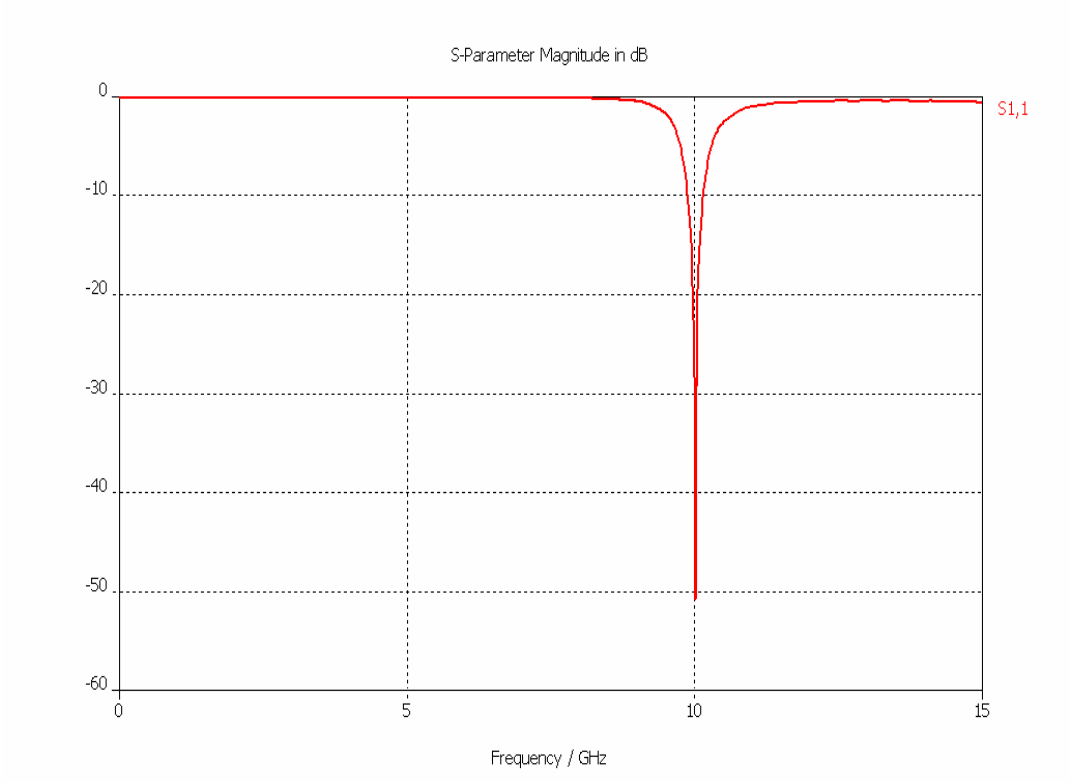

Figure 14. S11 Frequency Response of Circular Disc Design with Copper Cladding on Both Sides of $17\,\mu\mathrm{m}$ and Probe Feed Offset of 2 mm from the Center of the Antenna.

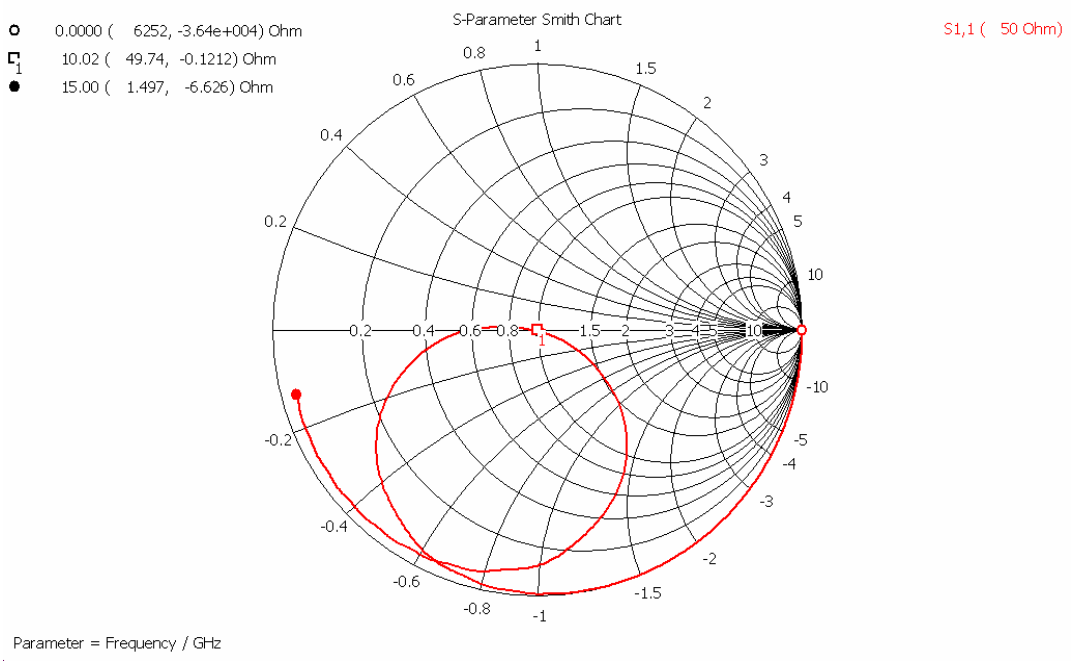

Figure 15. Smith Chart of Circular Disc Design with Cooper Cladding on Both Sides of $17\,\mu m$ and Probe Feed Offset at 2 mm from the Center of the Antenna.

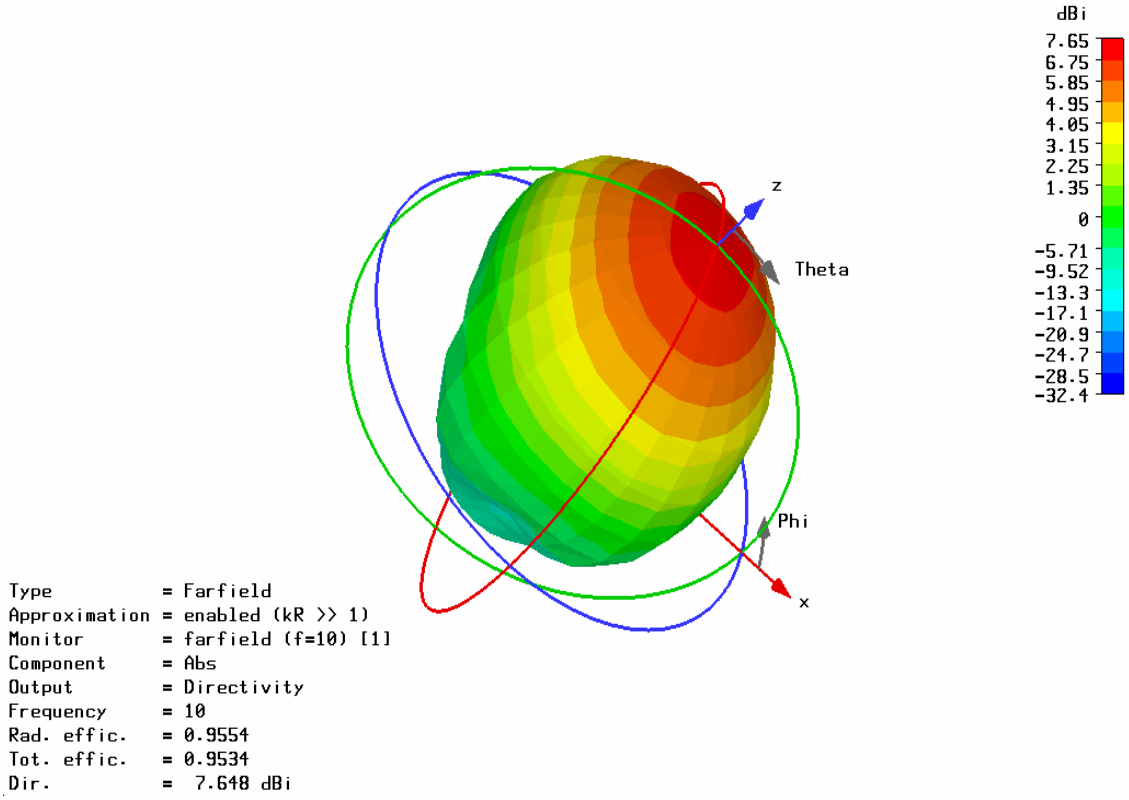

Figure 16. Far-field Radiation Pattern of the Circular Patch Antenna with Copper Cladding on Both Sides of $17\,\mu m$ and Probe Feed Offset at 2 mm from the Center of the Antenna.

C. DISCUSSION OF FILTER DESIGN

The purpose of the filters in the rectenna system is to: (1) attenuate the unwanted frequencies being rectified, (2) prevent the retransmission of harmonics generated by the non-linear I-V characteristics of the diode, and (3) select the DC from the frequency components for the load. This section discusses the design and simulation of the sixth order low-pass filter based on the dimensions provided by [4]. The purpose is to ascertain whether the filter design meets the criteria for a rectenna system application. The method used for microstrip filter design is discussed. The simulated result of the proposed design using Agilent Technologies Advanced Design System version 2005A is presented.

1. Introduction to Filters

Filters are widely used in communication systems for controlling the desired frequency response at certain parts of the system. An ideal filter allows the desired frequency to pass through without any attenuation and attenuates all other frequencies in the stop band region. Filters are categorized into three groups:

a. A low-pass filter allows frequencies between zero and cut-off frequency to pass through and attenuate all other frequencies.

b. A high-pass filter allows frequencies above the cut-off frequencies to pass through.

c. A band-pass filter allows frequencies between the lower cut-off frequencies and higher cut-off frequencies to pass through and attenuate all other signals outside this region.

The three categories of filters can be further divided into active and passive type filters. Figure 17 shows the three attenuation characteristic types of passive filters. The output power of passive filter is always less than the input power while an active filter allows power gain via the use of amplifier devices. The attenuation of a filter can be calculated using the following formula:

$$\text{Attenuation} = -20\log\left(\left|\frac{V_2(\omega)}{V_1(\omega)}\right|\right) = -20\log(|S_{21}|) = -20\log|\tau(\omega)| \qquad (3.8)$$

where $\omega = 2\pi f$, V_1 and V_2 are the incident and transmitted voltages and τ is the transmission coefficient. S_{21} is the scattering parameter that corresponds to the transmission coefficient.

There are several ways of designing filters. These include the image-parameter method (IPM) and the well-known insertion-loss method (ILM). For a frequency below 1.0 GHz, filters are usually implemented using lumped elements such as resistors, inductors, and capacitors. At the microwave frequency region, microstrip or waveguide filters are usually deployed. A microstrip filter has the advantage of being compact.

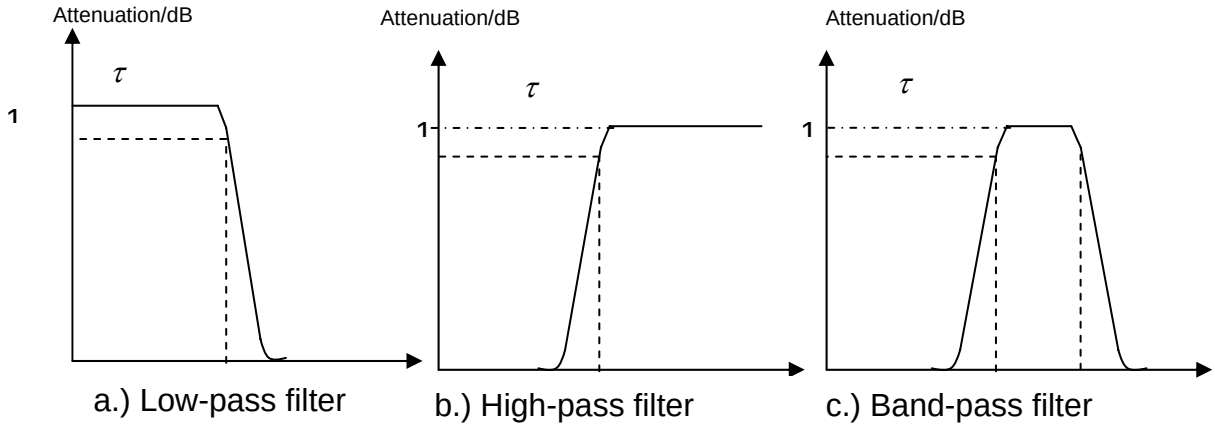

Figure 17. Various Types of Filters.

2. Insertion Method

In order to obtain a better roll-off rate and magnitude response, reference [2] proposed the use of a sixth-order low-pass filter with a cut-off frequency of 14 GHz instead of a fourth order low-pass filter with cut-off frequency of 12 GHz. The insertion method for designing the low-pass filter could be found in microwave textbook [30] and is summarized below.

a. Determine the type of filter intended for the application. In this case, a low-pass filter is used.

b. Determine the type of filter response. A Butterworth filter response is chosen as minimum ripple is desired.

c. Determine the order of the microstrip filter using Figure 18 in order to sufficiently attenuate the second harmonic at 20 GHz. The normalized frequency is

$$\left|\frac{\omega}{\omega_c}\right| - 1 = \frac{20}{12} = 0.66 \tag{3.9}$$

where $\omega_c = 2\pi f_c$, which corresponds to equal or at least a fourth-order filter. Eventually a sixth-order filter was chosen for a better roll-off rate and second harmonic isolation.

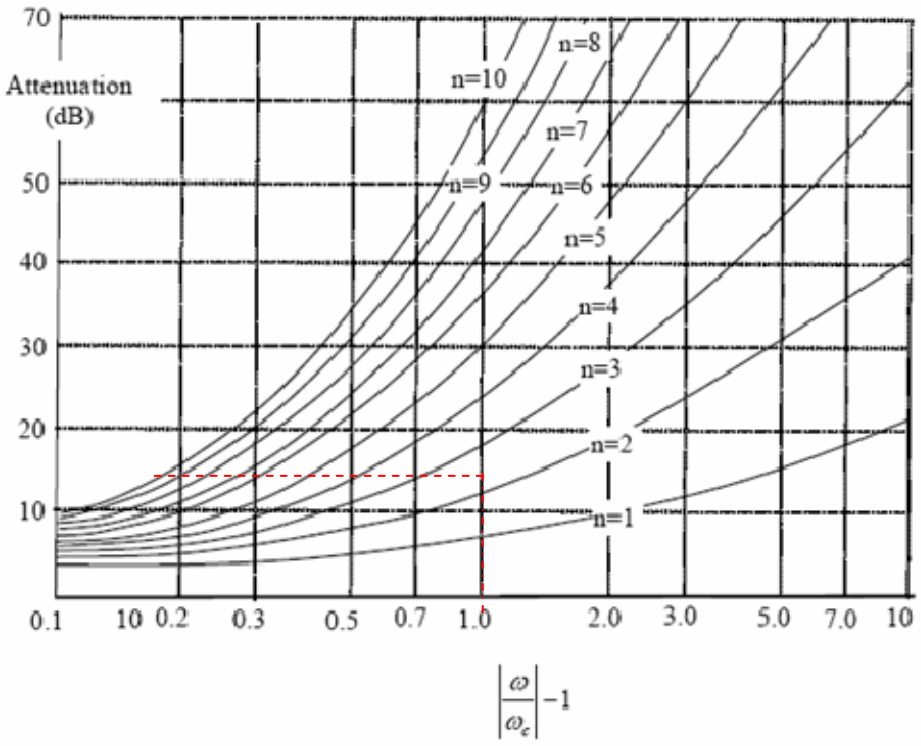

Figure 18. Attenuation Versus Normalized Frequency for Maximally Flat Filter Prototypes (From [30]).

d. Develop the prototype of a filter with a cut-off frequency of 1 Hz and 1Ω impedance. Reference [4] proposed the use of the shunt element prototype. Figure 19 shows the basic shunt element prototype of a low-pass filter. The values of g_1, g_2 and g_n can be found in Table 5. The element values for a maximally flat (Butterworth) low-pass prototype from [30].

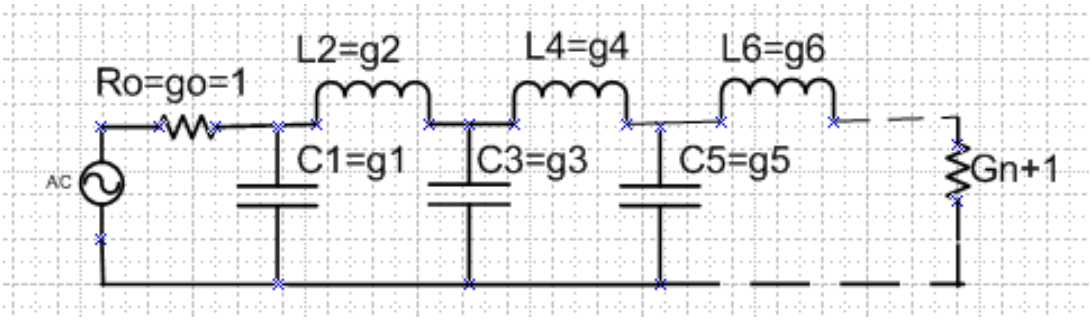

Figure 19. Ladder Representations for a Shunt and Series Element Low-pass Filter Beginning with the Shunt Element (After [30]).

N	g1	g2	g3	g4	g5	g6	g7	g8	g9
1	2.0000	1.0000							
2	1.4142	1.4142	1.0000						
3	1.0000	2.0000	1.0000	1.0000					
4	0.7654	1.8478	1.8478	0.7654	1.0000				
5	0.6180	1.6180	2.0000	1.6180	0.6180	1.0000			
6	0.5176	1.4142	1.9318	1.9318	1.4142	0.5176	1.0000		
7	0.4450	1.2470	1.8019	2.0000	1.8019	1.2470	0.4450	1.0000	
8	0.3902	1.1111	1.6629	1.9615	1.9615	1.6629	1.1111	0.3902	1.0000

Table 5. Element Values for a Butterworth Low-pass Filter Prototype (From [29]).

e. Determine the values of *C* and *L* through transformation. Based on the load impedance and cut-off frequency ω_c, the prototype values need to be transformed using

$$R = g_{N+1} R_L \tag{3.10}$$

$$L_i = \frac{I_i R_L}{\omega_c} \tag{3.11}$$

$$C_i = \frac{c_i}{R_L \omega_c} \tag{3.12}$$

where R_L is the load resistance. For R_L=30Ω and f_c =14 GHz, the capacitance and inductance values are shown in Table 6.

Elements	C_1 (F)	L_2 (H)	C_3 (F)	L_4 (H)	C_5 (F)	L_6 (H)
Values	1.961E-13	4.823E-10	7.32E-13	6.5883E-10	5.359E-13	1.7653E-10

Table 6. Values of a Sixth-order Low-pass Filter for Capacitance and Inductance.

The *C* and *L* values are converted into physical microstrip dimensions based on the cut-off frequency, dielectric height, dielectric constant, and width-length ratio by first determining the effective dielectric and characteristic impedance for each shunt and series elements. The effective dielectric constant for a microstrip needs to be determined because one side of the material is substrate and the other side of the microstrip is air which leads to a fringing E-fields.

The effective dielectric constant is:

$$\varepsilon_e = \frac{\varepsilon_r + 1}{2} + \frac{\varepsilon_r - 1}{2} \frac{1}{\sqrt{1 + 12d/W}} \tag{3.13}$$

where W is the width of the transmission line, d is the height of the substrate at 13 mm, and ε_r is the relative dielectric constant of the substrate, which is equal to 3. The width of the microstrip, W, is dependent on whether it represents a shunt or series element. For shunt elements, W is usually larger than h by 10 times or more. The opposite is true for series elements, where W is much smaller than h.

Once the effective dielectric is determined, the impedance of the shunt and series elements of width *(W)* and selected length ratio is [30]

$$Z_0 = \begin{cases} \dfrac{60}{\sqrt{\varepsilon_e}} \ln\left(\dfrac{8d}{W} + \dfrac{W}{4d}\right) & \text{for } W/d \le 1 \\ \dfrac{120\pi}{\sqrt{\varepsilon_e}\left[W/d + 1.393 + 0.667 \ln\left(W/d + 1.444\right)\right]} & \text{for } W/d \ge 1 \end{cases} \quad (3.14)$$

where ε_e is the effective dielectric constant of the substrate.

Based on [2] the low impedance section is Z_{low} = 10 Ω, and the high impedance section Z_{high} = 100 Ω, W/d_{ind} = 0.67 , W/d_{cap} = 21.26 respectively. With these values, the values of ε_{ehigh}, ε_{elow}, Z_{low} and Z_{high} can be calculated using Equations (3.13) and (3.14). The physical lengths of microstrip lines are calculated using

$$Length\_L_i = \frac{cL_i}{Z_{ind}\sqrt{\varepsilon_{eff\_ind}}} \quad (3.15)$$

$$Length\_C_i = \frac{cC_iZ_{cap}}{\sqrt{\varepsilon_{eff\_cap}}} \quad (3.16)$$

where C_i and L_i are the values calculated in Table 6. The physical lengths of the sixth-order low-pass filter shunt and series elements are shown in Table 7, and the layout of the sixth-order low-pass filter is shown in Figure 20.

Elements	C_1 (F)	L_2 (H)	C_3 (F)	L_4 (H)	C_5 (F)	L_6 (H)
Values	1.961E-13	4.823E-10	7.32E-13	6.5883E-10	5.359E-13	1.7653E-10
Physical Length of strip (mm)	0.3203	0.9670	1.1956	1.3209	0.8752	0.3539

Table 7. Physical Dimensions of Sixth-order Low-pass Filter Shunt and Series Elements.

The sixth-order filter was simulated using ADS software in order to ascertain its performance. Figure 21 shows the layout of the sixth-order low-pass filter in Agilent ADS software.

The sixth-order low-pass S12 and S21 insertion loss is -0.078 dB as shown in Figure 22. It has a transmittance of 98.2%, which is considered good. The simulation result using CST Microwave Studio is close to 94%. At 14 GHz, the attenuation is about -3.04 dB. At 20 GHz, the second harmonic isolation as shown in Figure 21 is about -14.5 dB, which is very close to the design requirements as show in Figure 17. The simulated and theoretical results are identical.

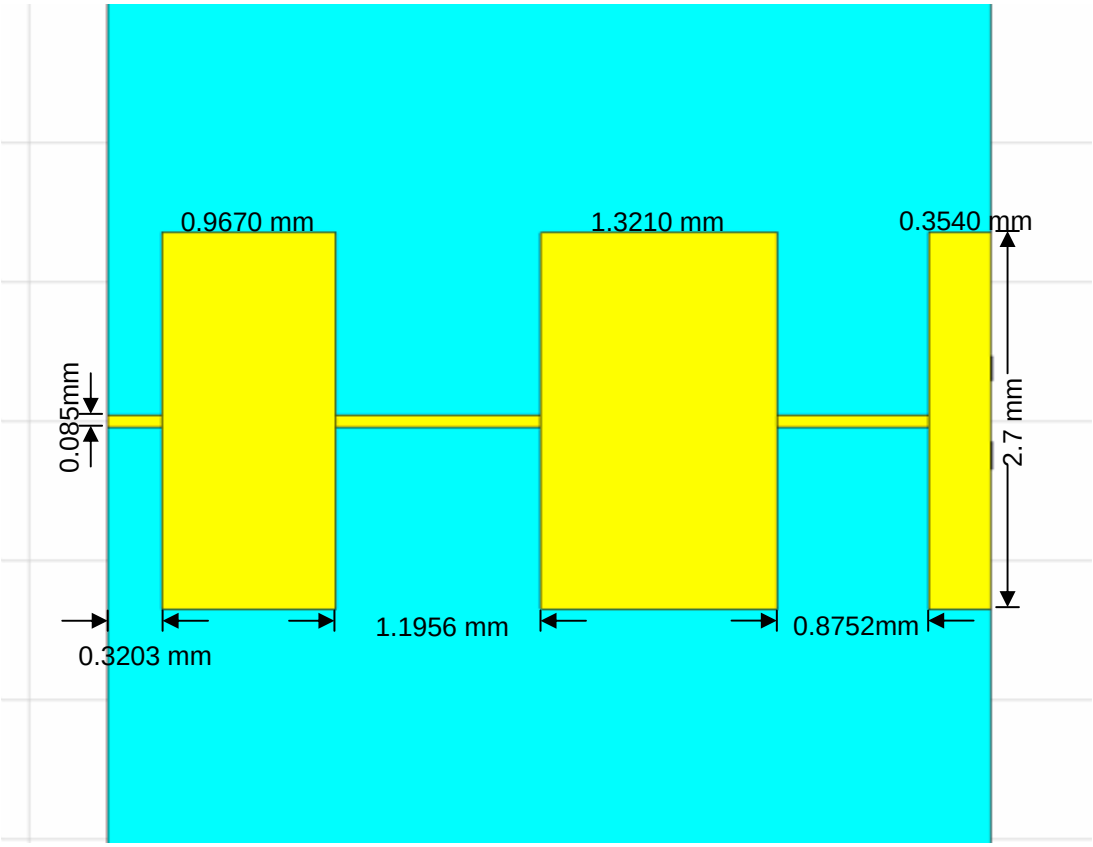

Figure 20. Physical Dimensions of the Sixth-order Low-pass Filter.

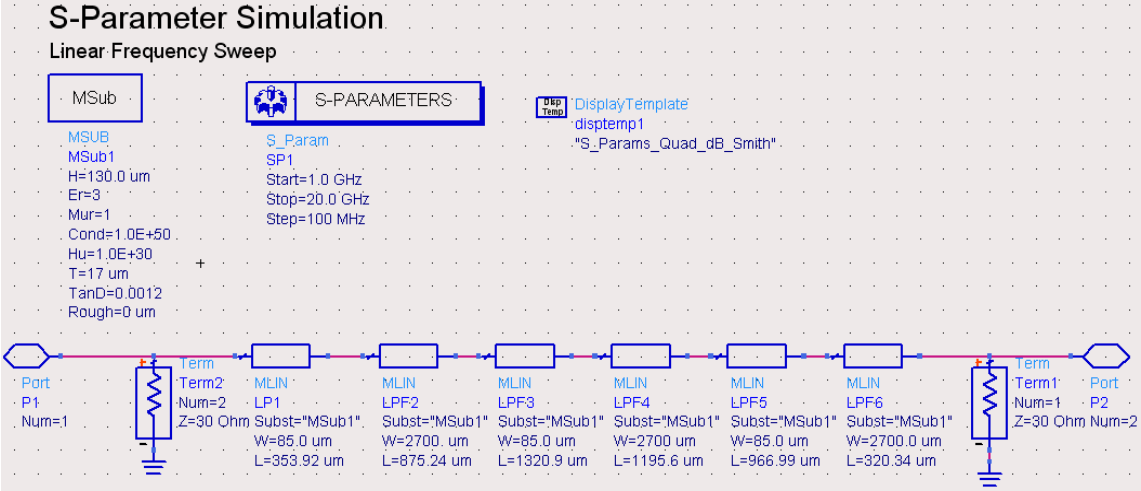

Figure 21. Layout of the Sixth-order Low-pass Filter in the Agilent ADS 2005 Software Environment.

Figure 23 shows the S22 response of the simulated sixth-order filter on the Smith chart. The impedance of the filter at the output is $1.266 + j0.021\Omega$. When normalized with a 30Ω characteristic impedance, the impedance is $37.98 + j0.63\Omega$. The output impedance of the sixth-order filter needs to match the input impedance of the diode. This is accomplished using a quarter-wave transformer and is elaborated in the next chapter.

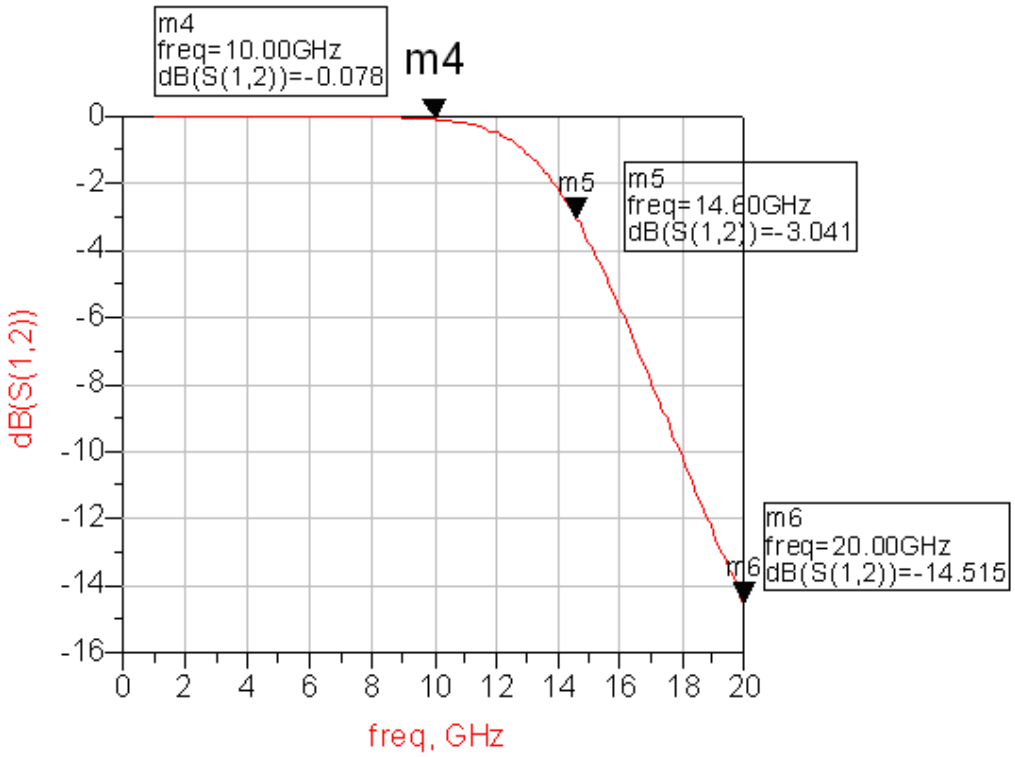

Figure 22. Response of the Sixth-order Low-pass Filter Simulated Using Agilent ADS Software.

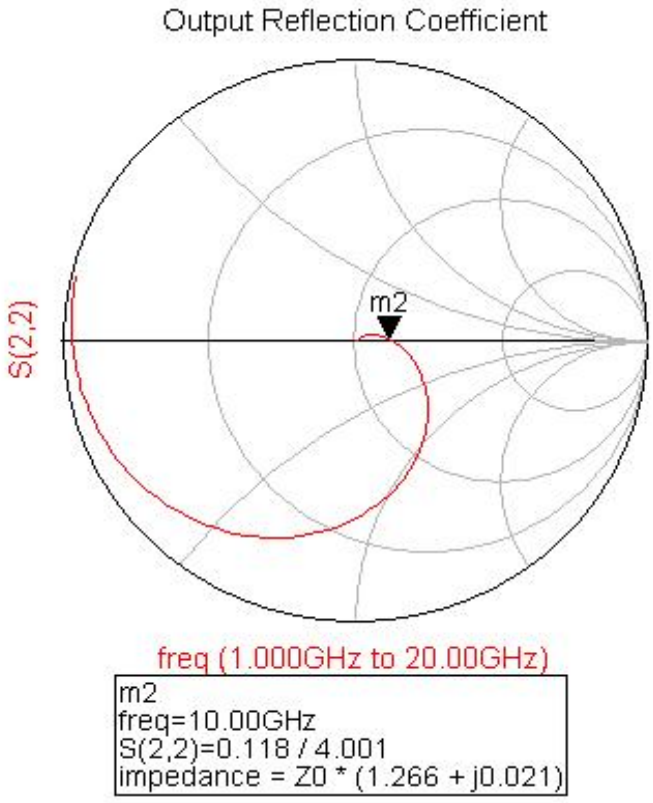

Figure 23. S22 Response of the Sixth-order Filter Simulated using ADS Software.

D. SCHOTTKY DIODE

The Schottky diode is majority doped with N-type carriers (electrons) and has a metal-semiconductor junction. The majority carriers (moving electrons) are injected into the conductor band of the metal contact on the other side as free-moving electrons resulting in very fast switching times as there is no P- and N-type carrier recombination.

The forward voltage of a silicon Schottky diode is typically 0.3-0.5V as compared to a PN junction diode which has a forward voltage drop of 0.6-0.8V. The disadvantages of the Schottky diode include high reverse leakage current and relatively low reverse voltage rating. The Schottky diode's fast switching time makes it ideal for rectenna application for rectifying an incoming AC signal. Figure 24 shows the schematic layout diagram of a two patch array rectenna system from [31] using the HSMS-8101 Schottky diode. A single rectenna

system was tested to have a maximum efficiency of 52% under ideal conditions for an input power of 10 mW and an overall efficiency of 44% for a three element array.

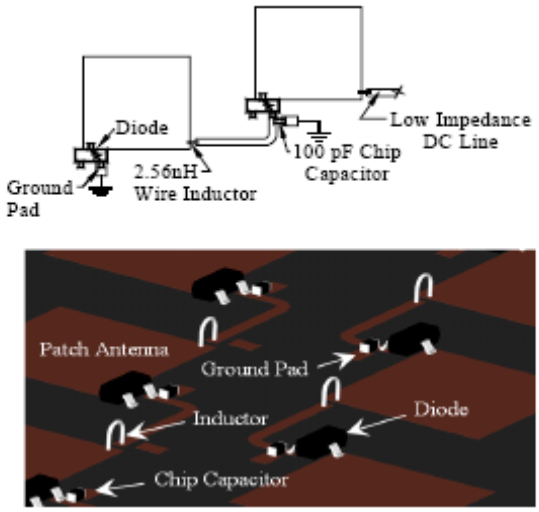

Figure 24. Schematic of Two Patch Rectennas Connected in an Array (top) and View of the Hardware Implementation (Bottom) (From [31]).

The Avago HSMS 8101 Schottky diode with an SOT-23 package component layout is used, as shown in Figure 25. The dimension for the Schottky diode's pin layout as shown in Figure 25 is transferred to the microstrip PCB board. The diode characteristic is given in Table 8.

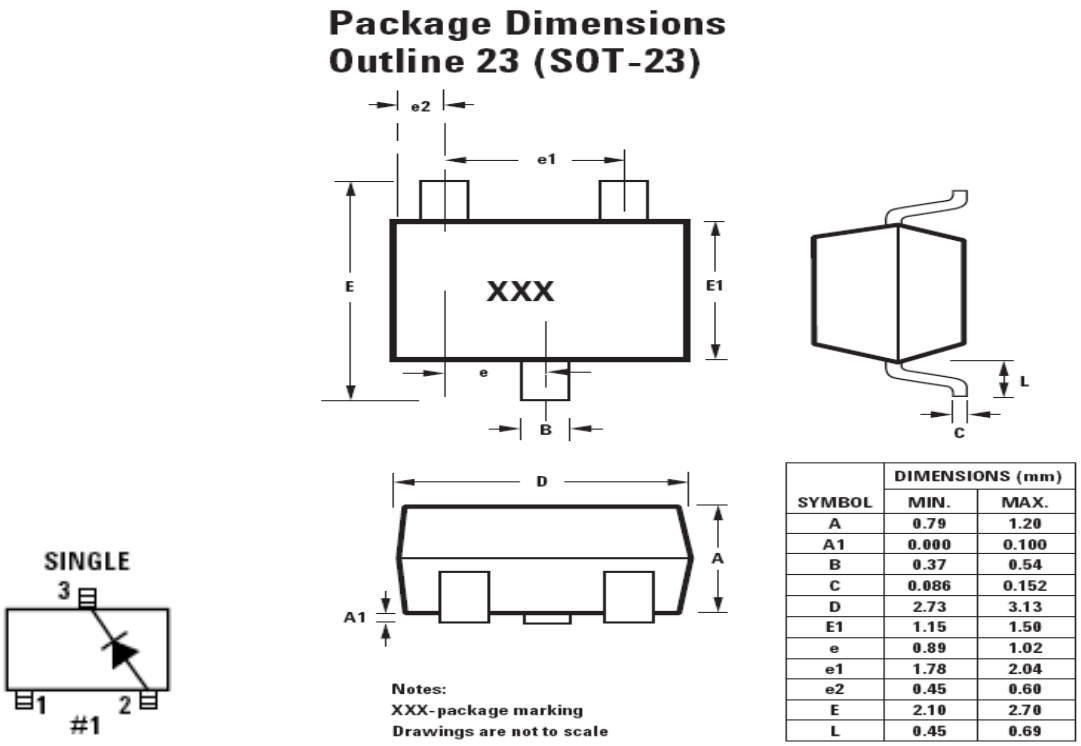

Figure 25. Schematic Layout of the Avago HSMS 8101 Schottky Layout (From [32]).

Electrical Characteristics of the HSMS-8101 Schottky Diode			
Symbol	Parameter	Unit	Value
P_T	Total Power Dissipation	mW	75
T_J	Junction Temperature	°C	+150
T_{OP}	Operating Temperature	°C	-65, +150
$V_{BR}(I_R\ 10\ \mu m)$	Breakdown Voltage	V	4(min)
C_T V_R=0 V, f=1 MHz	Total Capacitance	pF	0.26
I_S	Saturation Current	A	4.6×10^{-8}
n	Ideality Factor		1.09
R_S	Parasitic Series Resistance	Ω	6
C_J	Zero-bias junction capacitance	pF	0.18

Table 8. HSMS-8101 Electrical Characteristics (From [31]).

Reference [3] used a general diode model from [30] to compute the input impedance for the Schottky diode at 10 GHz. The result obtained for HSMS 8101 at 10 GHz using the general model as shown in Figure 26 has an impedance of $24.43 - j339.55\ \Omega$ for various input voltages between 0.6 and 2.6 V. According to [4], the result obtained was not accurate for the HSMS 8101 diode. The model for the HSMS 8101 from [32] is shown in Figure 26. The model includes inductance and capacitance caused by the packing of the HSMS 8101 diode. R_s is the series resistance and R_j is the junction resistance which is dependence on current.

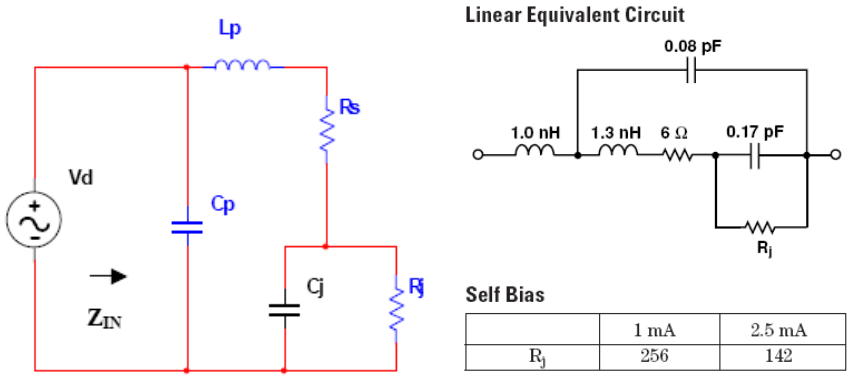

General diode model HSMS 8101 Schottky diode

Figure 26. General Diode Model (right) (From Ref. [29]); HSMS 8101 Schottky Diode (left) from Avago Data Sheet (From. [32]).

Reference [4] used the model as shown in Figure 27 and developed by references [33, 34] to calculate the efficiency and impedance of the Schottky diode by ignoring the inductance and capacitance of the package. The close-form formula to determine the efficiency of the diode with a $50\ \Omega$ load (motor) can be found in [4]. The Schottky diode efficiency versus output voltage is shown in Figure 28.

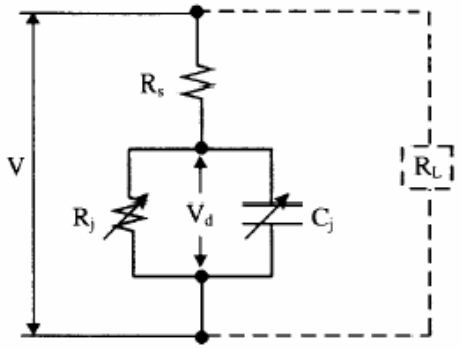

Figure 27. Circuit Model of Diode and Load (From [32]).

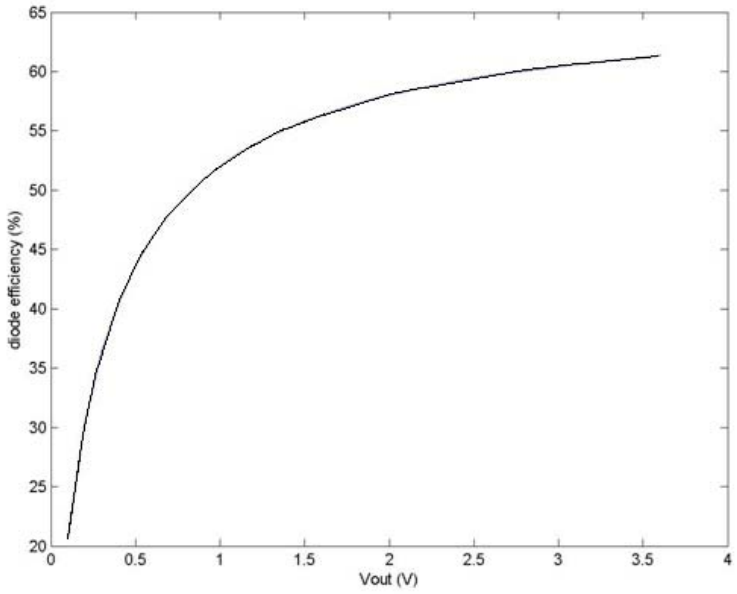

Figure 28. Diode Efficiency Versus Output Voltage for Load of 50Ω (From [4]).

Based on [4], the maximum efficiency for the diode is about 60% at maximum power with an input impedance of $45.5 - j13.9\ \Omega$ via the use of the following equations:

$$Z_{diode} = \frac{\pi R_S}{\cos\theta_{on}\left(\frac{\theta_{on}}{\theta_{on}} - \sin\theta_{on}\right) + j\omega R_S C_j\left(\frac{\pi - \theta_{on}}{\cos\theta_{on}} + \sin\theta_{on}\right)} \tag{3.17}$$

$$\tan(\theta_{on}) - \theta_{on} = \frac{\pi R_S}{R_L\left(1 + \frac{V_f}{V_O}\right)} \tag{3.18}$$

V_f is the forward bias voltage and θ_{on} is the forward bias turn on angle. This result is similar to the result of 60.5% obtained in [3]. The output voltage and power is calculated using

$$V_O = V_{BR}/2 \tag{3.19}$$

and

$$P_{OUT} = \frac{V_O^2}{R_L} \tag{3.20}$$

The Schottky diode HSMS-8101 has the following S21 response as shown in Figure 29. The S21 value is about -0.5 dB at 10 GHz. The S11 response for the diode is shown via a Smith chart in Figure 30 with input impedance of $54.7 - j40.05\Omega$. This real value is about 10Ω greater than the value obtained using Equation (3.17).

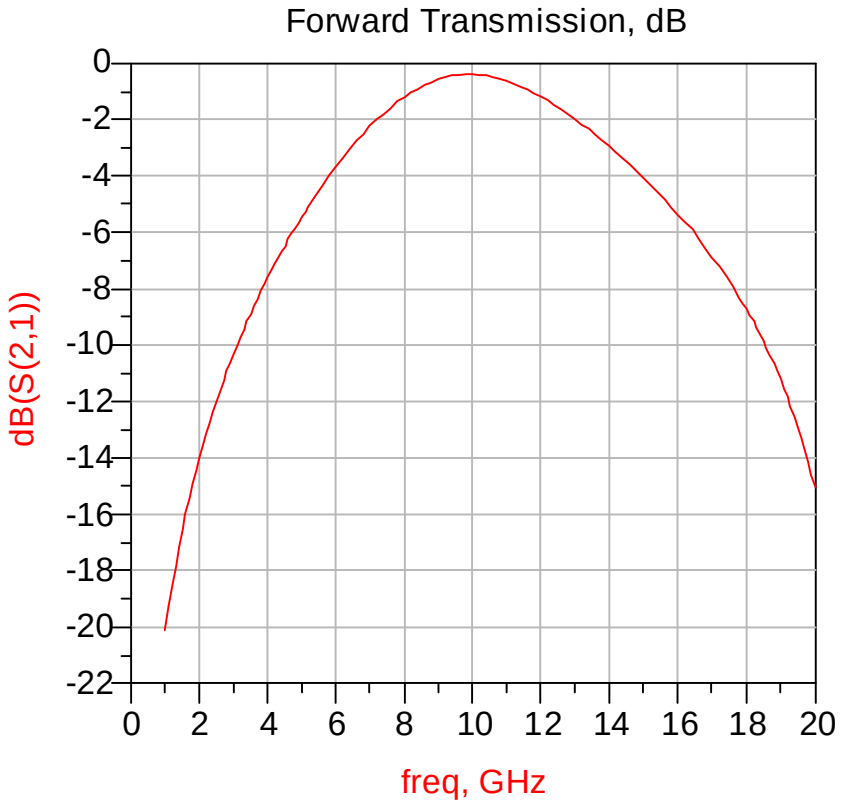

Figure 29. S21 Response of the Schottky Diode Simulated Using ADS 2005.

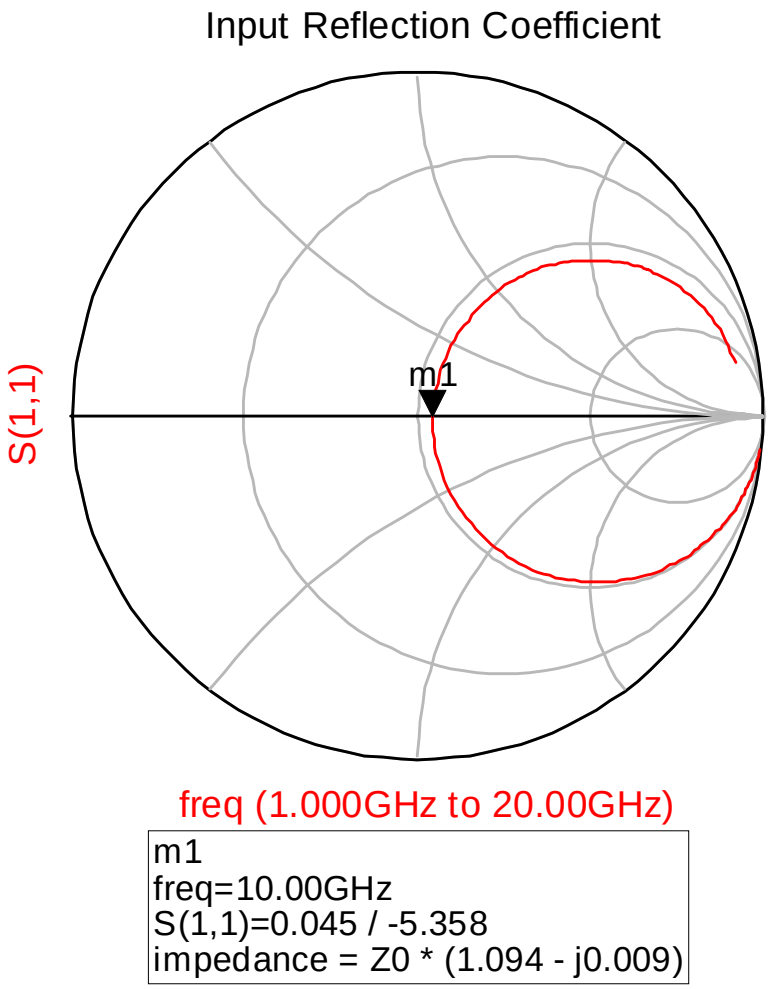

Figure 30. S11 of HSMS 8101 Schottky Diode Impedance at 10 GHz

E. SUMMARY

In this chapter, the rectenna subsystem theories have been presented. The 10 GHz circular patch antenna was simulated in CST Microwave Studio. The simulated 2 mm offset antenna has a gain of 7.65 dBi and efficiency of 96 %. The six order low-pass filter has a return loss of 0.008 dB and the Schottky Diode S21 impedance was used in simulations. The next chapter of this thesis discusses the need for an impedance matching unit.

THIS PAGE INTENTIONALLY LEFT BLANK

IV. RECTENNA IMPLEMENTATION

A. RECTENNA DESIGN

Chapter III discussed and analyzed the main components of the rectenna system. The main components are the circular patch antenna, sixth-order low-pass filter and HSMS 8101 diode. This chapter discusses the implementation and layout of the rectenna system and introduces the need for an impedance matching unit for the probe feed and a sixth-order low-pass filter for the rectenna system.

1. Probe Feed and Impedance

As the impedance of the antenna is assumed to be 50Ω, there was a need to match the 50Ω antenna with the correct probe feed dimension where a uniform E-field distribution was desirable. At 50Ω, the width of the microstrip was only 0.3 mm, which was too narrow for the probe feed hole to be drilled. The relief hole had a diameter of 1.1 mm (0.55 mm x 2). The width of the microstrip was calculated using the Matlab program in Appendix A. Therefore, the width of the microstrip was widened to 1.124 mm to accommodate the probe feed. Widening of the microstrip reduced the impedance to 20Ω. The 20Ω microstrip had a width of 1.124 mm and a length of 0.8 mm, was simulated in ADS software, and had an impedance of $(0.714 - j0.400)Z_o$ at 10 GHz. Z_o is the characteristic impedance. With the assumption that $Z_0 = 50\Omega$, the strip impedance was $35.7 - j20\Omega$.

A quarter-wave transformer was used for impedance matching. Reference [30] shows examples of using this method. The quarter-wave transformer equation was used to compute the impedance of the microstrip line

$$Z_{in} = \frac{Z_1 R_L + \tan kl}{Z_1 + jR_L \tan kl} \tag{4.1}$$

In order to have zero reflection coefficients, the input impedance Z_{in} must be equal to the characteristic impedance Z_o, and assuming $kl = \frac{2\pi}{\lambda}\frac{\lambda}{4} = \frac{\pi}{2}$, the characteristic impedance Z_1 for the quarter-wave transformer could be simplified and solved using

$$Z_{in} = Z_1 = \sqrt{Z_o R_L} \tag{4.2}$$

Figure 31 shows the general diagram for impedance matching. Γ is the reflection coefficient.

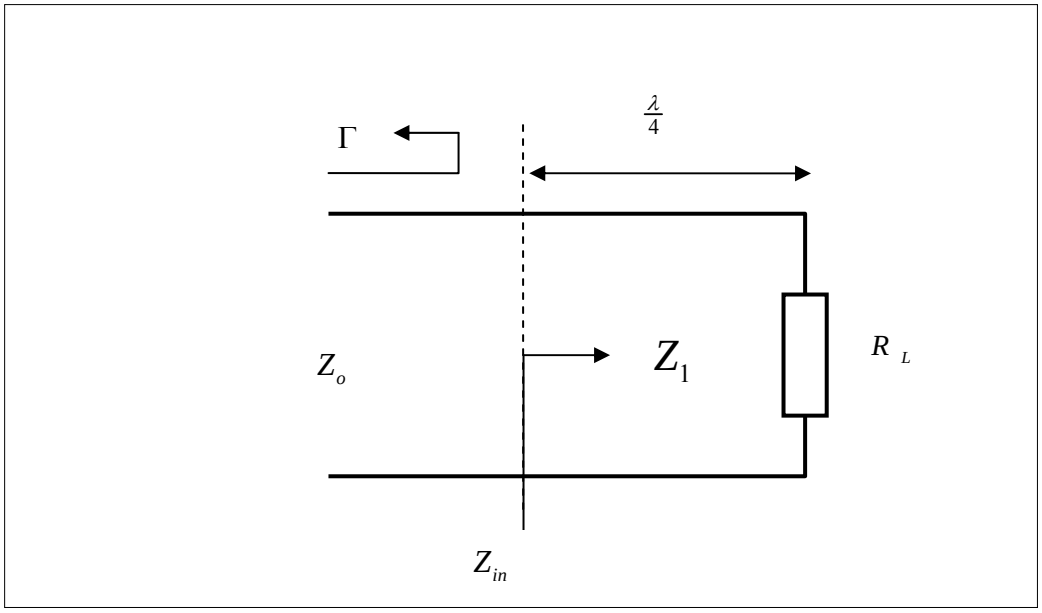

Figure 31. General Diagram Used for Quarter-wave Transformer Matching References.

Once the impedance of the quarter-wave transformer matching unit was obtained, the physical wavelength on the microstrip could be calculated using

$$\lambda = \frac{c}{2 f_o \sqrt{\varepsilon_{eff}}} \tag{4.3}$$

where ε_{eff} is the effective dielectric constant as shown in Equation (3.13).

Figure 32 shows the general block diagram of the rectenna design. The sixth-order input impedance of the low-pass filter simulated using ADS had a normalized impedance of $0.790 - j0.007\,\Omega$. When normalized with the 30Ω filter load, the impedance was $23.7 - j0.21\Omega$. By neglecting the imaginary term since it was small, $Z_{in} = \sqrt{50 \times 23.7} = 34.42\ \Omega$. This value is close to the 1.124 mm width strip line used for accommodating the probe feed. Using Equation (4.2), the length of the quarter-wave transformer strip was calculated to be 4.730 mm.

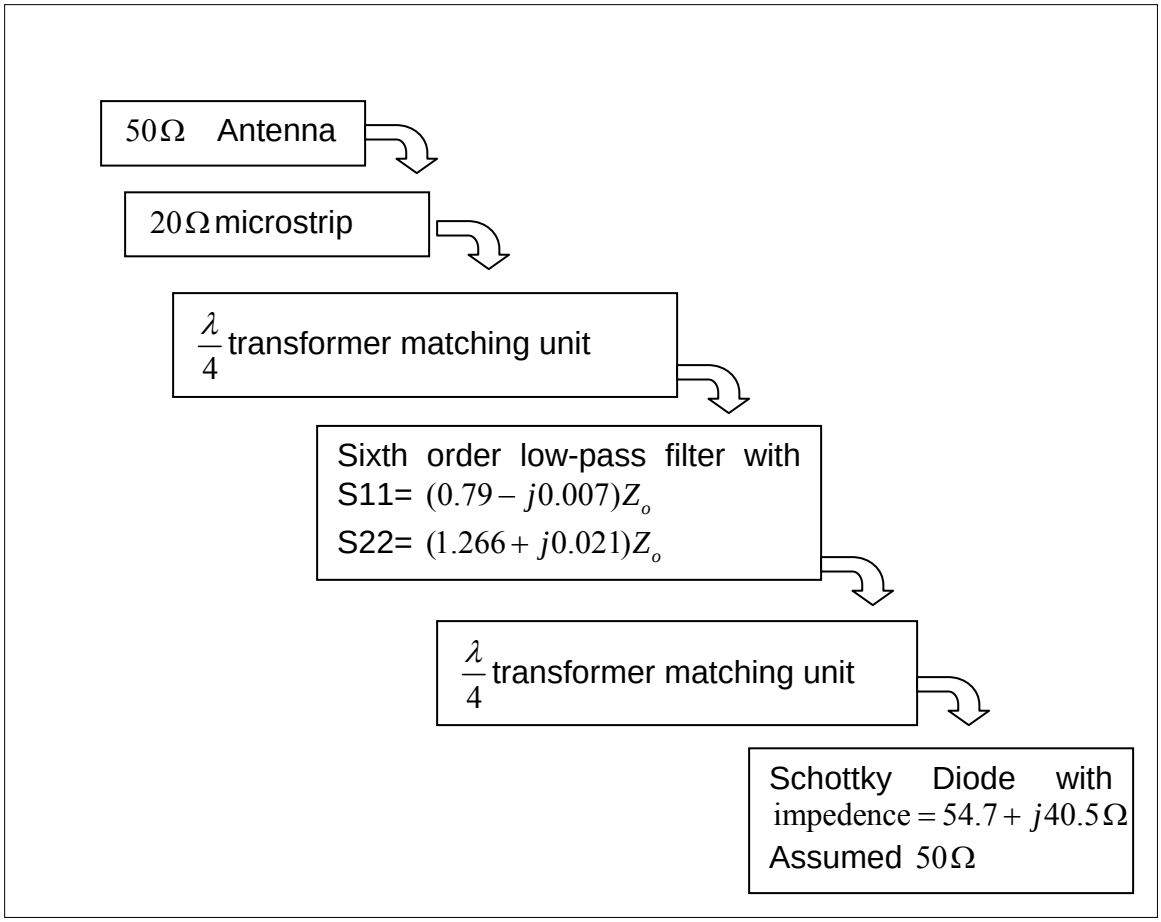

Figure 32. General Layout of the Rectenna System Showing the Matching Unit Location.

The use of a quarter-wave transformer allowed different widths of microstrip lines to connect together with minimum reflection coefficient. The next step was to use the quarter-wave transformer for diode impedance matching.

Based on the ADS simulation, the HSMS 8101 had an S22 characteristic impedance of $(1.094 + j0.802)Z_o = 54.7 + j40.05\Omega$ as shown in Chapter III. A Smith chart was used to determine the length of the quarter-wave transformer for impedance matching. The normalized impedance of the diode was plotted on the Smith chart in Figure 33.

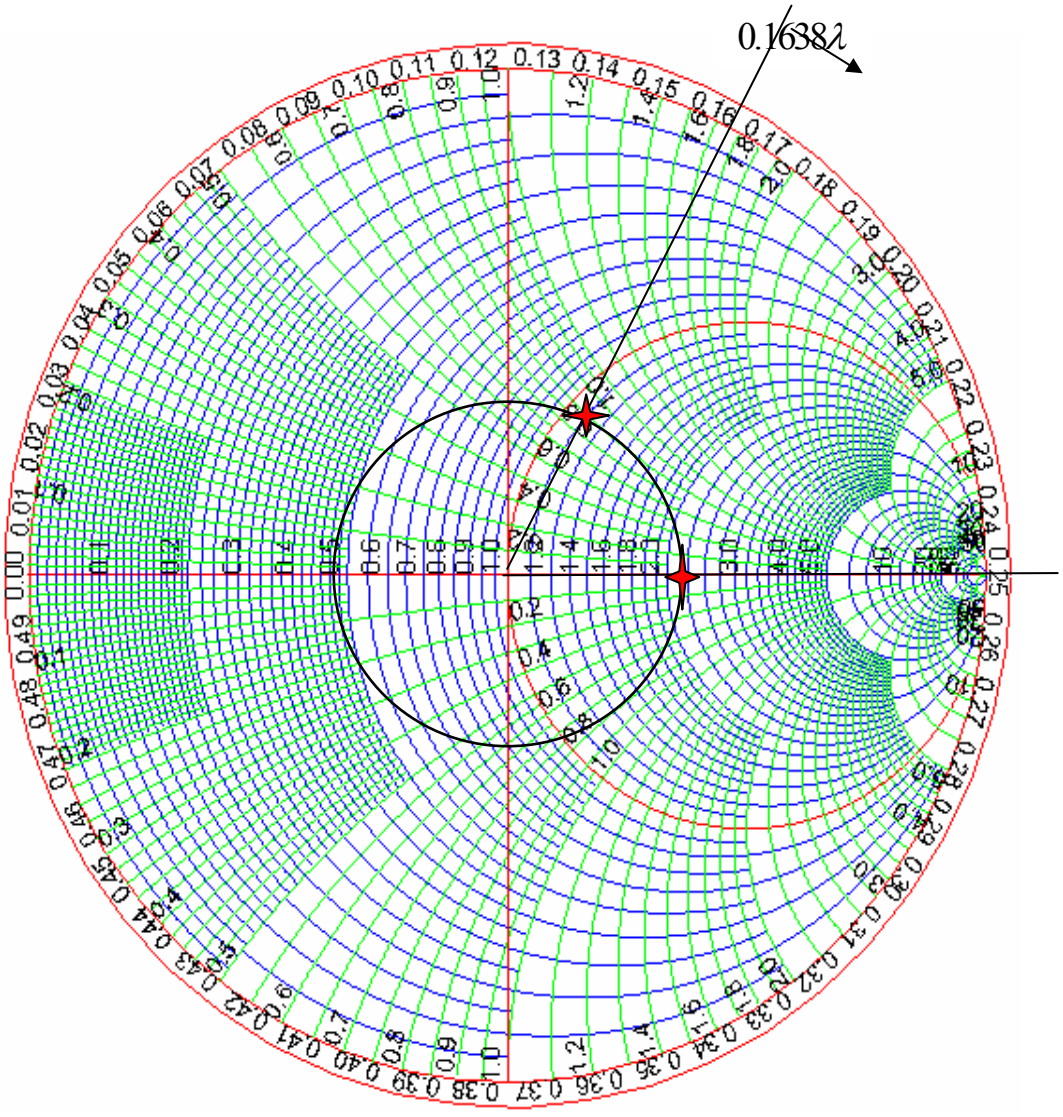

Figure 33. Smith Chart Showing the Normalized Diode Impedance and Shifting of Impedance Along the Normalized 100Ω Circle.

The diode's impedance was matched by employing two sections as shown in Figure 34. The impedance of Z_2 was arbitrarily chosen to be 100Ω and Z_1 was chosen as 50Ω for the diode. From the Smith chart in Figure 31, the reactance

$j0.801$ of the diode could be cancelled out by moving along the circle until it intercepted the horizontal axis. The real part of the diode impedance on the horizontal axis was 110Ω when normalized with 100Ω. The output of the low-pass filter had an impedance of 38Ω with negligible reactance as shown in the previous chapter. The purely resistive component of l_2 was $Z_{in} = \sqrt{38 \times 110} = 64.65\Omega$ at the $0.25\lambda - 0.1638\lambda = 0.0862\lambda$ location. This was equal to 19.581 mm on the PCB board. Therefore l_2=4.913 mm when a quarter-wave transformer was used. A Matlab program shown in Appendix A was used for the calculation.

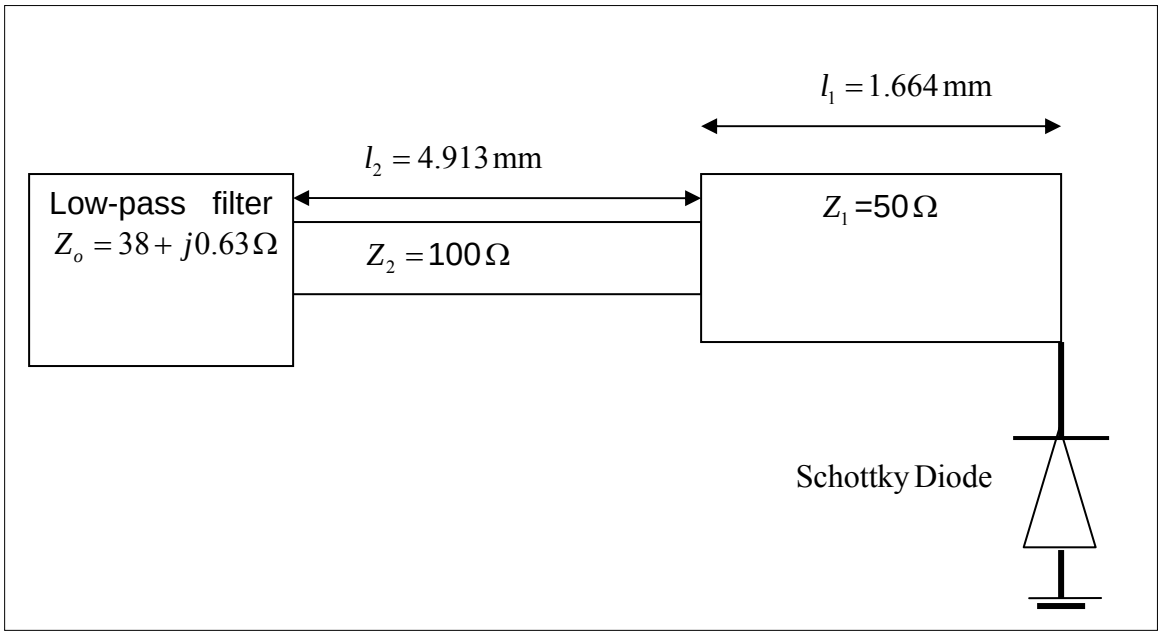

Figure 34. General Diagram for Schottky Diode Showing Impedance Matching Units.

With the assumption that the diode impedance was 50Ω, the width of the strip was about 0.320 mm using Equations (3.13) and (3.14). The length of the quarter-wave transformer strip l_1 was 1.664 mm.

2. Optimal Chamber Bend

In order to have had a compact design to reduce the footprint and weight of the PCB board, there was a need to bend the impedance matching unit. Bending of the microstrip at 90^o will create unwanted inductance as documented in most microstrip handbooks. To create an optimally 90^o chamfered bend as shown in Figure 35, the following equations from [35, 36] were used to calculate the dimension of the chamfered bend:

$$M = 52 + 65[\exp(-1.35\frac{W}{H})] \tag{4.4}$$

$$L = W(\frac{M}{50} - 1) \tag{4.5}$$

$$X = \frac{MD}{100} \tag{4.6}$$

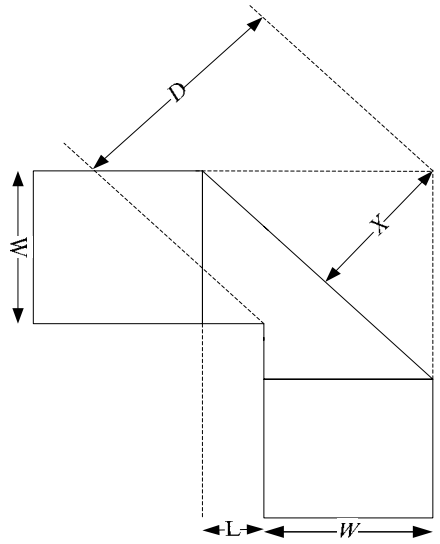

Figure 35. Optimally Chamfered Bend Used for the Rectenna Impedance Matching Unit Design (From [34, 35]).

A full CST software package was not available in school, the Schottky diode and other lumped elements could not be simulated in the CST environment. ADS was used for the circuit simulation with the HSMS-8101 diode. Figure 36 shows the dimensions of the filter component, impedance matching

unit, and diode of the rectenna system in the ADS environments. The simulated result for Figure 36 is captured in Figure 37. The S11 response of the rectenna system's low-pass filter with the diode had a return loss of 23.4 dB and bandwidth of 1.853 GHz at -10 dB. A higher bandwidth is desirable as it provides better design tolerance should the antenna bandwidth shift after fabrication. Higher bandwidth would deliver more energy to the diode as well.

As the full package of the ADS 2005 software package was not available for DXF conversion for fabrication purposes, the simulated rectenna's dimensions from ADS were transferred to CST and then converted to a DXF file format. The final design of the rectenna system without the circular antenna is shown in Figure 38. The capacitor was used to produce a smooth transient for the rectified current.

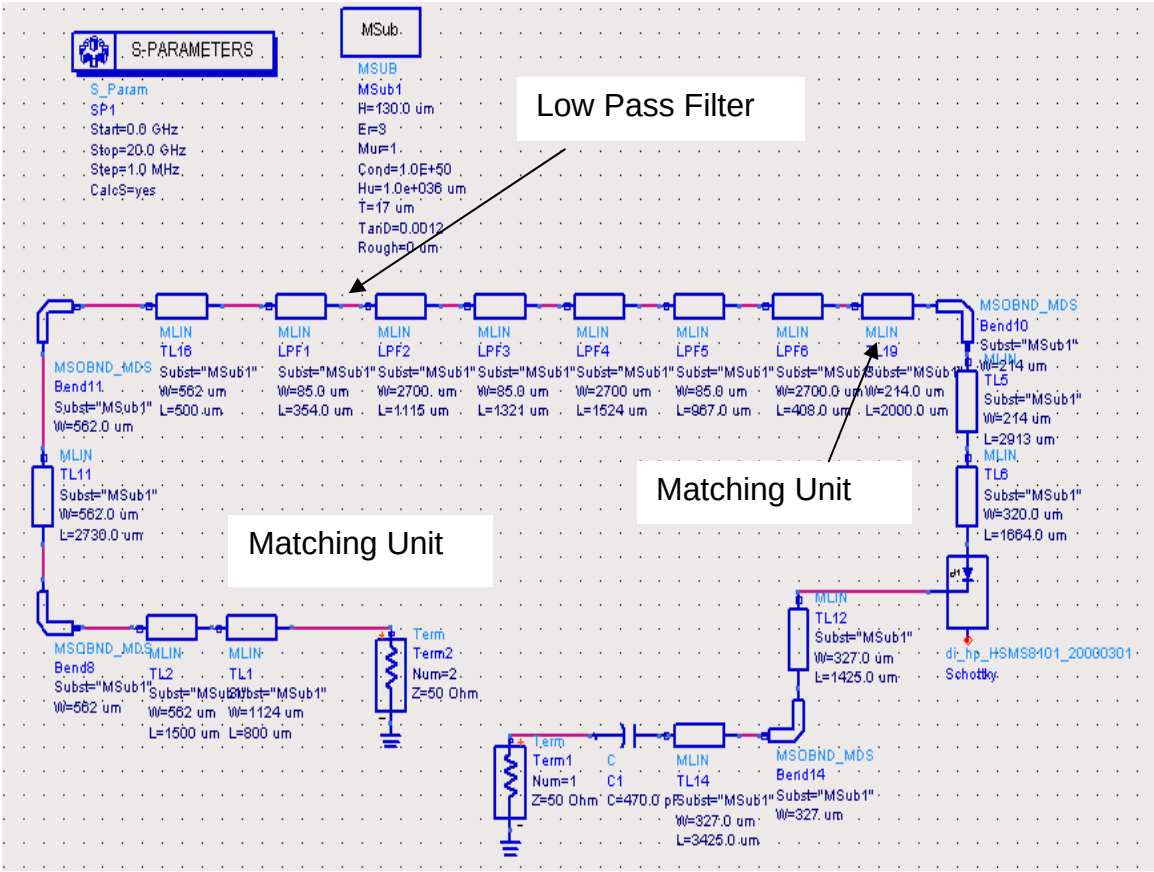

Figure 36. The Rectenna System Showing the Sixth-order Low-pass Filter, Impedance Matching Unit, and Schottky Diode.

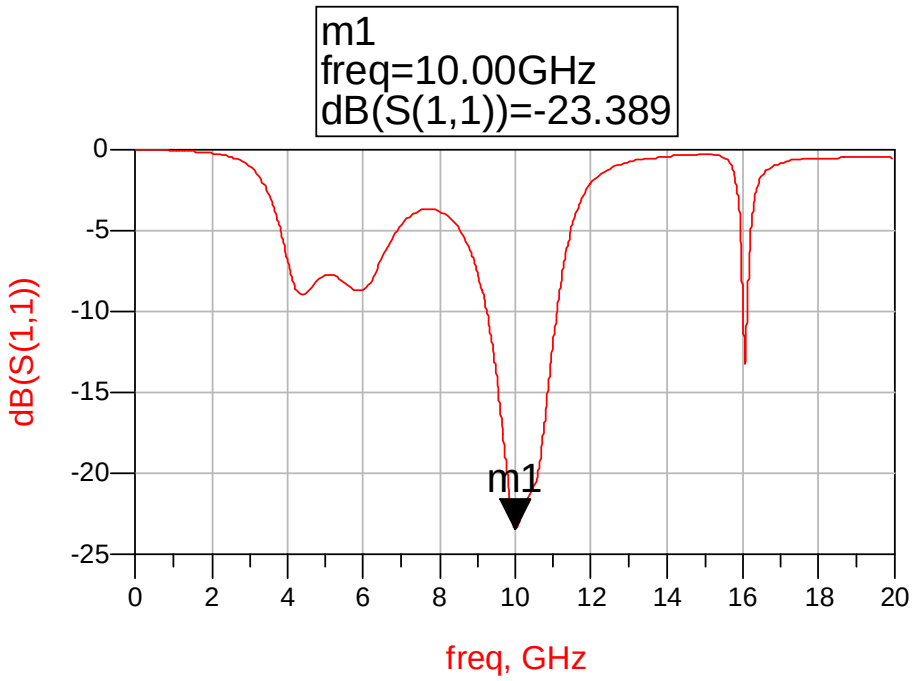

Figure 37. S11 Response of the Rectenna System Simulated in the ADS Environment.

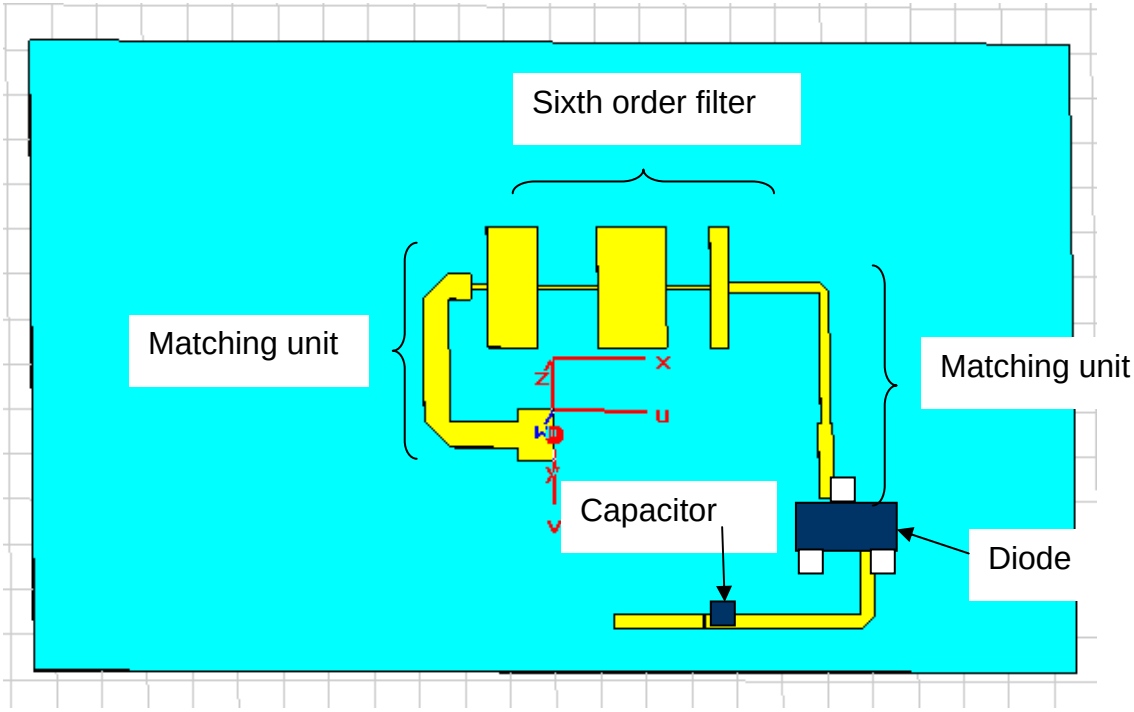

Figure 38. Final Design of the Rectenna System Excluding the Antenna.

3. Front End Matching for the Probe Feed

According to [28], at lower frequencies the probe feed may simply be connected to the end of a microstrip stub as shown in Figure 39 (a). However, at higher frequencies the feed line width must be larger than the dimension of the relief hole and extend beyond the probe feed such that the standing wave creates a uniform E-field between the probe and the edge of the relief hole. Thus, the microstrip width needed to be wider than the relief hole. This was the reason for using a 20Ω line with a width of 1.124 mm as explained in Section A of this chapter.

In order to have created a uniform E-field at the probe feed position, an extension of the stub at the probe feed position was needed as shown in Figure 39 (b). The length of the stub for a $20\ \Omega$ microstrip line could be calculated using Equation (4.3) as before. In order to have maximum power transfer from the antenna to the low-pass filter, the stub needed to behave like an opened circuit at the far end while shorted at the probe feed position. Therefore, the length of the stub needs to be a half wavelength as shown in Figure 40. Using the Matlab program in Appendix A, the half-wave stub should have a length of 9.480 mm.

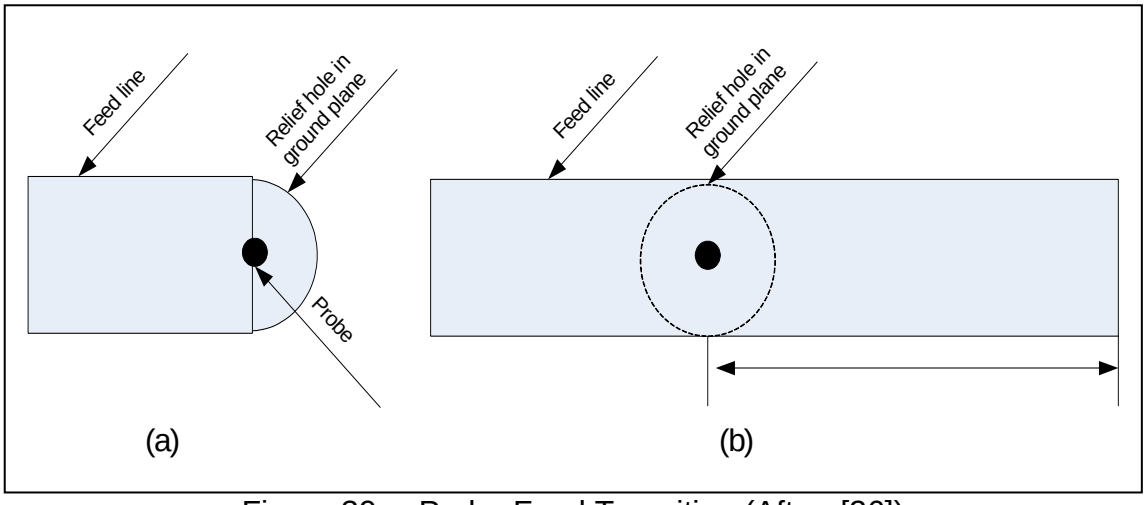

Figure 39. Probe Feed Transition (After. [26]).

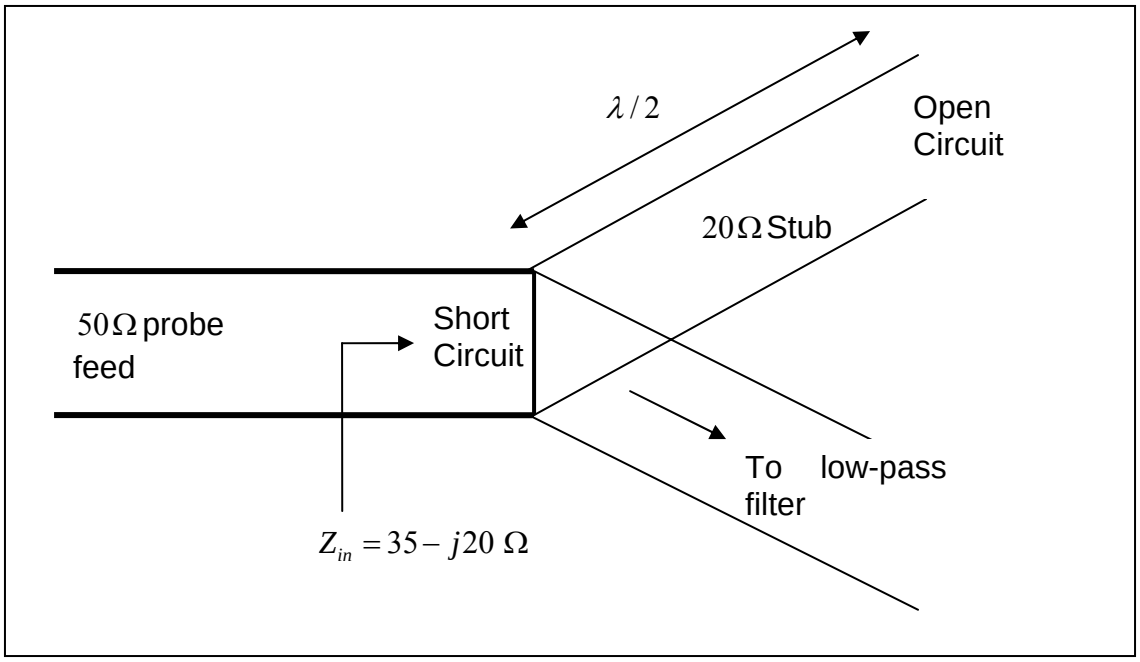

Figure 40. General Diagram Showing the 20 Ω Stub Position.

Figure 41 shows the rectenna diagram with the front end matching stub with two optimally chamfered bends. The length of the stub was fine tuned using ADS software. The final length of the stub was 9.220 mm. The impedance looking into the 20Ω stub from the probe feed is $35 - j20\Omega$ as mentioned in Section A of this chapter. The S11 response of the rectenna circuit is shown in Figure 42. It had a bandwidth of 1.357 GHz at -10 dB, which is 36 % lower than the rectenna circuit without front end matching stub as shown in Figure 38. The return loss at 10 GHz was 15.67 dB, 7.7 dB higher than Figure 36. This deterioration of the result was due to impedance mismatch, but it was still acceptable.

The half wavelength stub length could also be determined using the Smith chart. This was done by plotting the stub impedance $35 - j20\ \Omega$ on the Smith chart and moving it towards the right-hand side of the horizontal axis. The half wavelength stub length could be calculated using Equation (4.3).

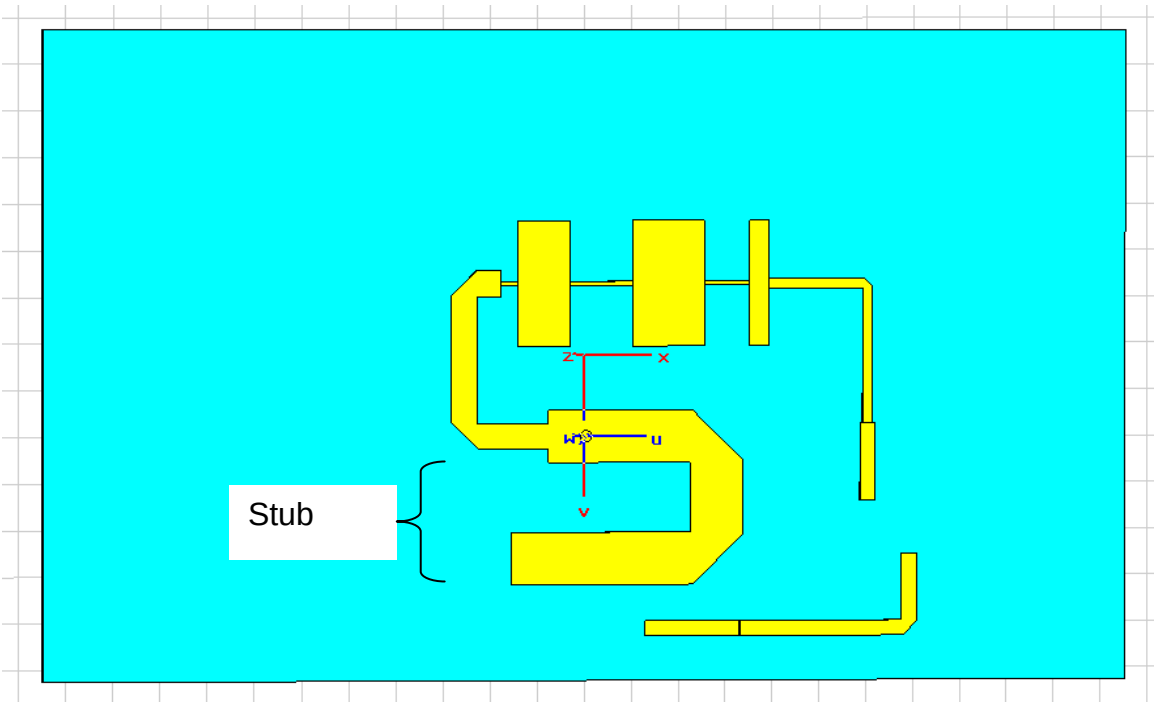

Figure 41. Rectenna Circuit Showing the Front End Matching Stub.

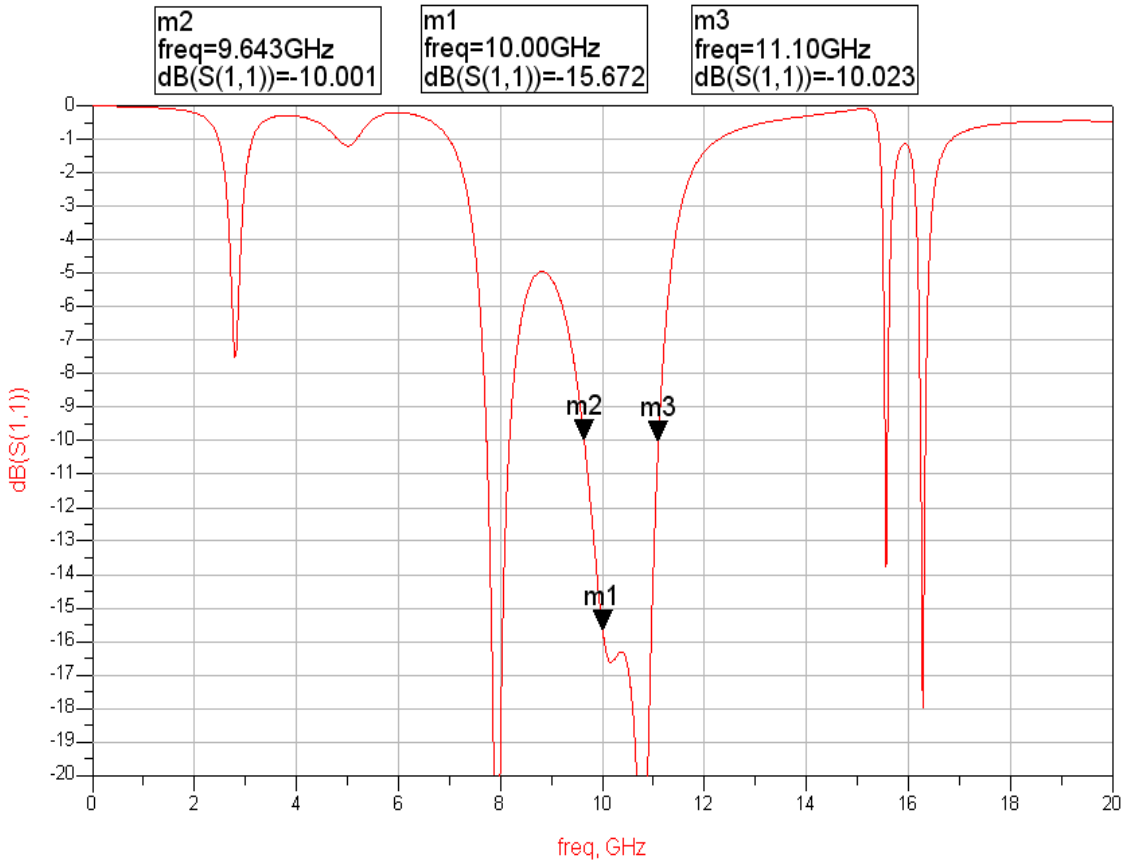

Figure 42. S11 Response of the Rectenna System with the Front Matching Unit.

B. ANTENNA ARRAY

Based on [3], the first helicopter motor prototype DMMK06-10 needs about 5.5 V with 100 mA to hover. Reference [3] performed extensive testing on the prototype motor and the measured data for the motor is reproduced in Table 9. The proposed motor was tested and confirmed that the data in Table 9 was accurate. For every increase in weight of 5 g, the electrical voltage and current required to allow an UAV to hover would increase dramatically.

DIMMK06-10 Motor's characteristic under test							
Weight (g)	net	5	10	15	20	25	30
Voltage (V)	5.5	7	8.1	9.9	11.5	14	16
Current (A)	0.1	0.136	0.17	0.22	0.264	0.319	0.357
Resistance (Ω)	54.9	51.4	47.4	45	43.5	43.8	44.8
Power (W)	0.55	0.952	1.3817	2.1780	3.0360	4.4660	5.7120
Round Per Minute	1200	1440	1620	1740	1770	1800	2100

Table 9. Measured Data for the MAV Motor Prototype (After [3]).

In order to produce the required electrical voltage and current for the MAV, the rectenna system needed to be connected in series. According to the manufacturer specification of the HSMS 8101 diode, the maximum power dissipation for the diode was 75 mW. If the motor needed 0.952 watts to hover, at least 22 antenna elements are needed. Therefore, an array of rectenna systems was needed to produce the required power. To investigate the effect of mutual coupling, two antennas were simulated side-by-side. The result of this rectenna simulation is shown in Figure 43. The S-parameter response clearly showed that the antenna coupling of the electric field occurred at all ranges of frequencies especially at 10 GHz. The S12 and S21 responses were -19.5 dB as shown in the figure. This is the transmission between antenna 1 and antenna 2. The antennas were spaced about three-quarter wavelength at 10 GHz.

To reduce the field coupling of the antennas, sufficient space needed to be provisioned. Figure 44 shows the S-parameter response of the antenna array when placed about one wavelength apart (20 mm). The mutual coupling was reduced to -23.58 dB.

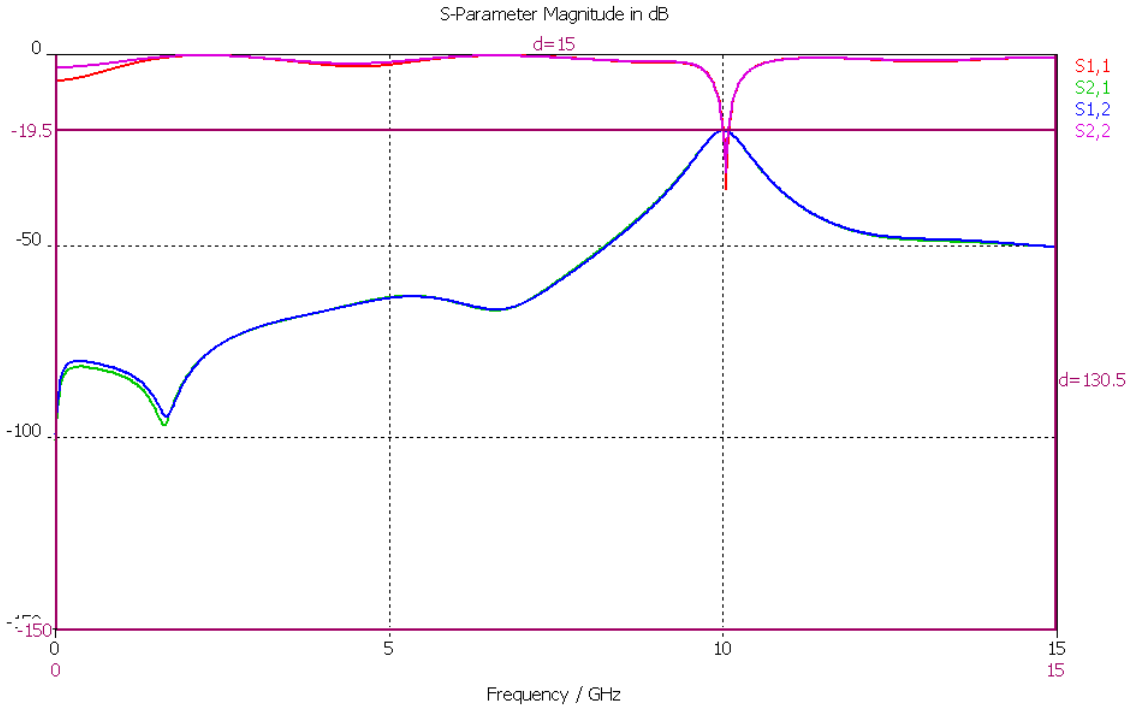

Figure 43. S-parameter Response of the Two Elements Antenna Array Showing Mutual Coupling When Both Antennas Were Placed Side-by-side.

As a rectenna array of 22 elements was required to produce the desirable voltage and current, Figure 45 shows four antenna elements arranged in the same direction, one wavelength apart from each other. The S-parameter response for the four antenna elements in Figure 46 showed little interference between the signals. The combined far-field radiation result is shown in Figure 47. The combined far-field directivity was 13.61 dBi, which was much better than a single antenna (7.65 dBi) as shown in Fig. 15. Ideally the gain increased as the number of elements increases.

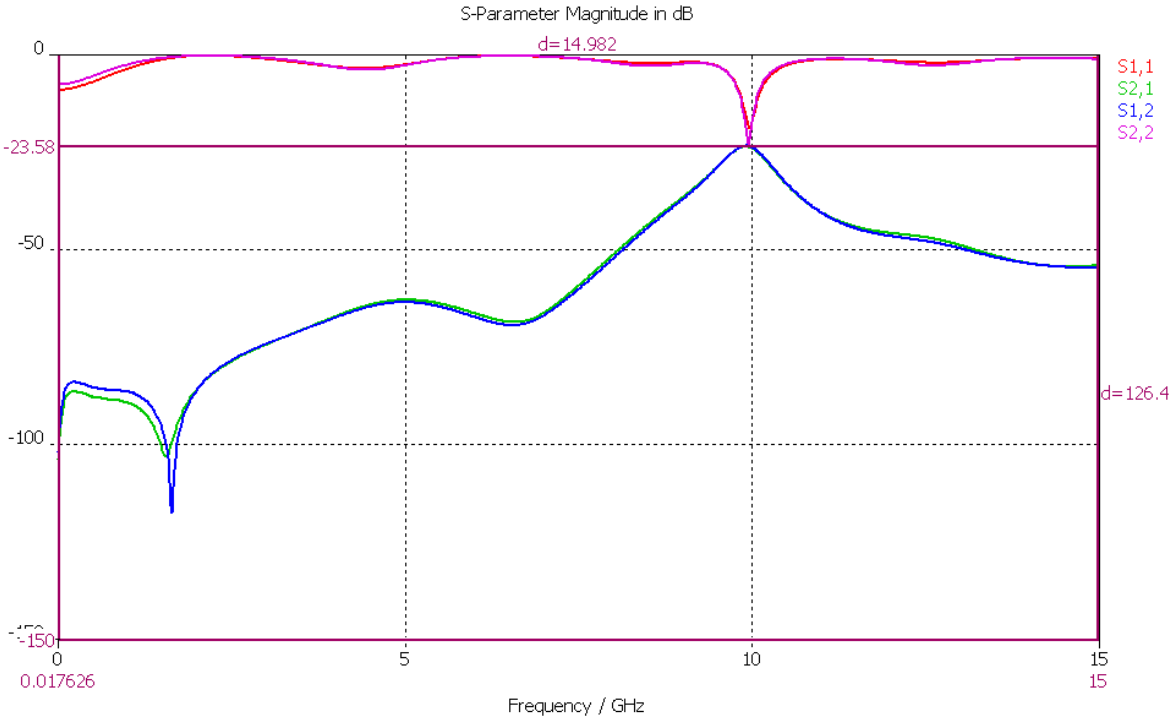

Figure 44. S-parameter Response of the Two Elements Antenna Array Showing Mutual Coupling When Both Antennas Were Placed One Wavelength Apart.

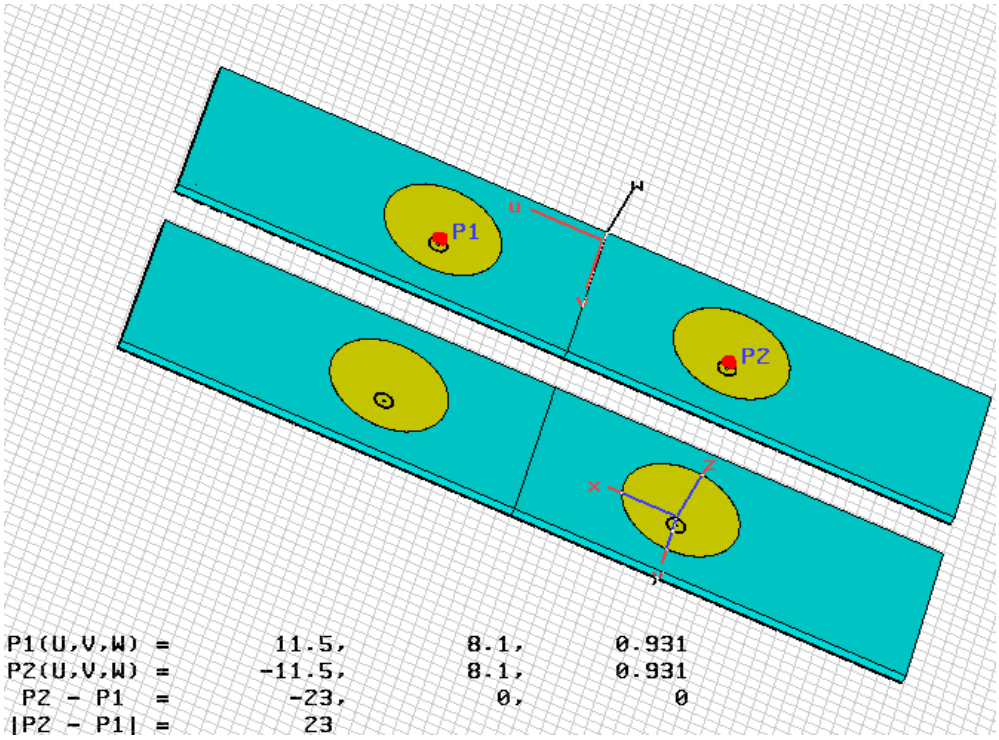

Figure 45. Four Antenna Elements Arranged in the Same Direction.

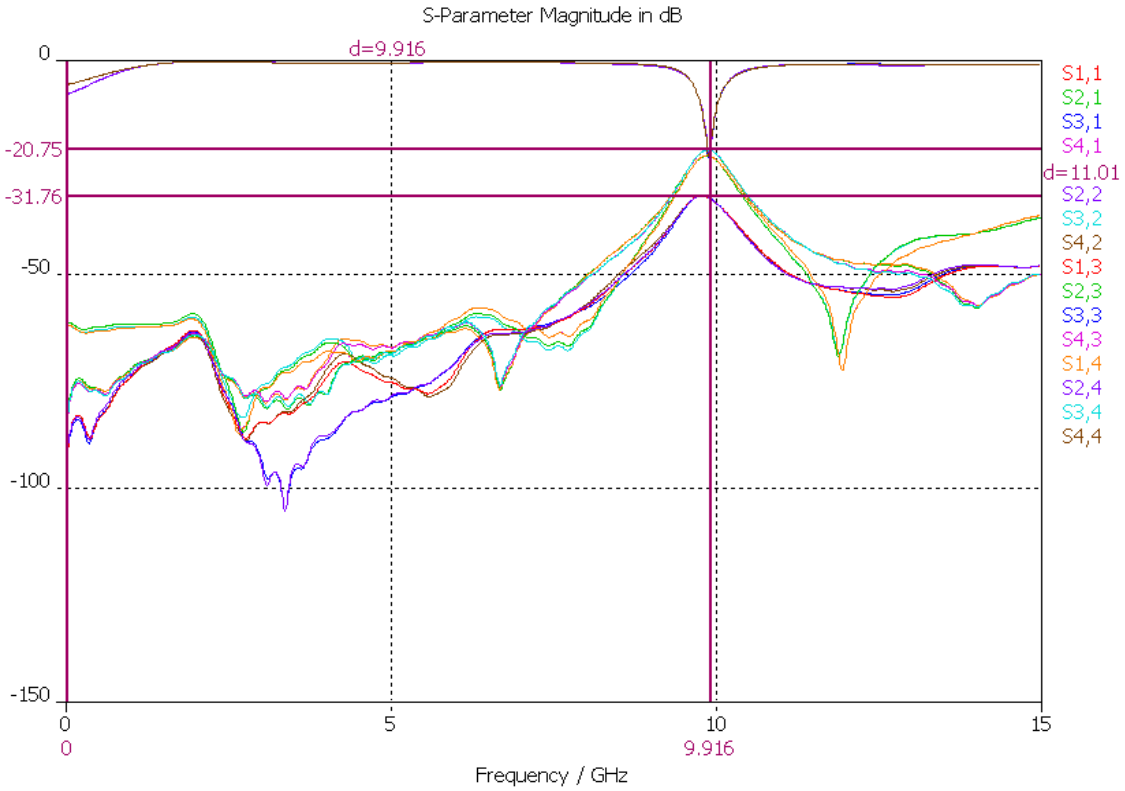

Figure 46. S-Parameter Response for Four Antenna Elements.

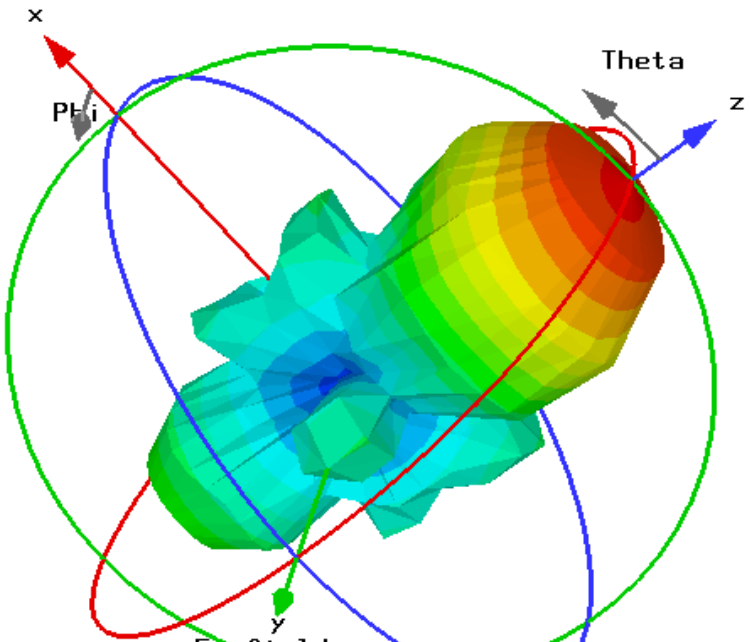


```
Type           = Far-field
Approximation  = enabled (kR >> 1)
Monitor        = farfield (f=10) [1[1,0]+2[1,0]+3[1,0]+4[1,0]]
Component      = Abs
Output         = Directivity
Frequency      = 10
Rad. effic.    = 0.9575
Tot. effic.    = 0.9159
Dir.           =  13.63 dBi
```

Figure 47. Combined Result of the Far-field Radiation for the Four Antenna Elements.

C. SUMMARY

In this chapter, the implementation and layout of the rectenna system were discussed. Quarter-wave transformers were introduced for impedance matching. Optimally 90^o chamfered bends were used to reduce the circuit footprint on the printed circuit board. Half-wave length stub was introduced at the probe feed for better E-fielding coupling. Rectenna arrays were stimulated using CST Microwave Studio and far-field results were presented.

V. RECTENNA TESTING AND ANALYSIS

A. ANTENNA ELEMENT

The DXF files for the rectenna design were sent to Cirexx International for fabrication. Figure 48 shows the measured return loss of the circular patch antenna using a HP Network Analyzer 8510C. The resonant frequency is at 10.15 GHz, which is 1.5 % off the desirable operating frequency. The S11 measured response measured is only -1.82 dB due to impedance mismatch as it was impossible to find any BNC connector with a probe feed diameter of 0.127 mm. To measure the input impedance accurately, it is necessary to build a custom test fixture, and this was not possible given the required time and cost.

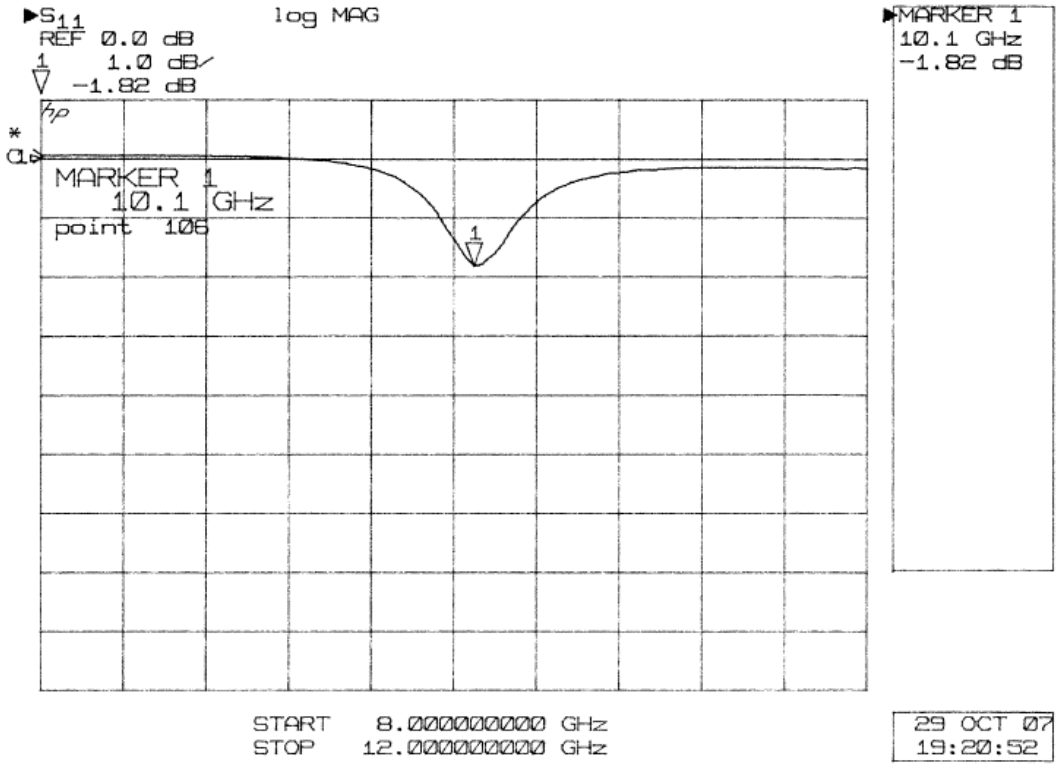

Figure 48. Response of a 10 GHz Circular Patch Antenna.

B. RECTIFIER ELEMENT

The HSMS 8101 diode was soldered onto the filter printed circuit board. The probe feed diameter was changed to 0.127 mm instead of 0.125 mm as

0.127 mm is the industrial standard. The soldering was extremely tedious as it was difficult due to the small line width. The filter and antenna boards were aligned and glued together using epoxy with the 0.127mm probe feed inserted. The weight of each rectenna element is less than 1 g. The area of each rectenna element is 11 mm x 23 mm.

C. RECTENNA ELEMENT

Figure 49 shows the set-up for the bench test. A horn antenna of area 91.3 mm x 73.9 mm was used for the transmitting antenna. An HP 8341B Synthesized Sweeper was used to produce the 10 GHz signal at an output of 10 dBm. This signal was amplified to 23 dBm using an HP 8349B Microwave Amplifier with a horn antenna. The rectenna element was placed in front of the horn antenna for current and DC voltage measurements.

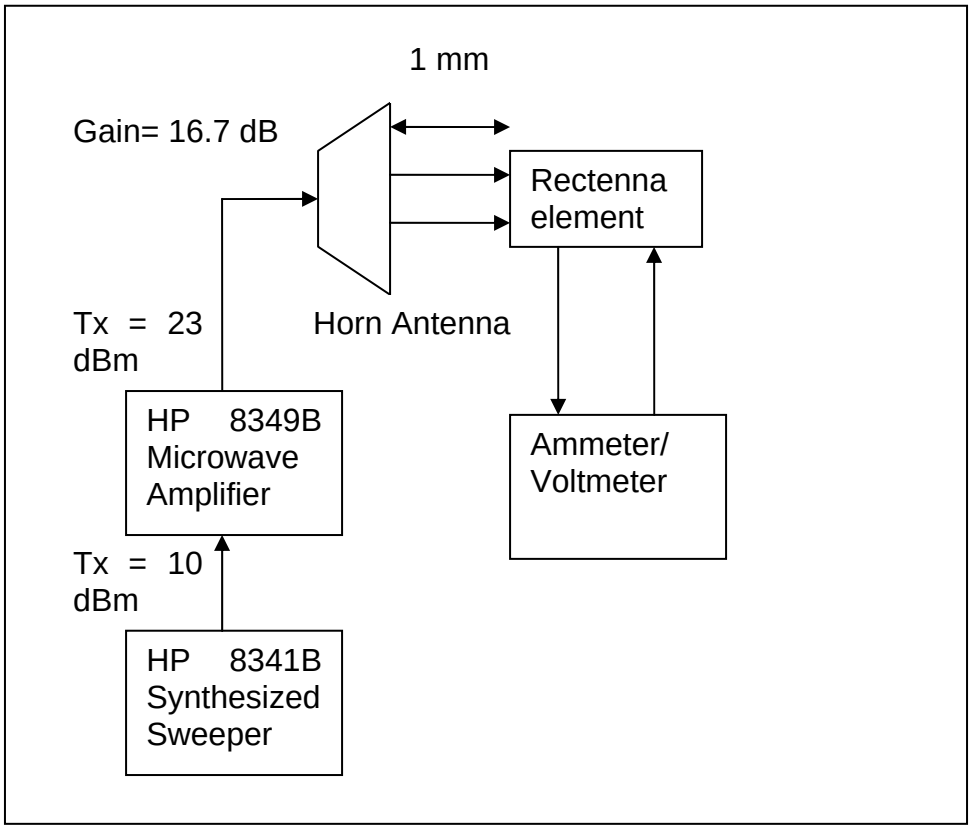

Figure 49. Setup of the Test Bench for Current and DC Voltage Measurement.

Figure 50 shows a rectenna element. To complete the DC loop, there is a need to add a grounding point before the diode. This was done by the wire stub. The wire before the diode acted as a quarter-wave shorted stub and was used to provide a closed DC current path. It was found that the result does not vary significantly without the 47 pF capacitor. Therefore, the capacitor was not used for sub-sequent testing as it was too small to solder correctly.

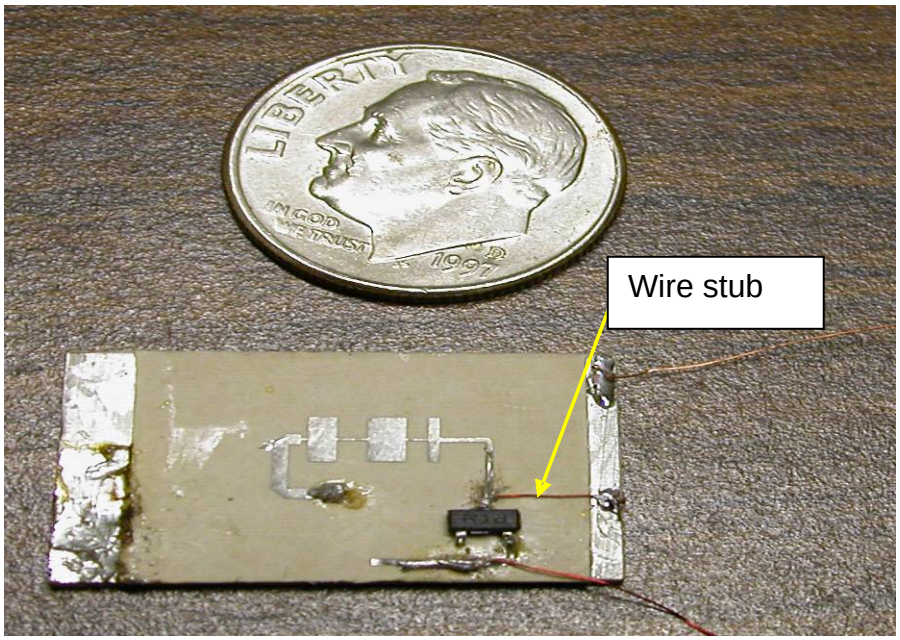

Figure 50. A Rectenna Element Compared with Dime Coin.

Table 10 shows the measured currents and DC voltages of a rectenna element under the test conditions. At 10 GHz, the current was 11.1 mA and DC voltage was 3.61 V. The maximum power produced by the rectenna element tested was 41.15 mW at 10 GHz.

Frequency (GHz)	Current (mA)	DC Voltage (V)	Power (mW)
9.00	-2.36	-2.01	4.74
9.10	-2.13	-2.51	5.35
9.20	-2.78	-1.7	4.73
9.30	-3.16	-1.38	4.36
9.40	-3.38	-1.14	3.85
9.50	-4.65	-1.12	5.21
9.60	-8.72	-1.15	10.03
9.70	-13.02	-1.92	25.00
9.80	-13.85	-2.31	31.99
9.90	-11.92	-2.85	33.97
10.00	-11.4	-3.61	41.15
10.10	-9.81	-3.91	38.36
10.20	-8.31	-3.83	31.83
10.30	-7.31	-3.62	26.46
10.40	-3.81	-2.62	9.98
10.50	-2.21	-1.54	3.40
10.60	-1.51	-1.1	1.66
10.70	-0.81	-0.68	0.55
10.80	-0.61	-0.38	0.23
10.90	-0.44	-0.41	0.18
11.00	-0.36	-0.4	0.14

Table 10. Measured Rectenna Currents and DC Voltages.

Figure 51 and Figure 52 show the voltage and current distributions of three tested rectenna elements tested. The values for the currents and voltages were affected by the position of the test point along the DC stripline. Rectenna 1 had an antenna offset of 1.70 mm from the centre of the patch. It's maximum power was about 31.46 mW at 10.3 GHz. Rectennas 2 and 3 had an antenna offset of 1.75 mm from the centre of the patch. Their maximum power was 41 mW and 36 mW at 10.0 GHz and 10.3 GHz respectively.

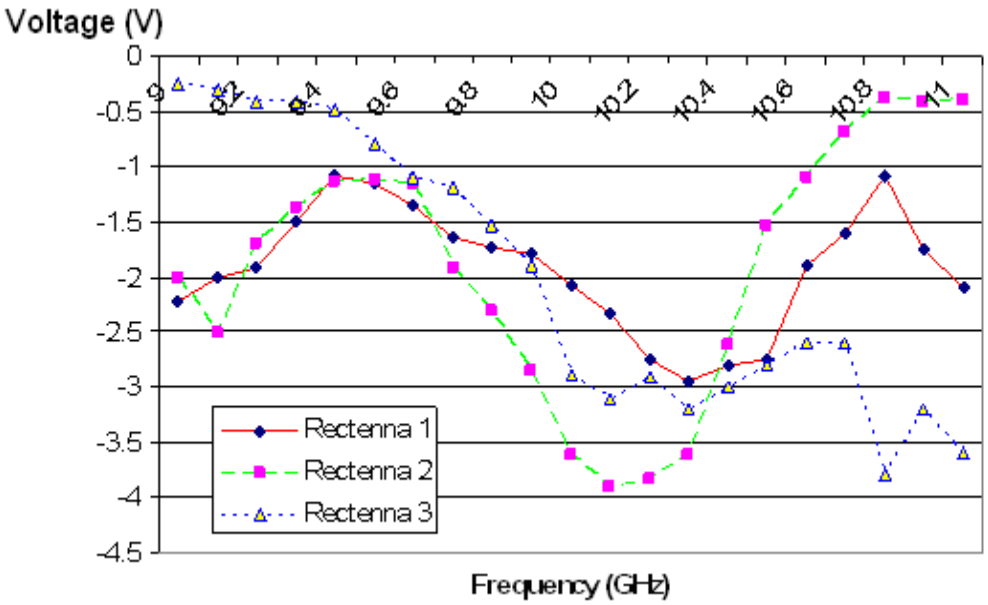

Figure 51. Voltage Distribution of Tested Rectenna Elements.

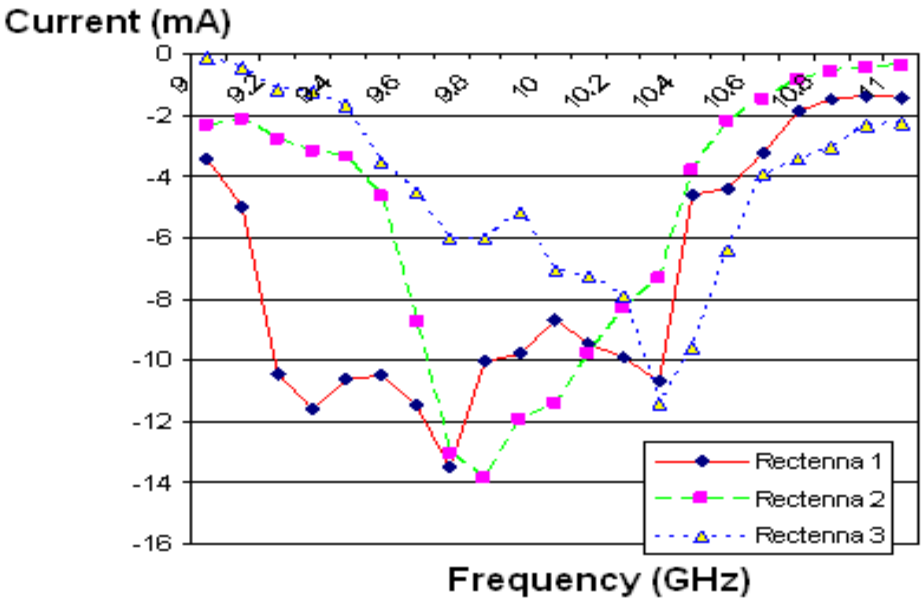

Figure 52. Current Distribution of Tested Rectenna Elements

In general, it was observed that the frequency range between 9.8 GHz and 10.3 GHz generated the highest power. The measured DC current and voltage results varied. These differences could be attributed to the soldering irregularities and length of the manually fabricated quarter-wave wire-stub which resulted in impedance variation.

D. RECTENNA EFFICIENCY

The overall efficiency of rectenna element is defined as the total output power at the load over the input power which is the incoming microwave power. Reference [34] showed that the efficiency of rectifier can be determined using

$$\eta = \frac{P_{dc}}{P_{rec}} = \frac{4\pi r^2 P_{dc}}{P_{trans} G_{trans} A_{eff}} \tag{5.1}$$

where G_{trans} is the gain of the transmitting antenna, P_{trans} is the transmitted power, *r* is the distance from the transmitting antenna, and A_{eff} is the area of the receiving antenna. This is based on the rectenna being in the far field of the transmitting antenna and the RF power is time-averaged.

The antenna effective area is a functional equivalent area from when the antenna is directed toward the source of the received electromagnetic waves. Usually, the antenna is terminated with a matched load to absorb the maximum power. The effective area of the circular patch antenna is calculated using

$$A_{eff} = \frac{\mathrm{P}_{rec}}{S} \tag{5.2}$$

where S is the power density. The relationship between A_{eff} and circular patch antenna gain G_{rec} is

$$A_{eff} = G_{rec} \frac{\lambda^2}{4\pi} \tag{5.3}$$

where λ is the wavelength in free space. The antenna gain of a single circular patch antenna element is the product of antenna directivity and radiation efficiency. Simulated results based on CST Microwave Studio indicated that the circular patch antenna with 1.75 mm offset from the centre had a radiation efficiency of 88% and directivity of 6.50 dBi. Therefore, the gain of the fabricated patch antenna was 5.94i dB. Using Equation (5.3), the effective area A_{eff} of the circular patch antenna was 0.2815 mm^2.

Figure 53 shows the test bench set-up for efficiency measurement. For far-field measurement, the rectenna element had to be placed at least 0.92 m away with the assumption that

$$\text{Far-field} = \frac{2d^2}{\lambda} = 0.92 \text{ m}, \tag{5.4}$$

where *d* is the diagonal length of the horn antenna measured at 117.46 mm with an area of 91.3 mm x 73.9 mm.

For the experiment setup, the rectenna element was placed 1 m away from the horn antenna. The transmitted power by the amplifier was 23 dBm. The horn antenna had a gain G_{trans} of 16.7 dB. Using Equation (5.1), the rectenna efficiency was about 29.6 % when the measured current and voltage measured was 220 μA and 0.281 V respectively. Table 11 summarizes the results for the four rectenna elements.

At 20 GHz, the measured current and voltage was almost zero. This verified that the six-order low-pass filter was working correctly to suppress the second harmonic. For the single rectenna element, the efficiency ranged between 26 % and 36 %. The maximum current and voltage obtained at 1 m is about 240 μW and 0.30 V respectively and the maximum power was about 72 μW. The differences were likely due to soldering irregularity and the length of the wire stub as it was manually constructed and approximated to a quarter wavelength.

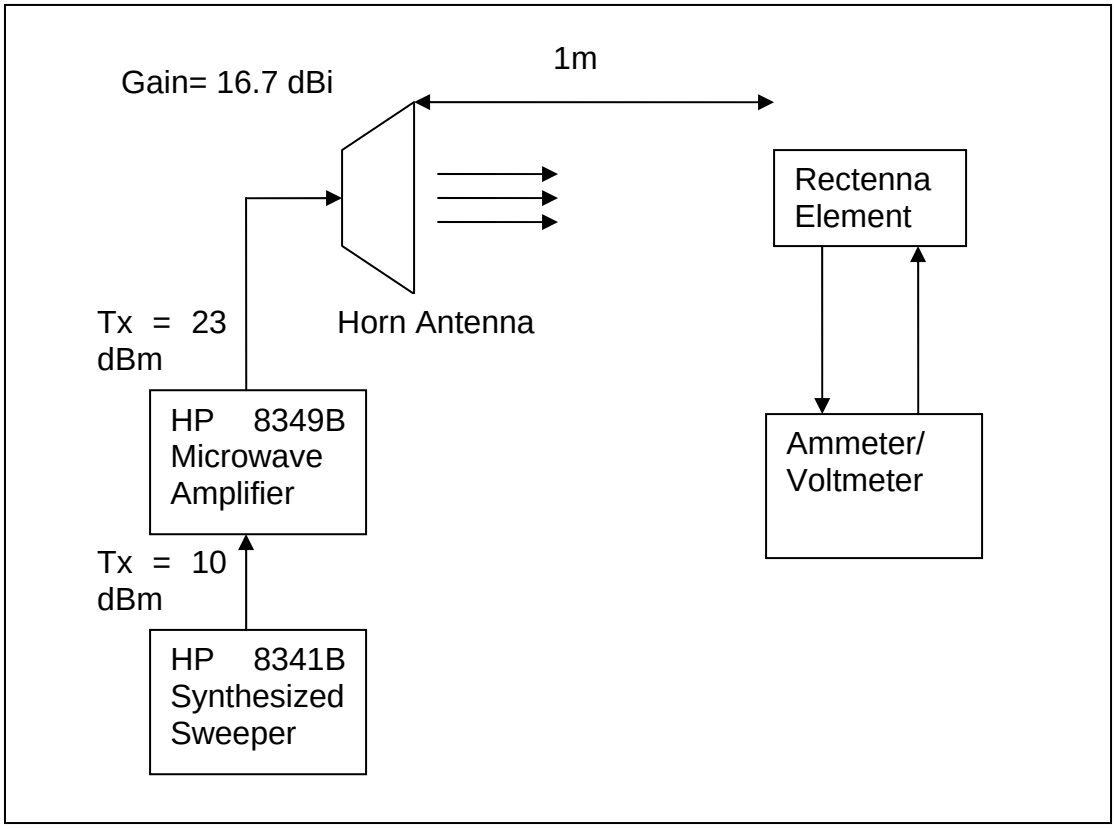

Figure 53. Experimental Setup for Rectenna Current and DC Voltage Measurements.

Rectenna element	Current (μA)	Voltage (V)	DC Power (μW)	Efficiency (%)
1	220	0.27	59	28.4
2	220	0.281	61.8	29.6
3	195	0.281	54.6	26
4	240	0.30	72	35.6

Table 11. Measured Data for the Four Rectenna Elements.

E. RECTENNA ARRAY TESTING

The individual rectenna elements were connected in series using the 0.127 mm diameter wire. They were placed about one wavelength apart to minimized E-field coupling of adjacent elements. The series rectenna array was placed close to the centre of the horn antenna which was transmitting at 23 dBm to produce a maximum voltage and current of -6 VDC and -9 mA respectively as shown in Figure 54. Typically, the output DC voltage range was about -3 V to -6 V. The amount of DC voltage and current produced depended on the position of the rectenna array relative to the horn antenna center. This was due to the TE_{10} mode amplitude tapered across the horn aperture.

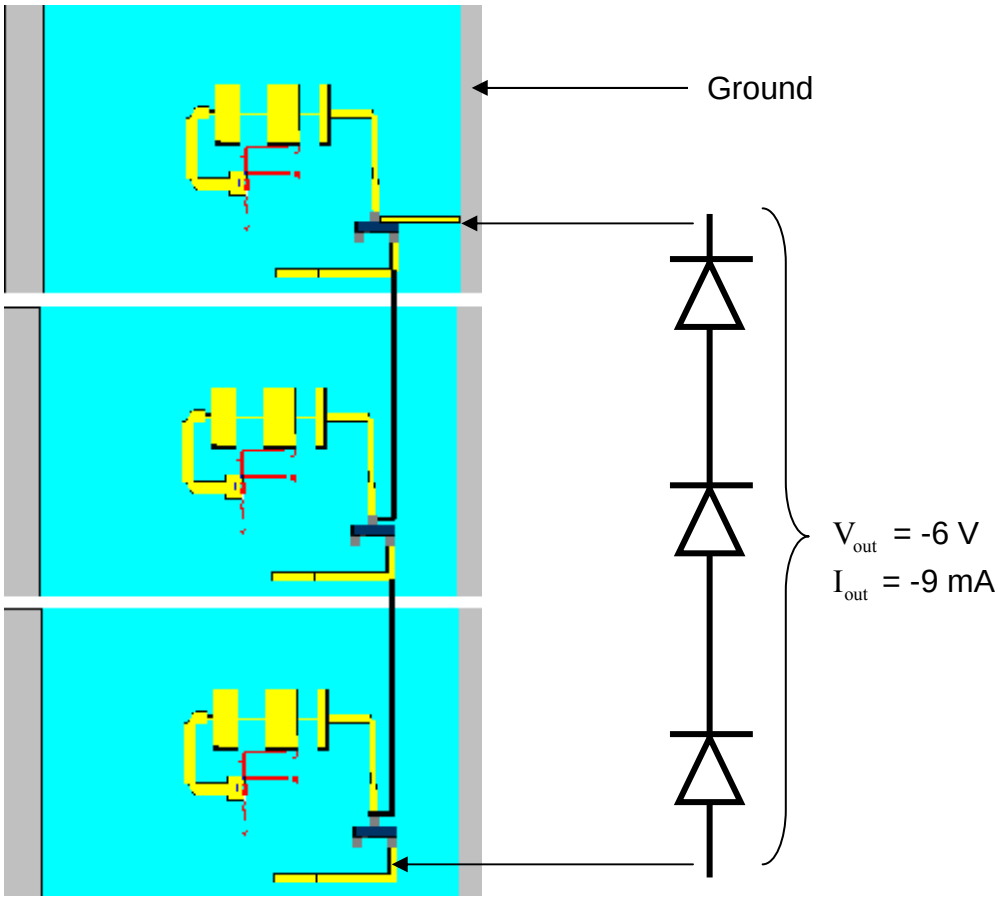

Figure 54. Rectenna Element in Series Setup.

Next, the individual rectenna elements were connected in parallel using the 0.127 mm diameter wire and placed close to the centre of the horn antenna which was transmitting at 23 dBm as shown in Figure 55. The parallel rectenna

elements produced a maximum voltage and current of -1.85 VDC and -29 mA respectively. The typical output current value for the three parallel rectenna elements ranged between -18 mA and -29 mA.

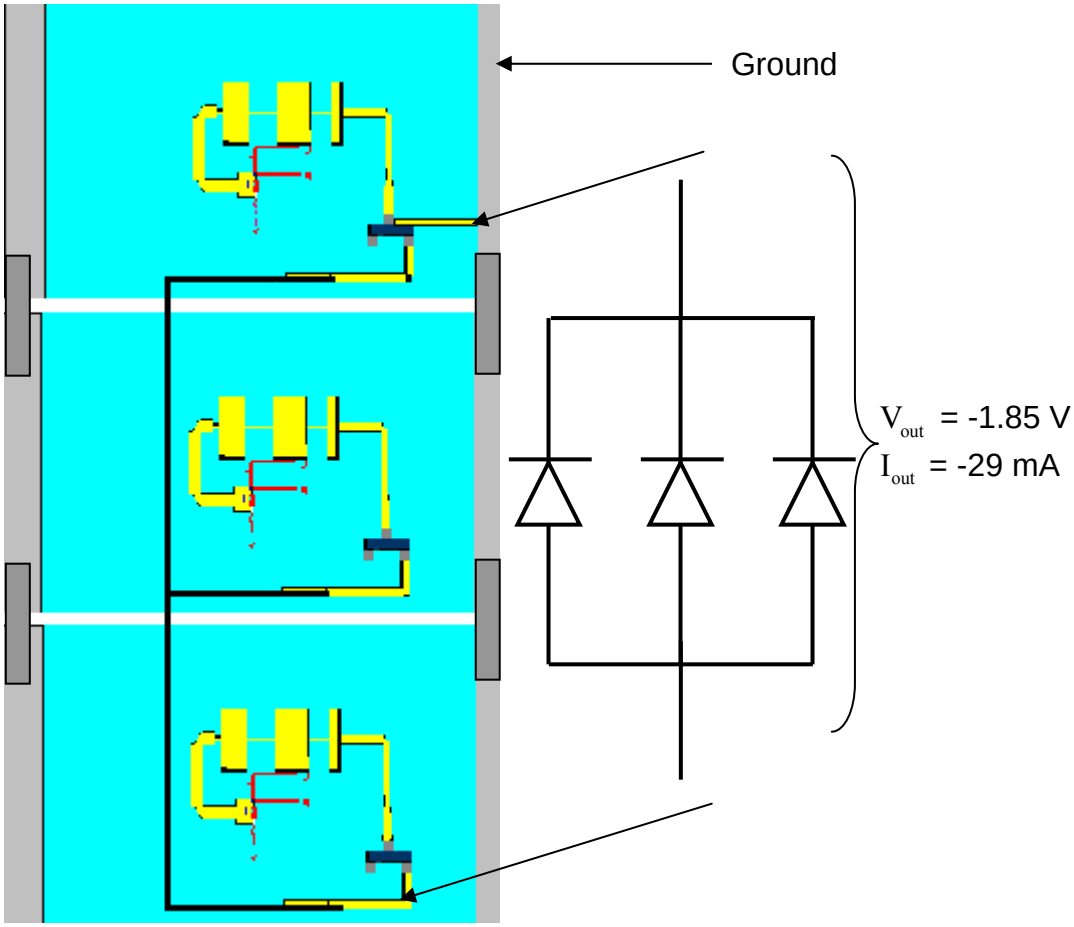

Figure 55. Rectenna Elements Connected in Parallel.

Finally, 16 rectenna elements were connected together to form a 4 x 4 array as shown in Figure 56. The array was placed close to the horn at 10.08 GHz antenna for voltage and current measurements. The column elements were in a series configuration to increase the voltage to about -4.25 VDC. The four columns of rectenna elements were connected in parallel to increase the current as shown in Figure 56. Figure 57 shows the 4 x 4 circular patch antennas. The maximum current obtained for the 4 x 4 array was about 23 mA, which was much less than the measured 36 mA when a single 1 x 4 row of array elements were

connected in parallel. The voltage measured for the 4 x 1 series configuration is listed in Table 12. The values are low as compared to the standalone testing of a 4 x 1 array. The reasons are likely due to soldering irregularity, misalignment, and a non-uniform electromagnetic field generated by the horn antenna. Another reason may include E-field coupling of adjacent antennas since they were placed less than one wavelength apart.

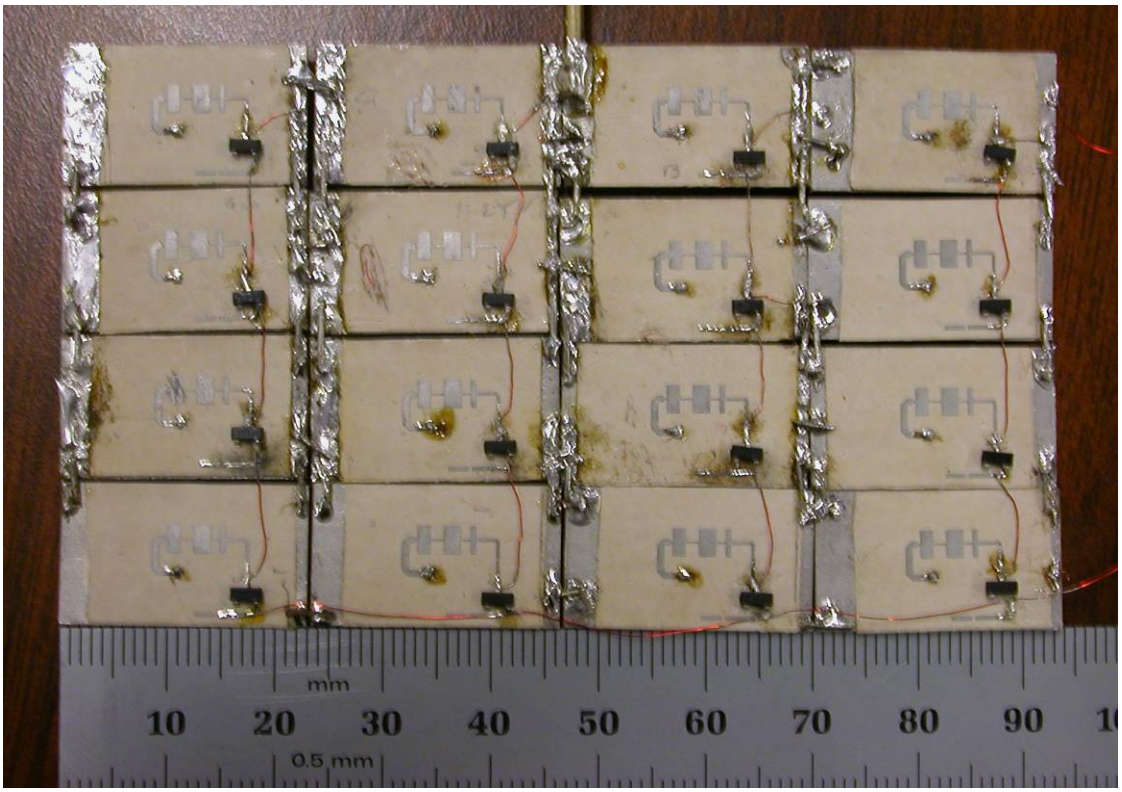

Figure 56. Rectenna's Rectifying Circuits Arranged in Series and Parallel.

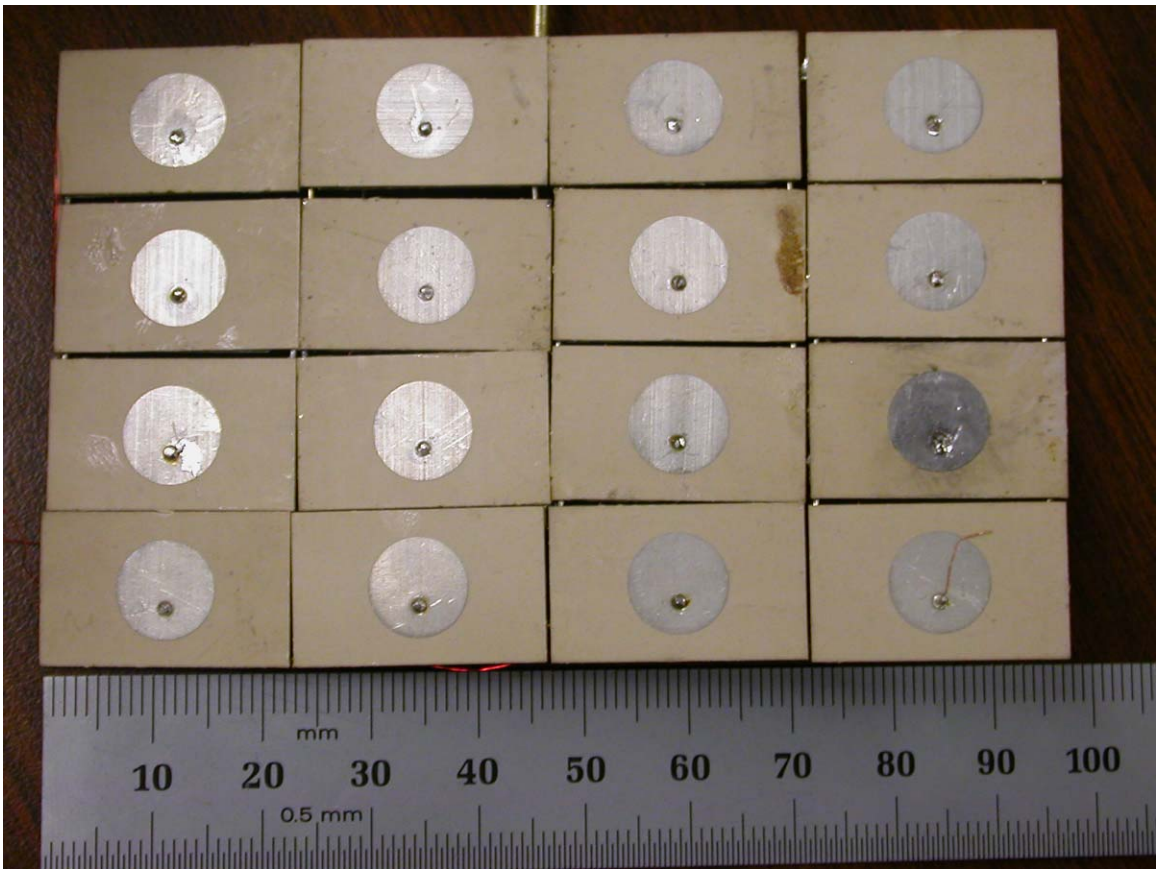

Figure 57. Rectenna' Circular Patch Antenna Array.

Rectenna Column	1	2	3	4
Voltage (V)	-4.01	-4.30	-4.25	-4.21
Current (mA)	-6.00	-6.20	-6.79	-5.85
Power (mW)	24.06	26.66	28.86	24.63

Table 12. Current and Voltage of the Rectenna Array Arranged in Series.

The 4 x 4 array was connected to the MAV prototype as shown in Figure 58 and 23 dBm was transmitted to the 16.7 dBi horn antenna. The MAV rotor blade rotated at a regular speed but did not manage to hover as there was too little current to drive the rotor motor. In order for the MAV to hover, at least 0.55 W is needed. This translates to at least 100 mA current needed.

Figure 58. Rotating MAV with 4 x 4 Rectenna Array.

F. SUMMARY

Based on the experimental results, it can be concluded that the proposed rectenna element has an efficiency range of 26% to 37%. A single rectenna element is capable of producing -1 VDC to -3.9 VDC and -3 mA to -10 mA using a single Schottky diode. At – 3 VDC, the efficiency of the HSMS 8101 Schottky diode is about 60%, which is in agreement with Diode efficiency curve presented as Figure 28.

As there was insufficient power produced by the 4 x 4 rectenna array, the MAV could not hover when 23 dBm of power was transmitted by the horn antenna.

THIS PAGE INTENTIONALLY LEFT BLANK

VI. CONCLUSIONS AND RECOMMENDATIONS

A. CONCLUSIONS

This thesis demonstrated the feasibility of powering a MAV using RF energy without the need of portable fuel. The rich history and background of wireless power transmission was covered in the first chapter. Research performed by NPS students from [3] and [4] was verified and improved upon. Individual elements that made up the rectenna system were simulated using CST Microwave Studio and Agilent ADS software. A quarter-wave microstrip transformer was introduced for impedance matching and an optimally bent microstrip was implemented to minimize the footprint of the circuit on the PCB board. This reduced the weight of the rectenna. The simulated results for individual elements were presented in this thesis.

The final design of the rectenna system was sent for fabrication. The HSMS 8101 Schottky diode and antenna were soldered together to form the rectenna element. Each rectenna element was tested to verify the performance. The efficiency of a single rectenna element varied between 26% and 37%. This is about four times better than the 7% obtained by [3]. The efficiency did not achieve the desired 60%, which was likely due to soldering irregularity and impedance mismatch. The rectenna elements were connected together to form a 4 x 4 rectenna array to power the MAV.

The prototype motor for the air vehicle was tested to verify the results documented by [3]. The antenna array was attached to the motor and tested. The MAV was not able to fly due to insufficient current generated by the rectenna array as there were insufficient rectenna elements and the efficiency of the rectenna array was too low.

B. RECOMMENDATIONS

The result of this thesis shows that in order to allow MAV to hover, the efficiency of the rectenna system needs to be improved. This can be done by:

1. Increasing the offset of the antenna from 1.75 mm to 2.00 mm from the centre of the circular patch antenna using 17 μm copper cladding with ε_r = 3. This would create a purely resistive 50 Ω circular patch antenna as shown in Chapter III.

2. Replacing the manually made wire-stub with a quarter-wave length microstrip stub for the first row of the rectenna array as well as and fine tuning the impedance matching units.

3. Reducing the rectenna PCB board size as the actual circuit occupied about only 70% of the rectenna surface.

4. Selecting a thinner antenna substrate to reduce the weight of the rectenna element. Using a thin substrate would reduce the antenna's bandwidth, this could be compensated for by using a lower dielectric constant (e.g. ε_r = 2.2) material instead of 3.

5. Redesigning the rectenna element using a three-layered PCB board instead of using two single double-layer boards. At 10 GHz, the circuit design might be too small for hand soldering. Therefore, machine soldering is a better option as micrometer accuracy is required.

6. Using a high power transmitter and high gain antenna to increase the power density on the rectenna array, and therefore increase the DC voltage and current produced.

7. Implementing a full-wave rectifier circuit. This is likely to produce more current per element for the MAV motor. A full-wave rectifier would rectify the positive and negative cycles, thus, producing twice the amount of current with the same DC voltage. In order to accommodate a full-wave rectifier circuit, the rectenna needs to be redesigned.

APPENDIX

This appendix contains a Matlab program that employs the microstrip equation to calculate the microstrip physical length based on the dielectric constant and operating frequency.

```
% characteristic impedance of a microstrip line
 clear
 er=3; d=.00013/0.0254; f=10e9;
% find w/d for given Zo
 Zref=50; Zo=Zref;
 A=Zo/60*sqrt((er+1)/2)+(er-1)/(er+1)*(.23+.11/er);
 B=377*pi/2/Zo/sqrt(er);
 ratio1=8*exp(A)/(exp(2*A)-2);
 ratio2=2/pi*(B-1-log(2*B-1)+(er-1)/2/er*(log(B-1)+.39-.61/er));
 if ratio1 < 2, ratio=ratio1; end
 if ratio2 >= 2, ratio=ratio2; end
 ee=(er+1)/2+(er-1)/2/sqrt(1+12/ratio);
% check the impedance using the reverse formulas
  if ratio <=1, Z0=60/sqrt(ee)*log(8/ratio+ratio/4); end
  if ratio >1, Z0=120*pi/sqrt(ee)/(ratio+1.393+.667*log(ratio+1.444));
end
 disp(['-------------- ',num2str(Zo),'  OHM LINE DIMENSIONS -----------
------']) 
 disp(['design characteristic impedance (ohms): ',num2str(Zo)])
 disp(['relative permittivity: ',num2str(er)])
 disp(['substrate thickness, (in): ',num2str(d),', (m):
',num2str(d*.0254)])
 disp(['effective relative permittivity: ',num2str(ee)])
 disp(['ratio W/d: ',num2str(ratio)])
 disp(['line width, W (in): ',num2str(ratio*d),', (m):
',num2str(ratio*d*.0254)])
 disp(['computed characteristic impedance (ohms): ',num2str(Z0)])
 % antenna and power splitter dimensions (if iant=0)
 iant=1;
 if iant==0
 wavl=3e8/f/sqrt(ee);
 L=wavl/2;
 disp('----------------- PATCH DIMENSIONS --------------------')
 disp(['frequency, f (GHz): ',num2str(f/1e9)])
 disp(['patch length, L (m): ',num2str(L)])
 disp(['patch length, L (in): ',num2str(L/.0254)])
% equal Y power splitter -- recompute new dimensions
 Zo=Zref*2;
 A=Zo/60*sqrt((er+1)/2)+(er-1)/(er+1)*(.23+.11/er);
 B=377*pi/2/Zo/sqrt(er);
 ratio1=8*exp(A)/(exp(2*A)-2);
 ratio2=2/pi*(B-1-log(2*B-1)+(er-1)/2/er*(log(B-1)+.39-.61/er));
 if ratio1 < 2, ratio=ratio1; end
 if ratio2 >= 2, ratio=ratio2; end
 ee=(er+1)/2+(er-1)/2/sqrt(1+12/ratio);
```

```
% check the impedance using the reverse formulas
  if ratio <=1, Z0=60/sqrt(ee)*log(8/ratio+ratio/4); end
  if ratio >1, Z0=120*pi/sqrt(ee)/(ratio+1.393+.667*log(ratio+1.444));
end
 disp('------------ POWER SPLITTER DIMENSIONS ----------------')
 disp(['design characteristic impedance (ohms): ',num2str(Zo)])
 disp(['relative permittivity: ',num2str(er)])
 disp(['effective relative permittivity: ',num2str(ee)])
 disp(['substrate thickness, (in): ',num2str(d),', (m):
',num2str(d*.0254)])
 disp(['ratio W/d: ',num2str(ratio)])
 disp(['line width, W (in): ',num2str(ratio*d),', (m):
',num2str(ratio*d*.0254)])
 disp(['computed characteristic impedance (ohms): ',num2str(Z0)])
 end
 disp(['design frequency (GHz): ',num2str(f/1e9)])
 wavl0=3e8/f/.0254;
 wavl=wavl0/sqrt(ee);
 disp(['free space wavelength (in): ',num2str(wavl0),', (m):
',num2str(wavl0*.0254)])
 disp(['wavelength in microstrip (in): ',num2str(wavl),', (m):
',num2str(wavl*.0254)])
```

Output of the program sample shows below:

---------- 50 OHM LINE DIMENSIONS ----------

design characteristic impedance (ohms): 50

relative permittivity: 3

substrate thickness, (in): 0.0051181, (m): 0.00013

effective relative permittivity: 2.4162

ratio W/d: 2.5138

line width, W (in): 0.012866, (m): 0.00032679

computed characteristic impedance (ohms): 50.2719

design frequency (GHz): 10

free space wavelength (in): 1.1811, (m): 0.03

wavelength in microstrip (in): 0.75984, (m): 0.0193

```
%Program to calculate length and width of microstrip Low Pass Filter
(Butterworth)
%note this uses a leading capacitor followed by alternating inductors
and
%capacitor
%Output are L_length_mm and C_length_mm. From [4].

clear

%Input parameteres and number of stages for filter
N = input('Please input number of N stages (1-6) = ');
Fc = input('Please input cutoff frew (GHz) = ');
Z0 = input('Please input Loading Impedance (Ohm) = ');

Er = input('Please input Er of substrate material = ');
d = input('Please input thickness height of substrate material(mm) =
');


%Calculated values
Fc = Fc * 1e9;
Wc = 2*pi*Fc;


%creating and determining the g factors
if N == 1
    g = 2.0;
elseif N == 2
    g(1)=1.4142; g(2)=1.4142;
elseif N == 3
    g(1)=1.0; g(2)=2.0; g(3)=1.0;
elseif N ==4
    g(1)=0.7654; g(2)=1.8478; g(3)=1.8478; g(4)=0.7654;
elseif N ==5
    g(1)=0.618; g(2)=1.618; g(3)=2.0; g(4)=1.618; g(5)=0.618;
elseif N == 6
    g(1)=0.5176; g(2)=1.4142; g(3)=1.9318; g(4)=1.9318; g(5)=1.4142;
g(6)=0.5176;
end

%now calculating the L & C values; Starting with  inductive load
followed by
%capacitive load
for I = 1:N,
    if mod(I,2) == 1            %odd function, i.e Capacitor C
        C(floor(I/2)+1) = g(I)/(Z0*Wc);
    else                      %even function, i.e Inductor L
        L(I/2) = g(I)*Z0/Wc;
    end
end

%Next stage is to determine the width and length of the respective
%capacitive and inductors parts;
```

```
Wdratiohigh = input ('Please input the expected Width to Height Ratio
for High Impedance (0.2 to 1) = ');   %capcitor
Wdratiolow = input ('Please input the expected Width to Height Ratio
for low Impedance (8 to 10) = ');      %inductor

Width_high = Wdratiohigh * d;       %actual width of capacitive stub
Width_low =  Wdratiolow *d;     %actual width of inductive stub
Ee_high = (Er+1.0)/2.0 + (Er-1.0)/(2.0*(sqrt(1.0+(12.0/Wdratiohigh))));
Ee_low  = (Er+1.0)/2.0 + (Er-1.0)/(2.0*(sqrt(1.0+(12.0/Wdratiolow))));

Z_high  = 60.0*log(8.0/Wdratiohigh + Wdratiohigh/4.0)/sqrt(Ee_high);
% for W/H < 1.0
Z_low   = 120.0*pi/(sqrt(Ee_low)*(Wdratiolow + 1.393 +
0.667*log(Wdratiolow + 1.444)));
% for W/H > 1.0

%now calculating the actual length of the L & C stubs.
for I = 1:N,
    if mod(I,2) == 1            %odd function, i.e capacitor C
        C_length_mm(floor(I/2)+1) =
3e11*C(floor(I/2)+1)*Z_low/sqrt(Ee_low);
    else                     %even function, i.e inductor L
        L_length_mm(I/2) = 3e11*L(I/2)/(Z_high*sqrt(Ee_high));
    end
end
```

LIST OF REFERENCES

[1] William C. Brown, “The History of Power Transmission by Radio Waves,” *IEEE Transactions of Microwave Theory and Techniques*, Vol MTT-32, No. 9, September 1984.

[2] N. Tesla, “The transmission of electrical energy without wires,” *Electrical World and Engineer*, New York, 5 March 1904.

[3] George Tsolis, “Theoretical and experimental study of micro air vehicle powered by RF Signal at 10 GHz,” Naval Postgraduate School, December 2003.

[4] Mark Tan Lee Meng, “Efficient Rectenna Design for Wireless Power Transmission For MAV application,” Naval Postgraduate School, December 2005.

[5] M. Cheney, Tesla, “Man Out of Time, “Englewood Cliffs, New Jersey, Prentice-Hall, 1981.

[6] G. Goubau and F. Schwering “On the guided propagation of electromagnetic wave beams,” *IRE Transaction on Antenna Propagation*, vol. AP-9, pp. 248-256, May 1961.

[7] W. C. Brown, “Description and operating characteristics of the platinotron – A new microwave tube device,” *Proceedings of the Institute of Radio Engineering (IRE),* vol. 45, no. 9, pp. 1209-1222, September 1957.

[8] W. C. Brown, “The amplitron, a super power microwave generator,” *Electron. Progress*., vol. 5, no. 1, pp. 1-5, July/August 1960.

[9] Joseph J. Schlesak, Adrian Alden and Tom Ohno, “A Microwave Powered High Altitude Platform,” IEEE MTT-S International, vol. 1, pp. 283-286, 25-27 May 1988.

[10] Matsumoto, H., “Research on Solar Power Station and Microwave Power Transmission in Space,” *IEEE Microwave Magazine*, December 2002, pp. 36-45.

[11] Nagatomo, S. Sasaki and Y. Naruo, 1994, "Conceptual study of a solar power satellite, SPS 2000,” 19th International Symposium on Space Technology and Science, Paper No. ISTS-94-e-04, pp. 469-476, May 1994.

[12] Advanced Concept Office, NASA Headquarters, and Advanced Space Analysis Office, NASA LeRC, SSP Technical Interchange Meeting, Washington, DC 1995, pp. 10-27.

[13] Dong-Gi Youn, Yang-Ha Park, Kwan-Ho Kim and Young-Chul Rhee, “A Study on the Fundamental Transmission Experiment for Wireless Power Transmission System,” IEEE Ten Conference, vol. 2, pp. 1419-1422, September 1999.

[14] James O. McSpadden, John C. Mankins, “Space Solar Power Programs and Microwave Wireless Power Transmission Technology,” *IEEE Microwave Magazine*, December 2002, pp. 46-57.

[15] Hiroshi Matsumoto, “Research on Solar Power Satellites and Microwave Power Transmission in Japan,” *IEEE Microwave Magazine*, December 2002, pp. 36-45.

[16] Hiroyuki Nagayama, “SSPS Activities in Japan,” Asia Pacific Radio Science Conference, 2004 Proceedings, pp. 615.

[17] Saurab Sood, Sivaparakash Kullanthasamy, Mohammad Shahidehpour, ”Solar Power Transmission: From Space to Earth,” IEEE 12 June 2005 Power Engineering Society General Meeting, pp. 605-610.

[18] Deng Hong Lei, Kong Li, “A Novel High-Efficiency Rectenna for 35 GHz Wireless Power Transmission,” 2004 4th International Conference on Microwave and Millimeter Wave Technology Proceedings.

[19] F. Steinsiek, K. H. Weber, W. P. Foth, H. J. Foth, C. Schafer, “Wireless Power Transmission Technology Development and Demonstrations,” The 4th International Conference on Solar Power from Space - SPS '04, Proceeding, 30 June- 2 July 2004, pp. 202.

[20] Yu-Jiun Ren, Kai Chang, “5.8 GHz Circularly Polarized Dual-Diode Rectenna Array for Microwave Power Transmission,” *IEEE Transaction on Microwave Theory and Techniques*, vol. 54, pp. 1495-1502, June 2006.

[21] Yu-Jiun Ren, Muhammad F. Farooqui, and Kai Chang, “A Compact Dual-Frequency Rectifying Antenna with High-Order Harmonic-Rejection,” *IEEE Transactions on Antennas and Propagation*, Vol. 55, No. 7, July 2007

[22] V.A. Vanke, V.L. Savin, “Cyclotron wave converter for SPS energy transmission system”, in Proceeding 2nd International Symposium, SPS 91 from Space, Paris, France, 1991, pp. 515-520.

[23] V.A. Vanke, H. Matsumoto, N. Shinohara, and A. Kita, “Cyclotron wave converter of microwave into dc,” *IEICE Transaction Electron*, vol. 81-C, no. 7, 1998, pp. 1136-1142.

[24] Jamal Zbitou, M. Latrach, “Hybrid Rectenna and Monolithic Integrated Zero-Bias Microwave Rectifier,” *IEEE Transaction on Microwave Theory and Techniques*, vol. 54, pp 147-152, January 2006.

[25] Robert L. Vitale, “Design and Prototype Development of a Wireless Power Transmission System For a Micro Air Vehicle (MAV),” Naval Postgraduate School, June 1999.

[26] Wadell, Brain C, *Transmission Line Design Handbook*, Artech House, 1991.

[27] Garg, Bhartia, Bahl and Ittipiboon, *Microstrip Antenna Design Handbook*, Chapter 9, pp. 539, Artech House, 2000.

[28] Balanis, Constantine A, Antenna Theory, Analysis and Design, 2nd Edition, John Wiley and Sons, 1997, ISBN 0-471-59268-4.

[29] Robert A. Sainati*, CAD of Microstrip Antennas for Wireless Applications,* Artech House, 1996, ISBN 0-89006-562-4.

[30] David M. Pozar, *Microwave Engineering*, John Wiley & Sons, Inc., New York, 1998.

[31] Zoya B. Popovic, “Wireless Powering for Low-Power Distributed Sensors,” Sixth International Symposium Nikola Tesla, 18-20 October 2006.

[32] Avago Technologies, “HSMS-8101, Surface Mount Microwave Schottky Mixer Diode,” 8 September 2006.

[33] James O. McSpadden, Lu Fan and Kai Chang, “Design and Experiments of a High-Conversion-Efficiency 5.8-GHz Rectenna,” *IEEE Transaction on Microwave Theory and Techniques*, vol. 46, no. 12, December 1998.

[34] Tae-Whan Yoo and Kai Chang, “Theoretical and Experimental Development of 10 and 35 GHz Rectennas”, *IEEE Transactions on microwave Theory and Techniques,* vol. 40, no. 6, June 1992.

[35] R. J. P. Douville and D.S. James, “Experimental Study of Symmetric Microstrip Bends and Their Compensation,” *IEEE Transactions on Microwave Theory and Techniques*, vol. MTT-26, March 1978, pp. 175-181.

[36] Hewlett Packard, “HP Advanced Design System, Circuit Components Vol. 2,” HP Part No. E8900-90082, January 1999.

INITIAL DISTRIBUTION LIST

1. Defense Technical Information Center
   Ft. Belvoir, Virginia

2. Dudley Knox Library
   Naval Postgraduate School
   Monterey, California

3. Chairman, Department of Electrical and Computer Engineering, Code EC
   Naval Postgraduate School
   Monterey, California

4. Professor David Jenn, Code EC/Jn
   Department of Electrical and Computer Engineering
   Naval Postgraduate School
   Monterey, California

5. Professor Michael Morgan, Code EC/Mw
   Department of Electrical and Computer Engineering
   Naval Postgraduate School
   Monterey, California

6. Leng Huei, Toh
   Defence Science and Technology Agency
   Singapore

7. Robert L. Vitale
   University of California, Santa Cruz, California

8. Garry Lee
   Lutronix Cooperation
   Del Mar, California